NUREG/IA-0510

International Agreement Report

MELCOR-ASTEC Crosswalk of the Accident at Fukushima-Daiichi Unit 1: Phase I Analysis

Prepared by:
N. Andrews[1], C. Faucett[1], S. Belon[2],
C. Bouillet[2], and H. Bonneville[2]

[1]Sandia National Laboratories
Albuquerque, NM 87185

[2]Institut de Radioprotection et de Surete Nucleaire
Cadarache, France, BP 3- 13115 St-Paul-Lez-Durance Cedex

D. Algama, NRC Project Manager

Division of Systems Analysis
Office of Nuclear Regulatory Research
U.S. Nuclear Regulatory Commission
Washington, DC 20555-0001

Manuscript Completed: May 2018
Date Published: June 2019

Prepared as part of
The Agreement on Research Participation and Technical Exchange
Under the Cooperative Severe Accident Research Program (CSARP)

Published by
U.S. Nuclear Regulatory Commission

AVAILABILITY OF REFERENCE MATERIALS IN NRC PUBLICATIONS

NRC Reference Material

As of November 1999, you may electronically access NUREG-series publications and other NRC records at NRC's Library at www.nrc.gov/reading-rm.html. Publicly released records include, to name a few, NUREG-series publications; *Federal Register* notices; applicant, licensee, and vendor documents and correspondence; NRC correspondence and internal memoranda; bulletins and information notices; inspection and investigative reports; licensee event reports; and Commission papers and their attachments.

NRC publications in the NUREG series, NRC regulations, and Title 10, "Energy," in the *Code of Federal Regulations* may also be purchased from one of these two sources.

1. **The Superintendent of Documents**
   U.S. Government Publishing Office
   Washington, DC 20402-0001
   Internet: bookstore.gpo.gov
   Telephone: (202) 512-1800
   Fax: (202) 512-2104

2. **The National Technical Information Service**
   5301 Shawnee Road
   Alexandria, VA 22312-0002
   www.ntis.gov
   1-800-553-6847 or, locally, (703) 605-6000

A single copy of each NRC draft report for comment is available free, to the extent of supply, upon written request as follows:

Address: **U.S. Nuclear Regulatory Commission**
Office of Administration
Multimedia, Graphics, and Storage & Distribution Branch
Washington, DC 20555-0001
E-mail: distribution.resource@nrc.gov
Facsimile: (301) 415-2289

Some publications in the NUREG series that are posted at NRC's Web site address www.nrc.gov/reading-rm/doc-collections/nuregs are updated periodically and may differ from the last printed version. Although references to material found on a Web site bear the date the material was accessed, the material available on the date cited may subsequently be removed from the site.

Non-NRC Reference Material

Documents available from public and special technical libraries include all open literature items, such as books, journal articles, transactions, *Federal Register* notices, Federal and State legislation, and congressional reports. Such documents as theses, dissertations, foreign reports and translations, and non-NRC conference proceedings may be purchased from their sponsoring organization.

Copies of industry codes and standards used in a substantive manner in the NRC regulatory process are maintained at—

The NRC Technical Library
Two White Flint North
11545 Rockville Pike
Rockville, MD 20852-2738

These standards are available in the library for reference use by the public. Codes and standards are usually copyrighted and may be purchased from the originating organization or, if they are American National Standards, from—

American National Standards Institute
11 West 42nd Street
New York, NY 10036-8002
www.ansi.org
(212) 642-4900

Legally binding regulatory requirements are stated only in laws; NRC regulations; licenses, including technical specifications; or orders, not in NUREG-series publications. The views expressed in contractorprepared publications in this series are not necessarily those of the NRC.

The NUREG series comprises (1) technical and administrative reports and books prepared by the staff (NUREG–XXXX) or agency contractors (NUREG/CR–XXXX), (2) proceedings of conferences (NUREG/CP–XXXX), (3) reports resulting from international agreements (NUREG/IA–XXXX), (4) brochures (NUREG/BR–XXXX), and (5) compilations of legal decisions and orders of the Commission and Atomic and Safety Licensing Boards and of Directors' decisions under Section 2.206 of NRC's regulations (NUREG–0750).

NUREG/IA-0510

International Agreement Report

MELCOR-ASTEC Crosswalk of the Accident at Fukushima-Daiichi Unit 1: Phase I Analysis

Prepared by:
N. Andrews[1], C. Faucett[1], S. Belon[2],
C. Bouillet[2], and H. Bonneville[2]

[1]Sandia National Laboratories
Albuquerque, NM 87185

[2]Institut de Radioprotection et de Surete Nucleaire
Cadarache, France, BP 3- 13115 St-Paul-Lez-Durance Cedex

D. Algama, NRC Project Manager

Division of Systems Analysis
Office of Nuclear Regulatory Research
U.S. Nuclear Regulatory Commission
Washington, DC 20555-0001

Manuscript Completed: May 2018
Date Published: June 2019

Prepared as part of
The Agreement on Research Participation and Technical Exchange
Under the Cooperative Severe Accident Research Program (CSARP)

Published by
U.S. Nuclear Regulatory Commission

ABSTRACT

This analysis compares Sandia National Laboratories' (SNL) MELCOR results for the first phase of the Modular Accident Analysis Program (MAAP)-MELCOR Crosswalk to the Accident Source Term Evaluation Code (ASTEC), developed by the Institut de Radioprotection et de Sureté Nucléaire (IRSN), results for the same accident scenario. Similar to the original MAAP-MELCOR Crosswalk, this analysis integrates system response of both containment and reactor pressure vessel (RPV), core degradation behavior, lower plenum behavior and lower head failure, and finally hydrogen behavior and generation.

The accident scenario developed by the Electric Power Research Institute (EPRI) and SNL for this analysis is stylized after accident progression of Fukushima Daiichi Unit 1 to better highlight areas of similarity and differences in the two computer codes studied. Hence, this work is not appropriate for extrapolation to the area of Fukushima forensic study. The behavior of the main steam line isolation valve, control rod drive mechanism, feedwater system, safety relief valve, and isolation condenser were made constant between the two codes. The MELCOR simulation was run to 16 hours, while the ASTEC simulation was run a slightly shorter amount of time before to the point of lower head failure. Ex-vessel behavior was not examined in this analysis.

Key differences in the system response were found to result from differing thermal-hydraulic models, how the two codes treat in-vessel core relocation, and how the codes treat debris generated. MELCOR treats the core debris primarily as particulate debris, whereas ASTEC treats debris in a single phase – called "magma" – which often resembles a molten pool. This has significant importance in predicting the total amount of hydrogen generated and the total amount of convective heat transfer away from degraded core materials. Key differences were also found in the total amount of core debris relocating to the lower plenum and then ex-vessel during the scenario, with ASTEC predicting significantly more core debris relocating.

FOREWORD

The contributions of EPRI in the original MAAP-MELCOR were integral in this analysis. Funding for this activity was provided to Sandia National Laboratories by the US Nuclear Regulatory Commission.

Sandia National Laboratories is a multi-mission laboratory managed and operated by National Technology and Engineering Solutions of Sandia LLC, a wholly owned subsidiary of Honeywell International Inc. for the U.S. Department of Energy's National Nuclear Security Administration under contract DE-NA0003525.

TABLE OF CONTENTS

LIST OF FIGURES

LIST OF TABLES

EXECUTIVE SUMMARY

To analyze the three accidents at Fukushima-Daiichi, integral severe accident codes are being used extensively for the simulation of core degradation and the core final damage state. This work presents a joint analysis between Sandia National Laboratories (SNL), under contract to the United States Nuclear Regulatory Commission (NRC), and the Institut de Radioprotection et de Sûreté Nucléaire (IRSN).

The U.S. Department of Energy (DOE) has sponsored collaborative work between the Electric Power Research Institute (EPRI) and SNL associated with the NRC, to compare the response of Modular Accident Analysis Program (MAAP5) and MELCOR severe accident analysis codes on a stylized Fukushima-Daiichi Unit 1-like scenario. (Humphries, 2014) This work, known as "MAAP/MELCOR Crosswalk Phase 1 Study," was completed in 2014 and highlighted some differences in the codes, which explain the differences in system behavior. (Luxat, 2014) Contemporarily to this work, the international Benchmark Study of the Accident at the Fukushima Daiichi Nuclear Power Station (BSAF) was launched in 2012 under the direction of the Organization for Economic Cooperation and Development (OECD) Nuclear Energy Agency (NEA). This collaborative benchmark includes, among others, EPRI, IRSN, SNL and the NRC. (OECD NEA, 2015)

Within this analysis, an extension of the original MAAP5-MELCOR Crosswalk was undertaken to include the Accident and Source Term Evaluation Code (ASTEC). (Chatelard, 2014) A comparison is made between MELCOR and ASTEC results on an accident scenario stylized after the events at Fuksuhima-Daiichi Unit 1. The main objective of the "Crosswalk Study" is to identify through a code-to-code comparison, which models or phenomenological representations are different and lead to significant deviations in the results.

The main events and assumptions of the scenario are presented in the Table ES-1. Given the different code frameworks in both MELCOR and ASTEC, an effort was made to reduce as much as possible the differences in the problem geometry and the initial conditions at the point of core uncovery. The decay heat evolution is imposed by setting a time dependent decay curve. The fission products release is represented in both simulations. (Luxat, 2014)

Table ES-1 Main Events and Assumptions for the Stylized Fukushima-Daiichi Unit 1 Scenario (Luxat, 2014)

Events, System or Operator Actions	Assumption and Details
Reactor scram and reactor cooled by the isolation condenser	Beginning of transient: t_0
Main Steam Isolation Valve (MSIV)[1]	Signal closure at t_0 + 52.5 s
Control Drive System	Flow stopped at SCRAM
Feedwater system	From t_0 to t_0 + 60 s
Isolation condenser	Imposed heat loss and isolation timings[1], Inefficient due to the SBO at t_0 + 55 min
Station Blackout (SBO) with total loss of normal and auxiliary power	t_0 + 55 min
Safety Relief Valves seizure[1]	t_0 + 7 h

[1] Conditions and parameters were defined and set as boundary conditions or as imposed entry parameters in both simulations to reduce the possible system behavior discrepancies.

Key event timings for core uncovery and degradation are presented in Table ES-2. (Luxat, 2014). Included are boil-off timings and key degradations events, such as the failure of core rings. The discrepancies between the two codes appear in loss of fuel integrity, which is modeled differently in the two different codes. MELCOR models fuel assembly failure as a function of time at temperature (loss of structural integrity), whereas ASTEC simulates a loss of integrity only if material melting conditions (phase change) are met.

Table ES-2 Key Events for Core Uncovery and Core Degradation (Luxat, 2014)

Accident Progression Event	MELCOR Timing	ASTEC Timing
Core water level at the Top of Active Fuel (TAF)	2.7 h	2.6 h
Core water level at 2/3 TAF	3.0 h	2.8 h
Core water level at 1/3 TAF	3.3 h	3.1 h
Onset of in-vessel hydrogen generation	3.6 h	3.4 h
Initial fuel assembly loss of integrity[1]		
Core ring 1	5.0 h	3.6 h
Core ring 2	8.4 h	3.7 h
Core ring 3	9.0 h	3.7 h
Core ring 4	no loss of integrity	3.9 h
Core ring 5	no loss of integrity	4.4 h
Initial core plate failure[2]	5.1 h	6.0 h
Lower plenum dryout	10.4 h	8.9 h
Initial RPV lower head breach	14.4 h	15.6 h

[1] Loss of integrity by collapse is defined by time & temperature criteria for MELCOR and by melting (temperature) criterion T_{fuel}>2550K for ASTEC.

[2] No mechanical core plate failure is predicted in ASTEC; only the melting is predicted. Debris and molten corium can leak through the plate holes.

The ASTEC simulation predicts that debris formation and relocation starts 0.2 hours after the onset of oxidation. That debris formation extends rapidly to the other rings (even to the outer core ring 5) due to a global heat-up of the core. In the MELCOR simulation, the first collapse is predicted 1.4 hours after the onset of oxidation. Compared to ASTEC, the heat-up of outer rings is significantly delayed. In MELCOR, the collapse of ring 2 and 3 occurs at 9.0 hours in the simulation, and the fuel rods in the outermost core rings (4 and 5) do not collapse until lower head rupture.

The RPV lower head failure times are predicted with nearly one hour of difference between the two simulations, and that deviation is noticeably less than what should be expected according to the timing differences on the fuel loss of integrity and lower plenum dry out.

The temperature fields during the accident transients are represented on Figures ES-1 and ES-2. Only the active core region is shown for MELCOR results, whereas the field for ASTEC is displayed in the active region and the top portion of the lower plenum (above the hemispherical portion).

In the MELCOR simulation, a hot spot over 2000 K occurs at the center of the upper half of the active region at 4.25 hours, which is later than in the ASTEC simulation. The overheating of the core is less than in the ASTEC simulation, and more localized. Core overheating quickly spreads from the hotspot to the rest of the core within ASTEC.

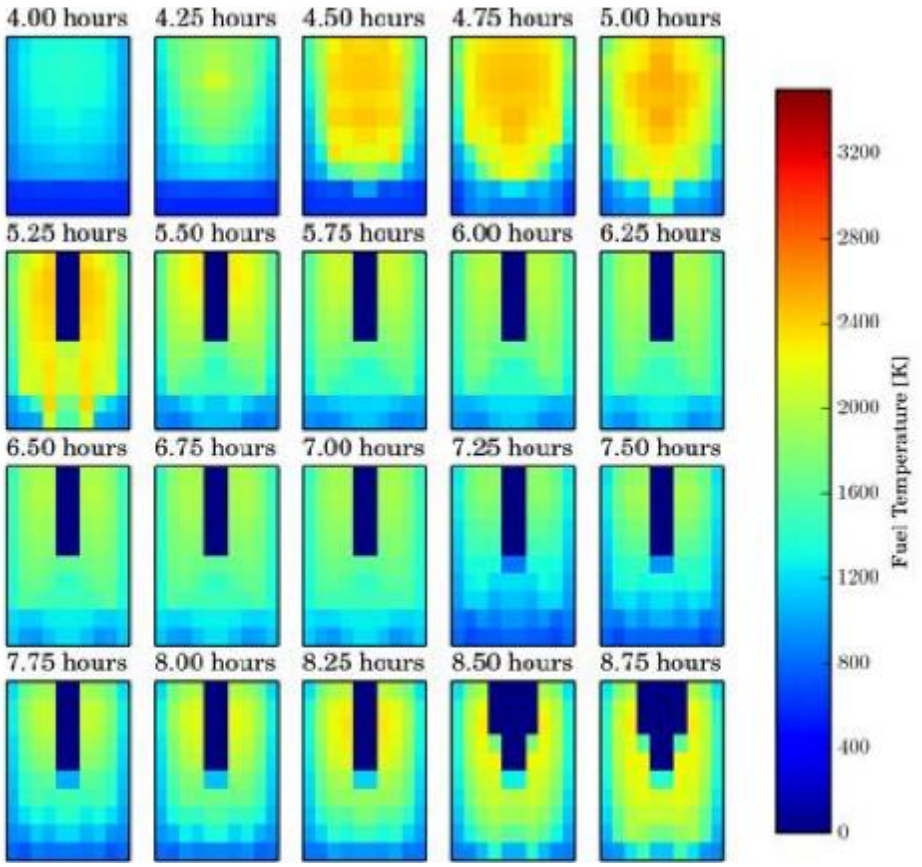

Figure ES-1 Distribution of Active Core Region Fuel Temperatures from Hours 4.0 to 8.75 from the MELCOR Simulation (Luxat, 2014)

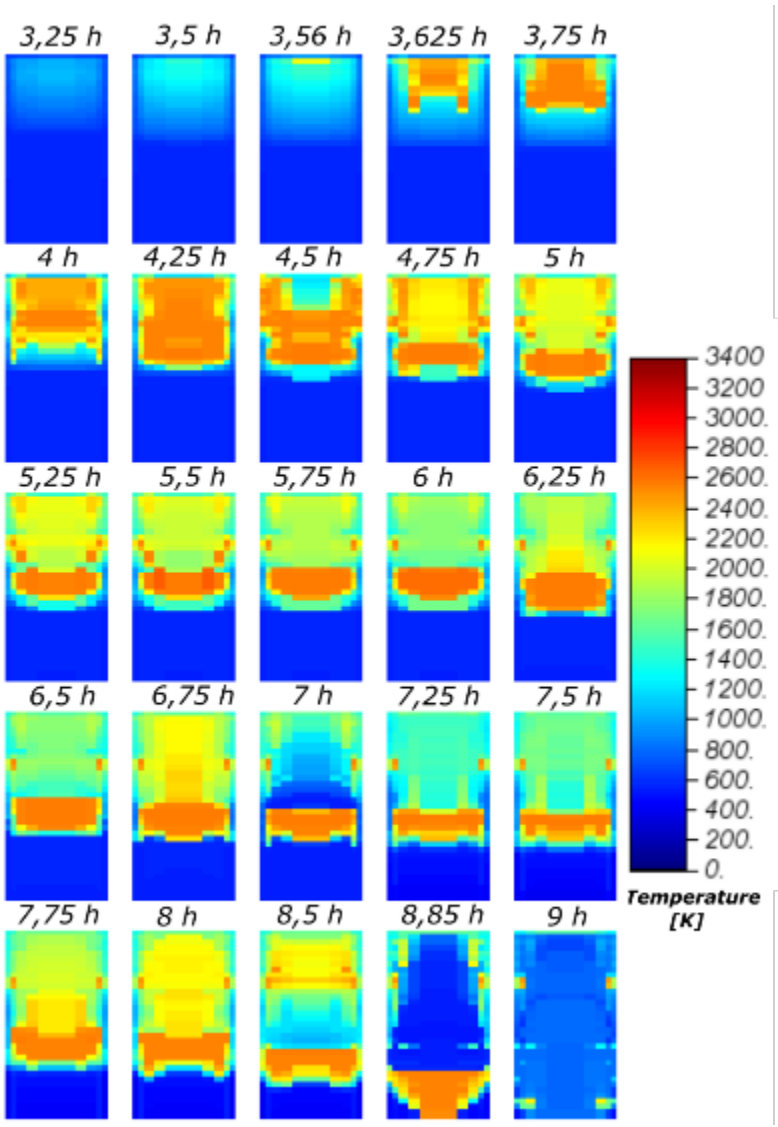

Figure ES-2 Distribution of Core Region Mesh-Average Temperatures from Hours 3.25 to 9.0 Hours from the ASTEC Simulation

The oxidation of Zircaloy, boron carbide and stainless steel by steam is modeled in both simulations. Within the lower plenum region, MELCOR applies the same model in both the active core region and lower plenum, whereas in ASTEC no oxidation model is available in the specific mesh used to model the hemispherical portion of the lower plenum. From the onset of oxidation to 5.0 hours, hydrogen production follows the same trend in both codes. However, the oxidation begins slightly sooner in the ASTEC simulation since core uncovery occurs sooner. The hydrogen generation curves can be seen in Figure ES-3.

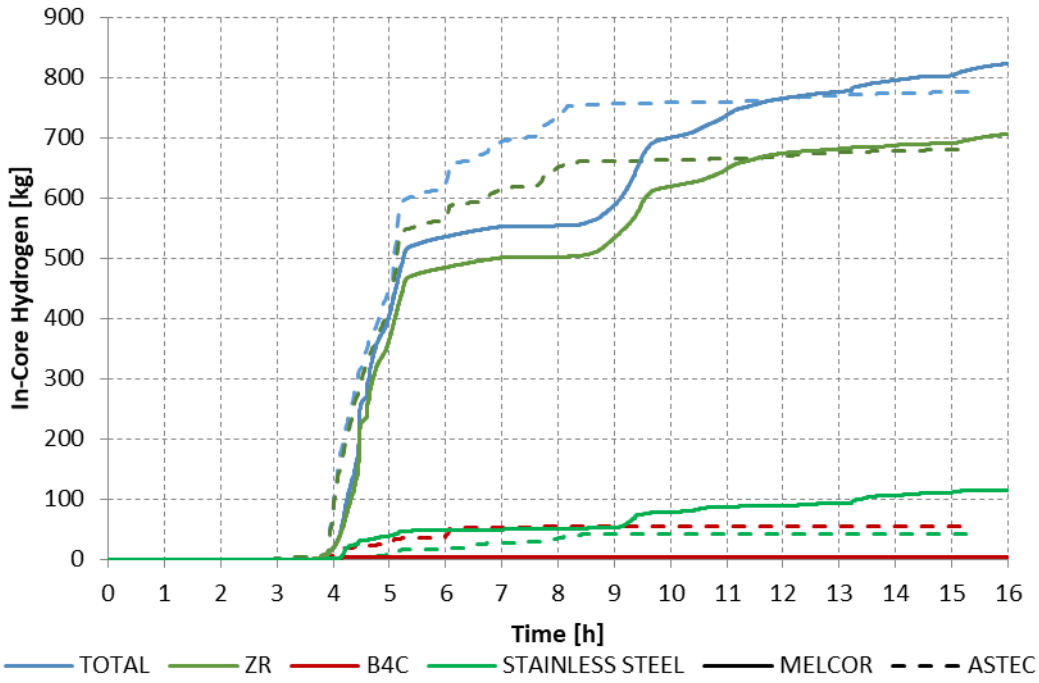

Figure ES-3 Cumulative Hydrogen Production by Oxidation for MELCOR (solid lines) and ASTEC (dashed lines) (Luxat, 2014)

MELCOR simulates two main phases of hydrogen production. The first phase corresponds to the core uncovery and heatup phase as in ASTEC simulation, except that after the first core ring collapse at 5.0 hours, the core temperature in MELCOR is stabilized by relocation of overheated debris to the lower plenum. MELCOR predicts a second phase of hydrogen production associated with a rise in temperature after the safety relief valve (SRV) seizure where steam flashing reignites the Zr-steam reaction. High core temperatures in rings 2 and 3 precipitate an increase in the hydrogen production rate until lower plenum dry out. After this, the hydrogen production still progresses but at a lower rate. Even if the final total hydrogen production is close between ASTEC and MELCOR simulations, the production kinetics differ clearly from 5 hours onward. At a given time, the difference in hydrogen production can reach 200 kg.

Within the remainder of this document, the phenomenological differences in the treatment of severe core damage progression is discussed in-depth. At a high level, this analysis underlines the fact that severe accident analysis codes assume different morphologies or modelling abstractions to describe and represent degraded core materials. MELCOR postulates the formation of primarily particulate debris on loss of rod-like geometry, with some molten debris components. ASTEC assumes the formation of a pool mainly composed of molten materials, but with a minimum gas flow area through the pool. Additionally, ASTEC and MELCOR model fuel assembly loss of integrity in different manners. ASTEC only models loss of integrity through the melting of core elements. Upon this melting event, the fuel becomes “magma.” MELCOR on the other hand models fuel assembly failure as a function of time and temperature.

These modeling abstractions directly impact the presumed porosity and surface area of debris, and thus have a significant impact on the coolability and oxidation of these materials. Accordingly, the thermal-hydraulic response can differ greatly at times between the two codes.

Despite the fact that the thermal-hydraulic behavior can differ between these codes, the overall oxidation predicted by the two codes interestingly does not differ significantly. Additionally, the time of predicted lower head failure between the two codes is also similar, even though the location of lower head failure is different.

ABBREVIATIONS AND ACRONYMS

1F1	Fukushima-Daiichi Unit 1
ASTEC	Accident Source Term Evaluation Code
BAF	bottom of active fuel
BSAF	Benchmark Study of the Accident at the Fukushima Daiichi Nuclear Power Station
BWR	boiling water reactor
CRD	control rod drive
CSARP	Cooperative Severe Accident Research Program
CV	control volume
DOE	Department of Energy
DCH	direct containment heating
EPRI	Electric Power Research Institute
FP	fission product
GRS	Gesellschaft für Anlagen und Reaktorsicherheit mbH
h	hour
IC	isolation condenser
IRSN	French Institut de Radioprotection et de Surete Nucleaire
J	joule
K	Kelvin
kg	kilogram
LOCA	loss of coolant accident
LP	lower plenum
m	meter
MAAP	Modular Accident Analysis Program
MCAP	MELCOR Cooperative Assessment Program
MCCI	molten core concrete interactions
MPa	Megapascal
MSIV	main steam isolation valve
MSL	main steam line
MW	megawatt
NEA	Nuclear Energy Agency
NCG	non-condensable gas
NRC	United States Nuclear Regulatory Commission
OECD	Organization for Economic Cooperation and Development
PCV	primary containment valve
PWR	pressurized water reactor
RPV	reactor pressure vessel
s	second
SNL	Sandia National Laboratories
SOARCA	State-of-the-Art Reactor Consequence Analyses
SRV	safety relief valve
TAF	top of active fuel
TEPCO	Tokyo Electric Power Company
TMI	Three Mile Island
µm	micron

1 INTRODUCTION AND DISCUSSION

1.1 Study Purpose and Objective

The Modular Accident Analysis Program (MAAP)-MELCOR Crosswalk Phase 1 Study was completed in November 2014, documenting differing behavior of the MAAP5 and MELCOR severe accident analysis codes during a stylized Fukushima Daiichi Unit 1 (1F1) event scenario. This was a collaborative effort between the Electric Power Research Institute (EPRI) and Sandia National Laboratories (SNL), sponsored by the U.S. Department of Energy (DOE). (Luxat, 2014)

The diverging behavior of the MAAP5 and MELCOR codes was brought to light by a DOE sponsored analysis of 1F1, which experts agree experienced significant core damage and saw core relocation ex-vessel due to a lack of water injection, using the codes MELTSPREAD and CORQUENCH where initial/boundary conditions were supplied by MELCOR and by MAAP. Of particular concern to these analyses were the reactor pressure vessel (RPV) pressure at the time of lower head breach, the fraction and temperature of molten core debris relocation into containment, and the rate of core debris relocation to and spreading within the containment. The crosswalk analysis sought to find the origin of these key divergences as well as any others that occurred during the in-vessel phase of a severe accident. (Luxat, 2014)

Accordingly, in the MAAP-MELCOR Crosswalk, relevant code deviations that could lead to a significant difference in system behavior were identified and attributed to the relevant models within the two codes. Deviations are described in more detail in the Modular Accident Analysis Program (MAAP)-MELCOR Crosswalk Phase 1 Study. These deviations included: (Luxat, 2014)

- Core energy balance
- RPV response
- Containment response
- Fuel assembly collapse
- Fuel canister failure
- Extent of downward relocation of particulate debris
- Flow and heat transfer area in the degraded core
- Fraction of core forming solid or molten debris
- Core region failure mechanism
- Rate of core debris slumping
- Molten fraction of debris slumping to lower plenum
- Molten fraction of debris in the lower plenum
- In-vessel hydrogen generation

At a high level, the MAAP5 code predicted core relocation behavior similar to that which occurred in Three Mile Island (TMI), in which a crucible containing a molten pool was formed in-core. The outer crust of this crucible insulated a significant amount of molten mass. On the other hand, the MELCOR code predicted a significantly higher amount of particulate debris within the core region. The increased porosity of the MELCOR debris leads to a higher steam and gas flow rate through the damaged core. Because of this, there is more convective heat removal and more in-vessel hydrogen generation in the MELCOR analysis. Figure 1-1 shows this difference in flow through the degraded core in both MAAP5 and MELCOR. (Luxat, 2014)

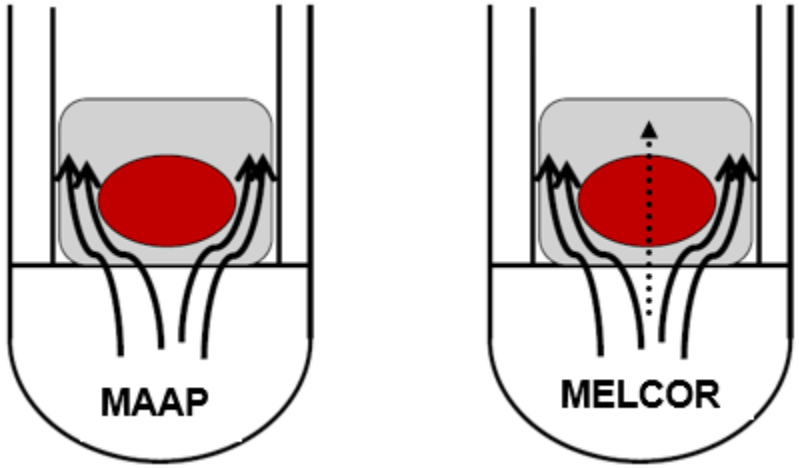

Figure 1-1 Illustration of Flow through a Degraded Reactor Core for both MAAP and MELCOR (Luxat, 2014)

Contemporary to the ongoing DOE-sponsored Fukushima analysis and forensics work, the French Institut de Radioprotection et de Sûreté Nucléaire (IRSN) Accident Source Term Evaluation Code (ASTEC) was also used to evaluate the accidents at the Fukushima site. Of particular note is the Organization for Economic Cooperation and Development (OECD): Nuclear Energy Agency's (NEA's) ongoing NEA Benchmark Study of the Accident at the Fukushima Daiichi Nuclear Power Station (BSAF) Project, which aims to gather international insights from code analysis of the accidents to inform the decommissioning of the reactors at the Fukushima site. The IRSN, EPRI, SNL and the U.S. Nuclear Regulatory Commission (U.S. NRC) have all taken part in this effort. (OECD NEA, 2015)

Following the publication of the results of the MAAP-MELCOR Crosswalk, IRSN, SNL and the U.S. NRC discussed the possibility of using both the Crosswalk and BSAF activities as a starting point for ASTEC to become involved in code crosswalk activities. This report compares the MELCOR results for the first phase of the MAAP-MELCOR Crosswalk to ASTEC results for the same accident scenario. This report aims to indicate key code modeling differences that result in the divergence of system behavior, similarly to what was done in the report on the first phase of the crosswalk.

Similar to both MAAP5 and MELCOR, ASTEC is a severe accident analysis tool for estimating core response to beyond design basis nuclear accidents. ASTEC simulates all the phenomena that occur during a severe accident in a water-cooled nuclear reactor, from the initiating event to the possible release of radioactive products outside the containment. ASTEC has been

developed jointly over a number of years by the IRSN and its German counterpart, the Gesellschaft für Anlagen und Reaktorsicherheit mbH (GRS) until 2015 and exclusively by IRSN since that time. (IRSN, 2017)

The version ASTEC V2.0 rev3 was used for the current crosswalk study; it was at the time of the start of this exercise the version used for safety analysis and to support the development of PSA level 2 at IRSN. This version presents some limits to describing the BWR geometry. The last version of ASTEC V2.1 rev1 , which was released at the beginning of 2017, overcomes those limitations by proposing new meshing and geometries adapted for canisters and new models such as oxidation in LP or double side oxidation of square canisters. (Chatelard, 2016) Even if IRSN has planned to update the present crosswalk study with the recently released version ASTEC V2.1 rev1, the simulation presented in that report with ASTEC V2.0 rev3 is useful for evaluating the essential differences in modeling of severe accident progression. In the rest of the report and unless explicitly mentioned, ASTEC means the V2.0 rev3 version documented in (Chatelard, 2014).

1.2 Code Description

1.2.1 MELCOR

MELCOR is a fully integrated, engineering-level computer code with the primary purpose of modeling the progression of accidents in light water reactor nuclear power plants. A broad spectrum of severe accident phenomena in both boiling and pressurized water reactors is treated in MELCOR in a unified framework. Uses of MELCOR include estimation accident progressions and the determination of fission product source terms. MELCOR can also be used to evaluate sensitivities and uncertainties of these calculations. (SNL, 2017)

The MELCOR code is composed of an executive driver and a number of major modules, or packages, that together model the major systems of a reactor plant and their generally coupled interactions. Reactor plant systems and their response to off-normal or accident conditions include: (SNL, 2017)

- Thermal-hydraulic response of the primary reactor coolant system, the reactor cavity, the containment, and the confinement buildings
- Core uncovering (loss of coolant), fuel heatup, cladding oxidation, fuel degradation (loss of rod geometry), and core material melting and relocation
- Heatup of reactor vessel lower head from relocated fuel materials and thermal and mechanical loading and failure of the vessel lower head, and transfer of core materials to the reactor vessel cavity
- Core-concrete attack and ensuing aerosol generation
- In-vessel and ex-vessel hydrogen production, transport, and combustion
- Fission product release (aerosol and vapor), transport, and deposition

- Behavior of radioactive aerosols in the reactor containment building, including scrubbing in water pools, and aerosol mechanics in the containment atmosphere such as particle agglomeration and gravitational settling

- Impact of engineered safety features on thermal-hydraulic and radionuclide behavior

The various code packages have been written using a modular structure with interfaces between them. This allows the exchange of information among them so that all phenomena are explicitly coupled at every step.

MELCOR is developed by Sandia National Laboratories under contract to the U.S. NRC. This analysis uses MELCOR 2.1, development build 5864, which is written in modern FORTRAN-95. (Humphries, 2014)

1.2.2 ASTEC

ASTEC covers the entire phenomenology of severe accidents except steam explosion (for which the IRSN uses the MC3D software) and the mechanical integrity of the containment (for which the IRSN uses the CEA CAST3M software package). Its modular structure simplifies qualification by comparing the simulated results with those obtained experimentally. (IRSN, 2017)

Each module simulates the phenomena occurring in one part of the reactor or at one stage of the accident. These include: (IRSN, 2017)

- The two-phase thermal-hydraulics of coolant flows in the reactor coolant primary and secondary systems using a numerical approach based on five equations.

- The degradation of the core geometry as the residual power causes a temperature rise resulting in chemical reactions between the constituent materials and even their melting, up to the formation of a mixture of molten materials named "corium". A dynamic management approach (appearance, disappearance, transformation, relocation) of the various components is used within a control volume of the core.

- The release of fission products (FP), particularly iodine, from fuel in the core, together with their transport and chemical behavior in the reactor coolant system and subsequently within the containment.

- The thermal-hydraulics and transport of aerosols within the containment using a lumped-parameter or 0D volume approach.

- The molten corium-concrete interaction (MCCI) in the reactor cavity following rupture of the reactor vessel, using a 0D volume and layer approach.

ASTEC also simulates other phenomena, associated with the accident, including direct containment heating (DCH) by the transfer of hot gases and corium droplets from the reactor cavity, following the rupture of the vessel; the combustion of hydrogen accumulated within the containment and the associated risk of explosion; and the radioactivity of the isotopes and the associated residual power in all parts of the reactor. (IRSN, 2017)

IRSN intends to implement in ASTEC models that incorporate the latest state-of-the-art knowledge. The models of fission product behavior in particular were reviewed based largely on knowledge derived from the results of the Phébus FP experiments[1]. (Chatelard, 2014)

1.3 Report Scope

This report compares the MELCOR results from the first phase of the MAAP-MELCOR Crosswalk to ASTEC results for the same accident scenario. It is a joint effort of the NRC, SNL and IRSN and covers the conclusions from ongoing discussions of these three organizations. Preliminary results of this analysis were presented at the 2016 Annual Cooperative Severe Accident Research Program (CSARP) and MELCOR Cooperative Assessment Program (MCAP) in order to gain the insight of other international partners and severe accident modeling experts. Additionally, guidance was provided by EPRI while writing this report. (Luxat, 2014)

This report maintains a similar structure to the original crosswalk report; however, instead of presenting plots in the appendices section, they are included in the body of the report to support the conclusions drawn. Where applicable, descriptions of the models taken from the corresponding code manuals are included in the report.

Separate chapters of this report cover:

- Executive summary discussing major conclusions from the report
- Introduction to the problem and codes
- Scenario description, plant models, and analysis methodology
- System response of both the containment and RPV
- Core degradation behavior
- Lower plenum behavior and lower head failure
- Hydrogen behavior, generation, and impact on the system, including safety relief valve response
- Conclusions and planned future work

[1] FP behavior models have been reviewed again in the lights of the OECD programs STEM, BIP and THAI in the ASTEC V2.1 that incorporates the latest state-of-the-art knowledge at the time of this report release.

2 PLANT MODEL, SCENARIO DESCRIPTION AND COMPARISON METHODOLOGY

This chapter details the plant models used in both the MELCOR and ASTEC simulations. Included is the discretization of the plant decks, values of key plant parameters, a description of the accident scenario, and the comparison methodology for the analysis.

2.1 Plant Models

2.1.1 MELCOR

MELCOR discretizes the core region, both axially and radially, into different regions. Within the core these regions are modeled with both control volumes and core nodes. The control volumes are used to represent thermal-hydraulic phenomena, while the core nodes represent the fuel, debris, and structures (control blades, canisters, guide tubes, tie plates, etc.) in the RPV. Both the control volume diagram and the discretization diagram can be seen in Figure 2-1.

Both codes represented the reactor core region using five radial rings. In the MELCOR model, five rings were used for both control volume setup and core cell nodalization. This is considered a best practice when modeling with MELCOR; however, MELCOR can use a higher or lower number of radial rings.

Axially, the MELCOR core cell model uses seventeen levels to represent the full reactor core. Within these core cells, component structures that represent both intact and subsequently degraded structures (including fuel, support structures and control blades) are defined by the user. This spans from the bottom of the lower plenum to the upper tie plate. The bottommost five regions X01 to X05 are in the lower plenum. The core region spans from X06 to X17, with X representing the relevant radial ring. The uppermost region X17 is for the top guide and upper tie plate. The region X06 is used for the lower core plate, lower tie plate, nose pieces and the “Elephant’s Foot.” The ten regions in between represent the active region of the core. As the core degrades, each core region becomes filled with debris, which is characterized as porous particulate debris or a molten debris.

The control volumes employed to model the RPV include one for the shroud dome and one for the lower plenum, as well as five separate axial levels for each axial ring of the core. Each of the five axial levels of control volumes in the active core region has two separate core cells within it. The topmost axial level of these core-region control volumes includes the upper tie plate.

This level of discretization is consistent with the Fukushima models developed by SNL for ongoing Fukushima analysis activities, including BSAF. These models are in turn based off of those developed as part of the State-of-the-Art Reactor Consequence Analysis (SOARCA) for the Peach Bottom Atomic Power Station, which is also a BWR with a Mark-1 containment. (OECD NEA, 2015) (Bixler, 2013)

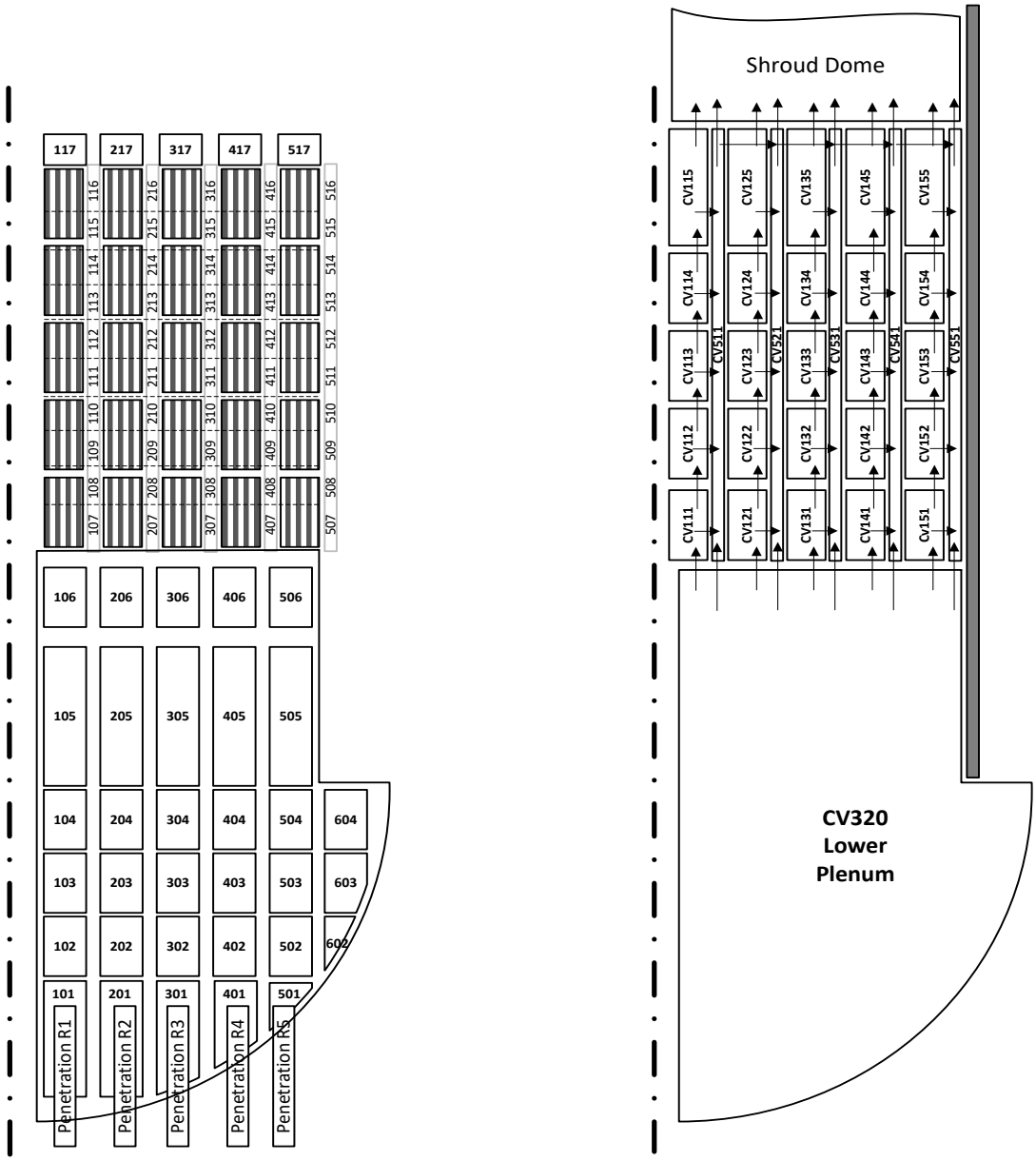

Figure 2-1 Reactor Pressure Vessel Core Cell Nodalization (left) and Control Volume Nodalization (right) used by MELCOR in this Simulation

2.1.2 ASTEC

In contrast to MELCOR, which has a separate discretization for core cells and control volumes, ASTEC uses a two-dimensional axisymmetric Eulerian grid to define a core "mesh." The geometrical space is entirely described by both axial segment and radial rings. The ASTEC plant model was adjusted to also have five radial rings, similar to what is recommended by ASTEC analysts for PWR900MWe (whereas 6 rings are commanded for PWR1300 or EPR®). (Chatelard, 2014)

Axially, ASTEC recommends a mesh height for an active zone of 20 cm. The dome and the steam dryers and separators are not modelled in the core degradation module but as control volume (in which no degradation phenomenon is simulated). As a consequence, the 2D vessel

meshing is limited axially to the top face of upper core plate. A diagram of this discretization can be seen in Figure 2-2. In the diagram, both the control volumes and core structure cells are shown. The difference between how the lower plenum is treated in the two codes is presented. Particularly, the lower plenum region in MELCOR is 2D discretized. Whereas, in ASTEC the "lower plenum" mesh region (homogeneous volume + OD corium/debris layers) extends only to the top of the bottom hemispherical portion. The top part of the lower plenum zone is represented by 2D ASTEC core meshing, which is similar to the active core region. (Chatelard, 2014)

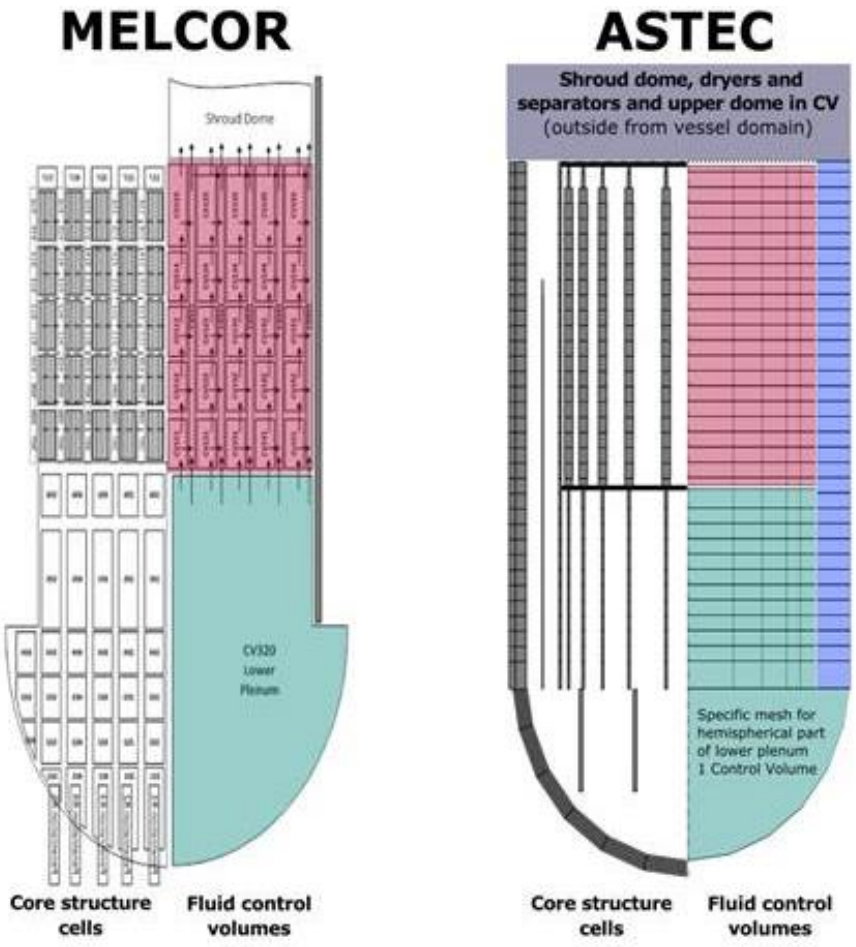

Figure 2-2 Reactor Pressure Vessel Nodalization (Both Fluid Control Volumes and Core Structure Cells) used by Both MELCOR and ASTEC Simulations

Within each mesh, ASTEC allows a user to specify geometric components. These components can include cylindrical structures (UO_2, fuel cladding, etc.), plates (core plate, upper tie plate, etc.), ellipsoidal or hemispherical structures (lower head), and fluid channels. Additionally, as the core degradation progresses, both fuel debris structures and corium are described by a specific field called "magma" component - especially devoted to deal with the 2D movement and relocation of the degraded materials. As fuel and other structures degrade during an accident, they are transferred internally within the code from fuel and structural components to this magma field. An illustration of the content of ASTEC meshes can be seen in Figure 2-3. (Chatelard, 2014)

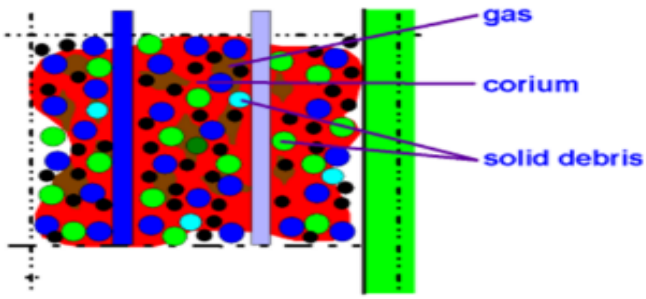

Figure 2-3 Components Inside a Mesh Region during the Fuel Relocation Portion of an Accident Sequence [Note that the solid debris includes structural components (green), fuel material and control blades (blue and gray)]

2.2 Plant Parameters

In order to determine the effect of the different models on the accident scenario, plant parameters were equated to the greatest extent possible. The key plant parameters for both ASTEC and MELCOR are presented in Table 2-1.

Table 2-1 Key Plant Model Parameters

Plant Parameters		MELCOR	ASTEC
Pressure Vessel	Total RPV water inventory (kg)	131,400	150,297[1]
Core Region	Number of fuel assemblies (#)	400	400
	Number of control blades (#)	97	97
	Mass of UO_2 (kg)	77,200	77,230
	Mass of active region Zircaloy cladding (kg)	16,799	16,799
	Mass of upper core, non-active region Zircaloy cladding (kg)	2,850	1,378[2]
	Mass of lower core, non-active region Zircaloy cladding (kg)	0	0
	Mass of Zircaloy in fuel canister (kg)	11,451	11,411
	Mass of stainless steel in control blades (kg)	9,000	9,000
	Mass of B_4C (kg)	540	540
	Mass of stainless steel in top guide tube and upper tie plate (kg)	4,420	3,727[3]
	Mass of stainless steel in core support plate and “elephants foot” (kg)	8,880	8,900
Lower Plenum Region	Mass of lower plenum structures (kg)	25,467	25,000
	Radius of lower plenum hemisphere (m)	2.4	2.4
	Height from lower head bottom to core support plate (m)	4.594	4.91[4]
	Height from lower head bottom to bottom of jet pumps (m)	2.4	2.25[4]
	Thickness of lower head (m)	0.205	0.205

[1] Modified to give the proper water inventory when all feedwater systems are lost at time of the tsunami.
[2] The value we used was obtained by assuming a 30 cm height of the cladding above the active region.
[3] Assuming a 6 cm height of the top guide and 97 holes with a diameter of 20 cm. The height of 6 cm is the height remaining if we have 3.66 cm of active region, 30 cm of non-active region, and a nozzle with 22.2 cm height.
[4] The height from the lower head bottom to the core support plate deviates because the MELCOR value is taken from the Peach Bottom SOARCA best practices, whereas the ASTEC value is based on Fukushima-specific numbers. Since the crosswalk calculations, the MELCOR numbers have been modified to better reflect Fuksuhima-specific numbers.

It can be seen that the majority of the inputs and boundary conditions are the same in the ASTEC model as in the MELCOR model used in the original MAAP-MELCOR crosswalk. Distinct differences can be seen in the RPV water inventory, the mass of upper core Zircaloy cladding, mass of stainless steel in top guide tube and upper tie plate, and the heights of the core support and jet pumps from the lower bottom head. Differences between in-core structural masses can be explained by the differences between the two codes in how the core region is defined.

It should be noted that the MELCOR water inventory additionally does not include water above top of active fuel (TAF) in the calculation of water mass in the core region. MELCOR and ASTEC employ different two-phase fluid models, which leads to different steady-state conditions and void fractions within the core, and therefore different masses of liquid water in the RPV.

The decay heat curve used in this analysis is shown in Figure 2-4. The decay power uses a Fukushima Unit 1 inventory developed by SNL. This decay heat curve was then used for both the ASTEC and MELCOR analyses. It can be seen that the decay power relation used by the codes in this analysis corresponds to the decay power approximations published by the Tokyo Electric Power Company (TEPCO), the owners of the Fukushima Daiichi site. (Cardoni, 2014)

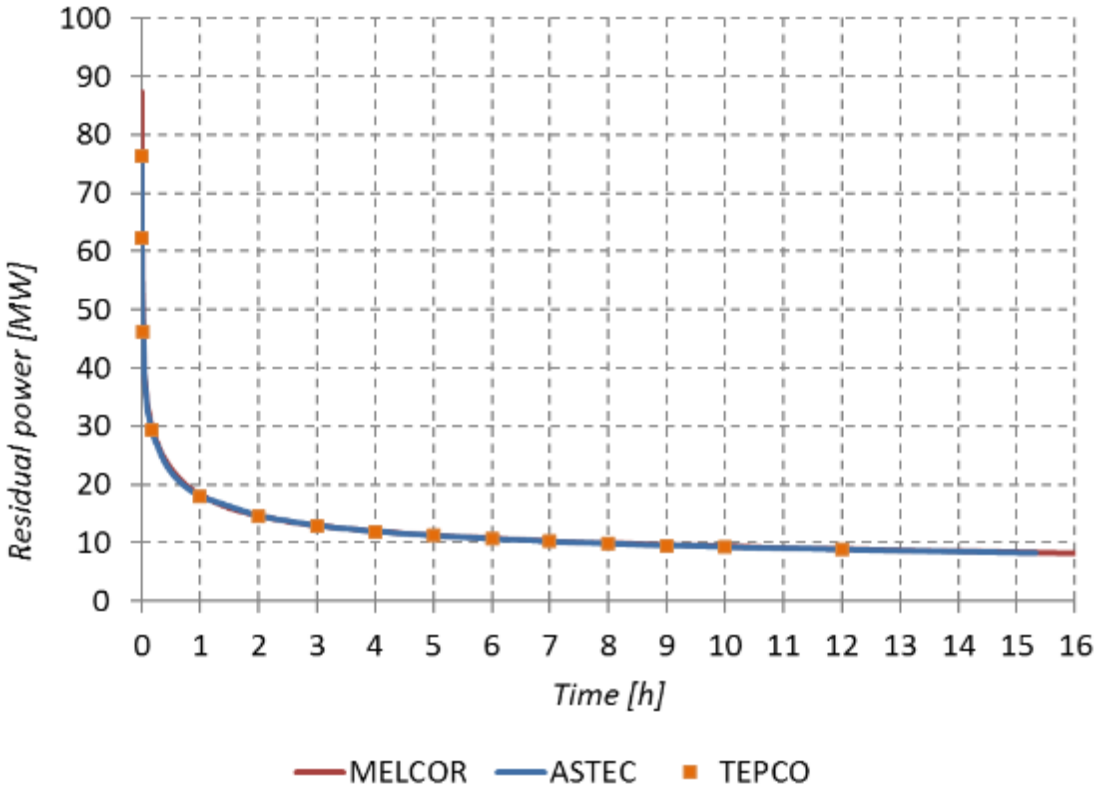

Figure 2-4 Decay Heat Curve Used by ASTEC and MELCOR, with TEPCO Approximation (Cardoni, 2014)

2.3 Accident Scenario

The accident scenario developed by EPRI and SNL for this analysis is stylized after accident progression of Fukushima Daiichi Unit 1. However, this accident scenario is for the purpose of code comparison and not for Fukushima Daiichi forensic efforts. The behaviors of key systems in the plant are summarized in Table 2-2. The behaviors of the main steam line isolation valve, control rod drive mechanism, feedwater system, safety relief valve and isolation condenser were made consistent between the two codes. This ensures that the differences in system behavior during the accident sequence originate from the differing in-core phenomenological treatment of the two codes. The MELCOR simulation was run to 16 hours, while the ASTEC simulation was run to 15.6 hours (time of lower head failure). Ex-vessel behavior was not examined in this analysis.

Table 2-2 Behavior of Key Systems in Simulated Fukushima Accident Scenario (Luxat, 2014)

System	Behavior
Main Steam Line Isolation Valve (MSIV)	MSIV closure signal at 52.5 s after SCRAM
	MSIV open area reducing from fully open to fully closed over a 3 s interval from the time of the closure signal
Control Rod Drive (CRD)	At reactor scram it is assumed that the CRD injection flow ceases
Feedwater System	The feedwater system is assumed to inject for the first 60 s following the initiating event
	The feedwater injection transient is an imposed boundary condition - the detailed injection transient can be seen in Figure 2-5
	The specific enthalpy of feedwater is assumed to be 792 kJ/kg
Safety Relief Valve (SRV)	SRV seizure is assumed to occur at 7 hours after SCRAM
	All discharge through the seized SRV is assumed to go into the suppression pool
Isolation Condenser (IC)	IC heat removal is assumed to be constant with pressure at 42.4 MW per train
	The periods of IC operation are shown in Table 2-3

The cumulative feedwater flow into the RPV is given in Figure 2-5. This value was held constant between the two analyses. Both MELCOR and ASTEC also used the same isolation condenser operation periods, which are shown in Table 2-3.

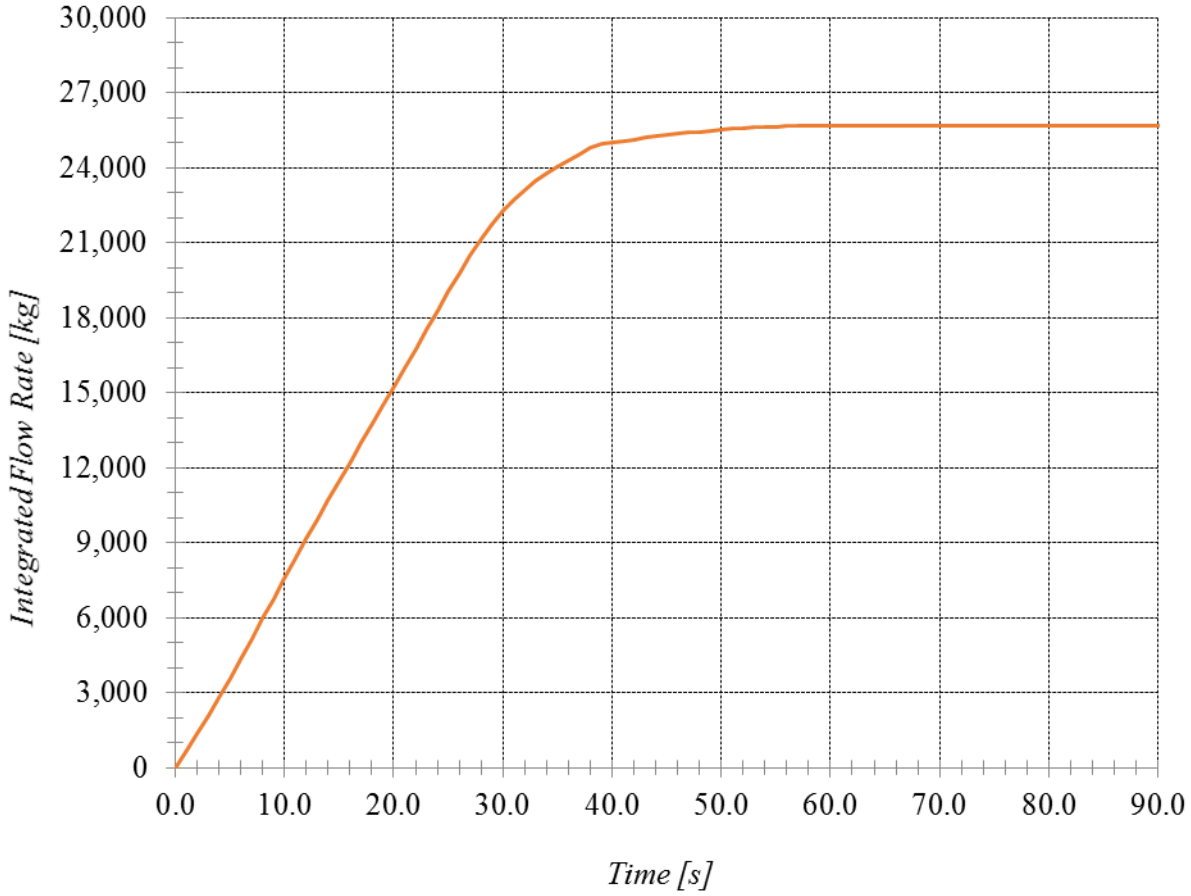

Figure 2-5 Cumulative Feedwater Flow into the RPV (Luxat, 2014)

Table 2-3 Isolation Condenser Operation Parameters

Time Isolation Condenser Operation Starts (s)	Time Isolation Condenser Operation Ceases (s)	Number of IC Trains Operating (#)
360	400	2
1,860	1,980	1
2,280	2,400	1
2,760	2,880	1

2.4 Comparison Methodology

The behavior of the codes as they progress through the prescribed accident sequence is evaluated according to event timings and simulated behavior. Key areas addressed are the system response behavior, core degradation and relocation behavior, debris slumping to lower plenum, debris behavior in lower plenum, and lower head breach mechanisms. The comparisons of the code prediction in these four key areas are then compared between MELCOR and ASTEC. Divergent behavior between the two codes is then evaluated and attributed to the relevant physical model(s) for each of these event timings and behaviors in the "Conclusions" section of this report.

The full list of relevant parameters compared is summarized in this section. It is believed that this list covers relevant behavior for this accident scenario, which can be compared between the MELCOR and ASTEC codes. A more in-depth discussion of the rationale for the inclusion of each of these parameters in this study can be found in the MAAP-MELCOR crosswalk report (Luxat, 2014).

Comparisons are also fitted to the capabilities, models and features of each code. For instance, ASTEC treats fuel debris in a single "magma" field, which contains both particulate and molten debris. On the other hand, MELCOR has separate fields for both particulate and molten debris. There is therefore not a completely equivalent comparison of particulate debris mass in both ASTEC and MELCOR, an analysis that was of key importance in the MAAP-MELCOR crosswalk. (Luxat, 2014) (Chatelard, 2014)

Key event timings:

- Core oxidation onset
- Core melting commencement
- First failure of fuel assemblies due to loss of structural integrity
- Relocation of core materials to the lower plenum
- Formation of molten debris pools in the lower plenum
- Initial RPV lower head breach
- Gross relocation of core debris into containment

System response behavior:

- RPV pressure
- RPV water level
- RPV water mass
- Energy removal by isolation condenser

- Mass and energy flow rate of steam through MSL
- Mass and energy flow rate of steam through the SRV
- Integrated mass and energy flow of steam through the SRV
- Flow rate of hydrogen through the SRV
- Integrated mass and energy flow of hydrogen through the SRV
- The flow rate of high temperature steam and hydrogen through a failure site in the RPV pressure boundary to the containment

Core degradation and relocation behavior:

- Core oxidation behavior
  - Peak cladding/core temperature
  - In-vessel mass of hydrogen generated
- Core melting behavior
  - Debris formation transient
  - Initial onset of loss of core structure integrity
  - Fuel cladding failure and degradation
  - Fuel assembly failure and degradation
- Core plate failure
  - Melt flow through the core plate
  - Challenge to core plate integrity, both thermal and mechanical

Debris slumping to lower plenum:

- Total mass of core debris within core region
- Mass of water in lower plenum
- Cumulative fraction of core debris that slumps into the lower plenum
- Core debris relocation mode into the lower plenum
- Criteria triggering relocation of core debris into the lower plenum
- Temperature of core debris slumping into the lower plenum
- Rate of core debris slumping into the lower plenum
- Distribution of debris between molten material and particulate material in the lower plenum

Debris behavior in lower plenum and lower head breach:

- Total mass of debris in lower plenum
- Temperature of lower head wall
- The timing of RPV lower head breach
- The mode of RPV lower head breach, which includes the various ways in which the lower head penetrations could result in a failure site of the lower head
- The RPV lower head temperature transient
- The fraction of core debris that relocates out of the RPV into containment
- The temperature of the debris relocating from the RPV into containment

3 PLANT AND SYSTEM-LEVEL RESPONSE

This chapter discusses the bulk system response predicted by MELCOR and ASTEC. Generally speaking, the bulk system response encompasses the thermal-hydraulic response to mass and heat transfer from core degradation. In particular, different fission product, core degradation, and core relocation behaviors in MELCOR and ASTEC heavily influence simulation predictions between both codes. The surviving core geometry also influences the system response to some extent. For the purposes of this chapter, the system response includes the RPV pressure, the RPV steam dome temperature, the RPV water level, the isolation cooler (IC) heat removal, containment pressure, and wetwell temperature.

The timings of key system level events are shown in Table 3-1. Good agreement between the two codes can be seen in the timings of boildown until the point TAF is reached. Afterwards, the boildown proceeds slightly faster in ASTEC; this leads to the onset of hydrogen generation occurring slightly sooner.

Concerning fuel rod/assembly behavior, the collapse of fuel rods in ring 1 simulated by MELCOR occurs 1.5 hours after the onset of melting of those rods simulated in ASTEC. Moreover, one can notice that within less than 1.0 hour, melting of fuel occurs in all the core rings in the ASTEC simulation, whereas no collapse is observed in the MELCOR simulation. One key difference highlighted by that table is the treatment of fuel rod loss of integrity.

MELCOR uses a time-at-temperature lifetime criterion that triggers the collapse of fuel assemblies, which instantaneously forms particulate debris. The portions of the fuel assemblies above the failed assembly portion are also assumed to collapse. In contrast, ASTEC simulates a progressive melting according to the temperature of the fuel rods in each mesh. Then ASTEC simulates a production of debris that is more continuous without a threshold or drastic change in geometry (induced by collapse for instance). The failure of the core plate occurs gradually in MELCOR beginning at 5.1 hours into the scenario, whereas in ASTEC the melting of this component occurred later in the transient when more debris had built up on top. (Humphries, 2014) (Chatelard, 2014)

The BWR core plate model in MELCOR is supported by beams and is loaded only by its own weight and that of debris on it. Although it does not bear the weight of the fuel and canisters, the presence of the plate is required for lateral stability of the control blade drive tubes and to force flow from the lower plenum region into the individually-orificed fuel assemblies and to provide some bypass flow to the fuel canister interstitial region. Fuel assemblies are supported by the control blade drive tubes and the fuel support piece (elephants foot) and this weight is transferred to the lower vessel head where the drive tubes are welded to the vessel. Any singular ring is not dependent on support from adjacent radial rings, or in any other core cell. When the plate fails in any ring, it loses the ability to support particulate debris that has fallen into the interstitial space between fuel canisters, which will then fall, but adjacent plate portions will remain in place until they fail. (Humphries, 2014)

Table 3-1 Timings of Key Events in the Simulated Accident Scenario

Accident Progression Event	MELCOR Timing		ASTEC Timing
Core water level at TAF	2.7 h		2.6 h
Core water level at 2/3 TAF	3.0 h		2.8 h
Core water level at 1/3 TAF	3.3 h		3.1 h
Onset of in-vessel hydrogen generation	3.6 h		3.4 h
Initial fuel assembly loss of integrity in Ring 1 (collapse for MELCOR, T_{fuel}>2550K for ASTEC)	5.0 h		3.6 h
Initial fuel assembly loss of integrity in Ring 2 (collapse for MELCOR, T_{fuel}>2550K for ASTEC)	8.4 h		3.7 h
Initial fuel assembly loss of integrity in Ring 3 (collapse for MELCOR, T_{fuel}>2550K for ASTEC)	9.0 h		3,7 h
Initial fuel assembly loss of integrity in Ring 4 (collapse for MELCOR, T_{fuel}>2550K for ASTEC)	no collapse		3.9 h
Initial fuel assembly loss of integrity in Ring 5 (collapse for MELCOR, T_{fuel}>2550K for ASTEC)	no collapse		4.4 h
Initial core plate failure (melting for ASTEC)	5.1 h		6.0 h
Lower plenum dryout, absence of liquid water in the lower plenum	10.4 h		8.9 h
Initial RPV lower head breach	14.4 h		15.6 h

3.1 Energy Balance

The two major sources of energy in a core undergoing a severe accident are decay heat and oxidation energy. Initially, severe reactor accidents are driven by the decay heat from fission products inside the fuel. As an accident progresses, fuel uncovery and high core temperatures (>1200 K) lead to the oxidation of metals in the core such as Zircaloy and stainless steel. Oxidation of Zircaloy is an intense exothermic process that, under runaway conditions, can surpass the energy from decay heat.

Typical heat transfer processes make up the energy sinks in the core. Convective heat transfer accounts for the majority of heat removal from the fuel. When the core uncovers, boiling removes heat from the core. After core uncovery, the steam generated in the lower plenum crosses the heated core and still removes some heat by gas phase convection. After the core boils down, eventually that cooling is not sufficient to prevent core heatup and degradation. Convection can also occur in the lower plenum as the falling debris (solid or molten) from core collapse is quenched in whatever pool remains during the accident progression.

Radiative heat transfer is the second heat removal process. As the name implies, radiative heat transfer occurs when heat from the core material radiates to boundary structures in the core (e.g., the upper tie plate). Both convective and radiative heat transfer are directly proportional to

their heat transfer surface areas. As such, fuel and debris configuration and flow channel integrity can largely affect the rate of heat transfer from core materials. This introduces some uncertainty, as core collapse patterns can differ significantly on a code-to-code basis.

A comparison of the system energy balances for both MELCOR and ASTEC is shown in Figure 3-1. It can be seen as the accident progresses that the amount of heat removal from convective heat transfer is higher in MELCOR than in ASTEC after the point of initial cladding oxidation. Prior to this point nearly all decay heat was removed via convective heat transfer, which includes steam cooling. ASTEC has more radiative heat loss compared to MELCOR for the first ten hours of the transient; however, after ten hours this trend reverses. At 9.0 hours, the core relocates to the lower plenum in the ASTEC simulation; within the lower plenum radiative heat transfer is not treated. Total oxidation energy in both codes is similar, with MELCOR showing slightly more oxidation than ASTEC. This difference may be due to the treatment of the oxidation of the mixture (U, O, Zr) in the ASTEC code and the associated difference in chemical reaction power. The majority of oxidation occurs sooner in ASTEC than in MELCOR.

The MELCOR simulation has both more convective and radiative heat transfer out of the degraded core and core debris. Additionally, the total amount of stored energy in the MELCOR core debris is less than that predicted by ASTEC. It is likely that these differences are due to how the two codes treat the core degradation process. ASTEC predicts a molten pool with a crust that reduces the total flow area through the core, limiting convective heat transfer, whereas MELCOR predicts the generation of a significant amount of particulate debris with a higher porosity and surface area.

The higher stored energy in the ASTEC simulation indicates that the pour of the fuel debris out of the RPV predicted will be at a higher temperature and consequently less viscous. Additionally, in the ASTEC simulation, at the point of RPV failure, nearly all of the debris relocates ex-vessel, taking the stored energy with it whereas a significant amount of debris, and thus stored energy, remains in the RPV in the MELCOR simulation.

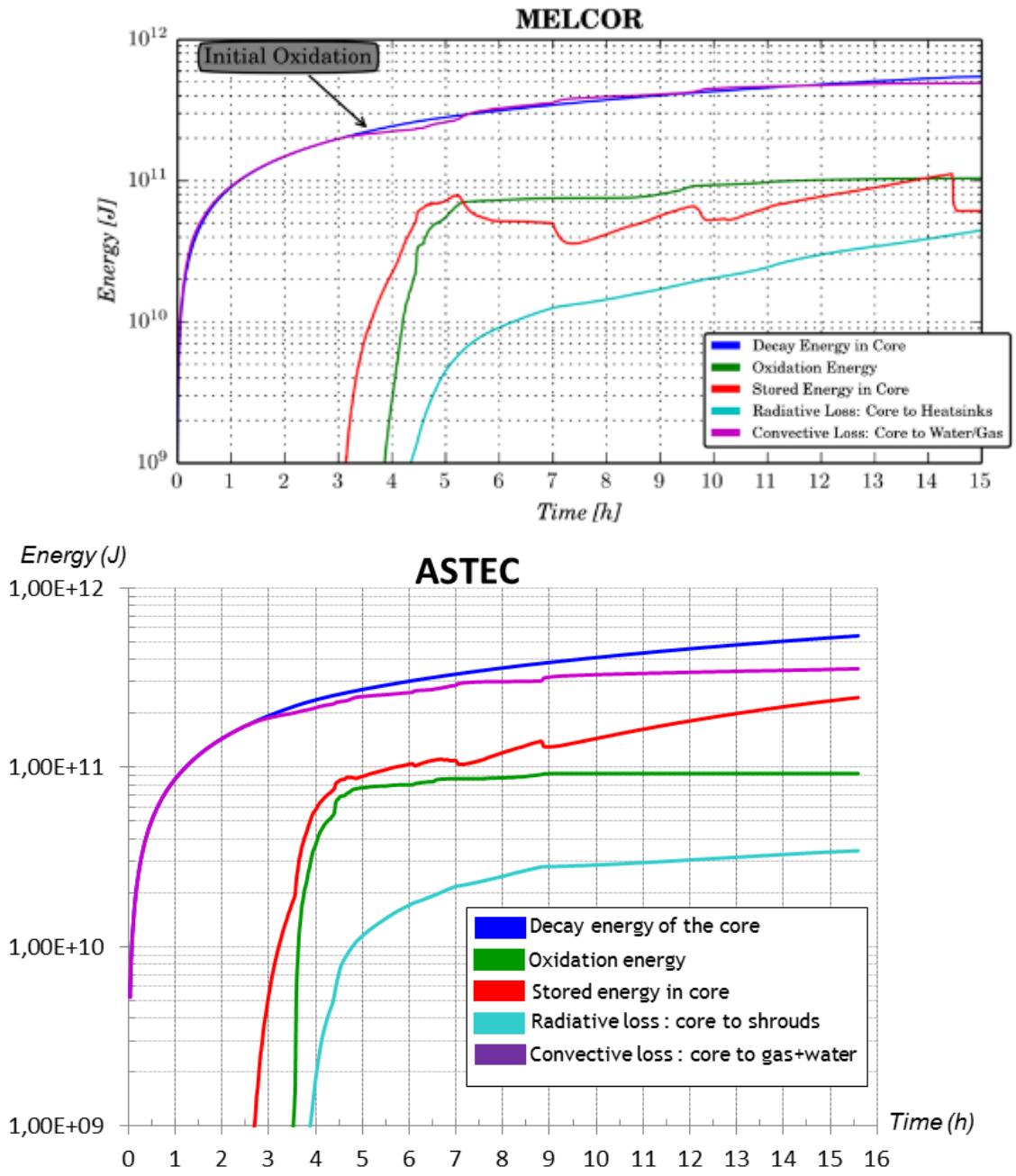

Figure 3-1 Comparison of System Energy Balance, Showing Both Energy Sources and Sinks

3.2 RPV Pressure

During IC operation both codes are in close agreement. First, there is an initial depressurization as 84.4 MW of decay heat is removed by the isolation condenser. Then the RPV re-pressurizes to the SRV setpoint of 7.75 MPa at 1 hour after the start of the accident. Steam generation in the core results in RPV pressurization to the SRV setpoint. Once RPV pressure reaches the

SRV setpoint, the SRV cycles, releasing coolant to the wetwell. Figure 3-2 shows a comparison of the RPV pressure transients between MELCOR and ASTEC.

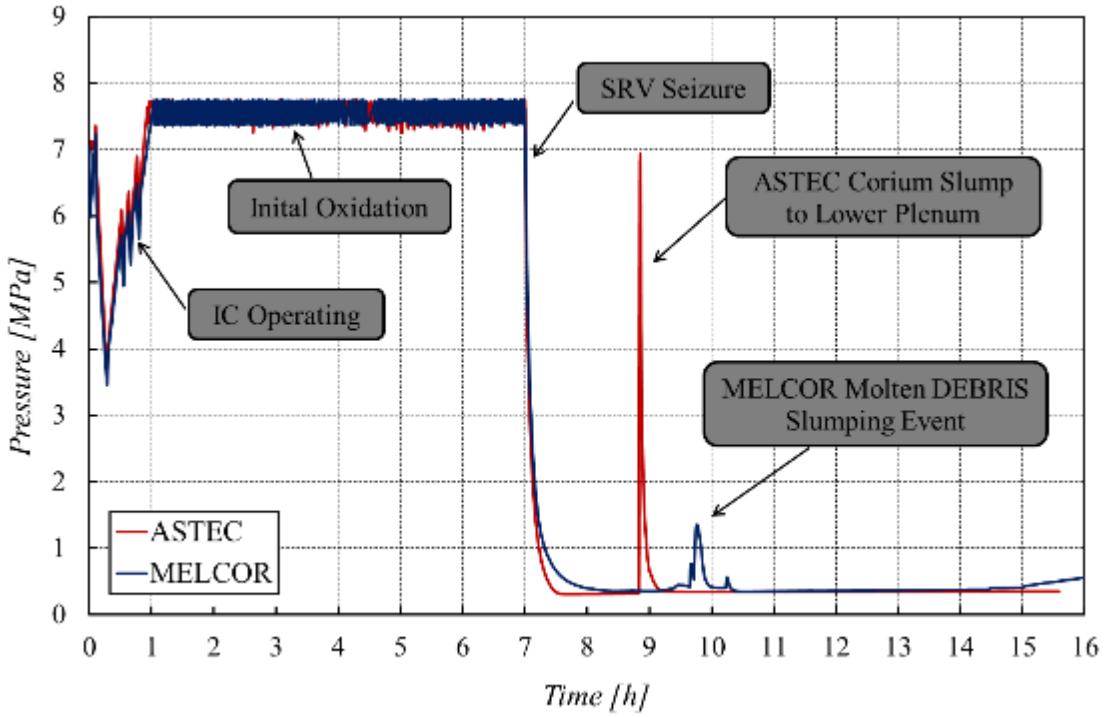

Figure 3-2 RPV Pressure Transients for the ASTEC and MELCOR Simulations

After 7 hours into each simulation, the SRV seizes, resulting in a rapid depressurization of the RPV. While both codes calculate a post-seizure pressure of 0.34 MPa, MELCOR calculates a relatively gradual decrease in pressure where the final pressure is reached an hour after the SRV seizure. ASTEC calculates a sharp drop in pressure over 0.25 hours. The difference in depressurization rates may be tied to a steam flow rate out of the SRV immediately after failure, with ASTEC predicting more steam discharge than MELCOR.

After SRV seizure, both codes experience pressure transients as debris slumps to a pool in the lower plenum. ASTEC simulates a pressures spike to nearly a 7.0 MPa surge at 8.8 hours lasting 0.3 hours. However, the core does not slump in MELCOR until 9.3 hours, and, when the slumping event occurs, MELCOR simulates a slower developing pressure transient lasting 1.1 hours with individual peaks of 0.74, 1.30, and 0.56 MPa. It is likely that the slumping transients are governed by how each code simulates core support plate failure.

In MELCOR, the core support structures may fail individually. For example, the innermost radial support structures may fail, resulting in a core slump, but some material may be left in the outer support structures. If the outer portion of the core support plate fails, this would lead to another large slumping event. The ASTEC core plate failure is based on a material melting model. The first melting of the center of the core plate occurs at 6.0 hours. After the failure of the core plate, the molten pool in ASTEC gradually progresses downwards, refreezing on support structures and then melting once again. The lower plenum is reached at 8.8 hours, causing a large spike in RPV pressure.

3.3 Steam Dome Temperature

The steam dome temperature transients predicted in each simulation are shown in Figure 3-3. Generally, both codes predict an increase in steam dome temperature followed by a temperature decrease when the SRV seizes. A second steam dome temperature decease occurs as the core slumps. ASTEC predicts a larger increase in the steam dome temperature after relocation to the lower plenum compared to MELCOR. This increase is gradual and smooth, as nearly all debris relocates to the lower plenum when the core plate fails in ASTEC. The decreases in steam dome temperature in the final eight hours correspond to fuel collapse and subsequent debris quenching in the lower plenum. The decreases in temperature are due to the rapid release of saturated steam due to the slumping events. It drives the RPV conditions back towards the saturation curve.

Until the onset of core uncovery at approximately 2.6 hours for ASTEC and 2.7 hours for MELCOR, both codes show nearly identical temperature predictions.

As the fuel begins to uncover in the MELCOR simulation, the steam dome temperature begins to increase linearly as the fuel temperature increases from decay heat deposition. Then, as fuel begins to degrade, oxidation releases energy into the core, increasing the steam dome temperature exponentially.

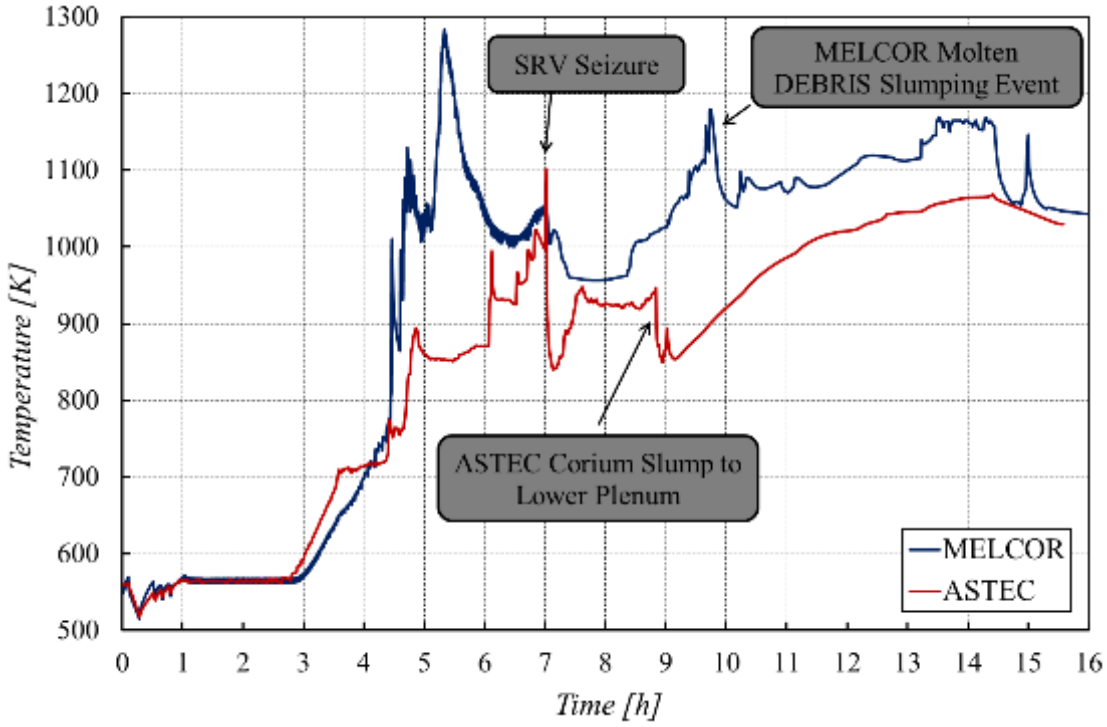

Figure 3-3 Comparison of the Steam Dome Temperature Transients in MELCOR and ASTEC

As core uncovery begins in ASTEC, the temperature linearly increases until a brief transient occurs at 2.9 hours, likely caused by energy release from the onset of oxidation. Unlike MELCOR, ASTEC predicts gradual increases and plateaus in the steam dome temperature as seen from 3.3 hours to 4.4 hours and 5.2 hours to 6 hours. These plateaus align with reduced

SRV cycling frequencies, resulting from less convective heat transfer, which could be a result of increased radiative heat transfer or reduced heat transfer area (e.g., from blockage). The drop in convective heat transfer in the ASTEC simulation results in a smaller steam generation and consequently less steam superheating. MELCOR allows significant steam flow through its particulate debris, which results in more convective heat transfer and leads to higher steam dome temperatures.

After each code's slumping event, steam dome temperature increases are predicted in MELCOR and ASTEC. ASTEC predicts a steady increase with minor fluctuations beginning at 12 hours. MELCOR's predictions are in sharp contrast to ASTEC. MELCOR predicts a general increase, but not at a steady rate. In ASTEC, the entire core collapsed, but in MELCOR, a significant portion of the core survived in the outer rings. See Figure 4-12 for an illustration of the status of the core and intact fuel after 8 hours. The variations in the steam dome temperature increase in MELCOR could be from oxidation and relocation of fuel material in the outer rings. The steam dome temperature in MELCOR drops after the failure of the lower head at 14.4 hours.

3.4 Core Water Level

The water levels for the MELCOR core and downcomer, as well as the ASTEC core, are shown in Figure 3-4. The water level for both codes increases as the IC operates until its shutdown at 1 hour. After IC operation ceases at 1.0 hours, both codes predict similar decreases in the RPV water level as water is boiled and released to the wetwell by the SRV. Core uncovery begins at approximately 2.6 hours and 2.7 hours for ASTEC and MELCOR respectively.

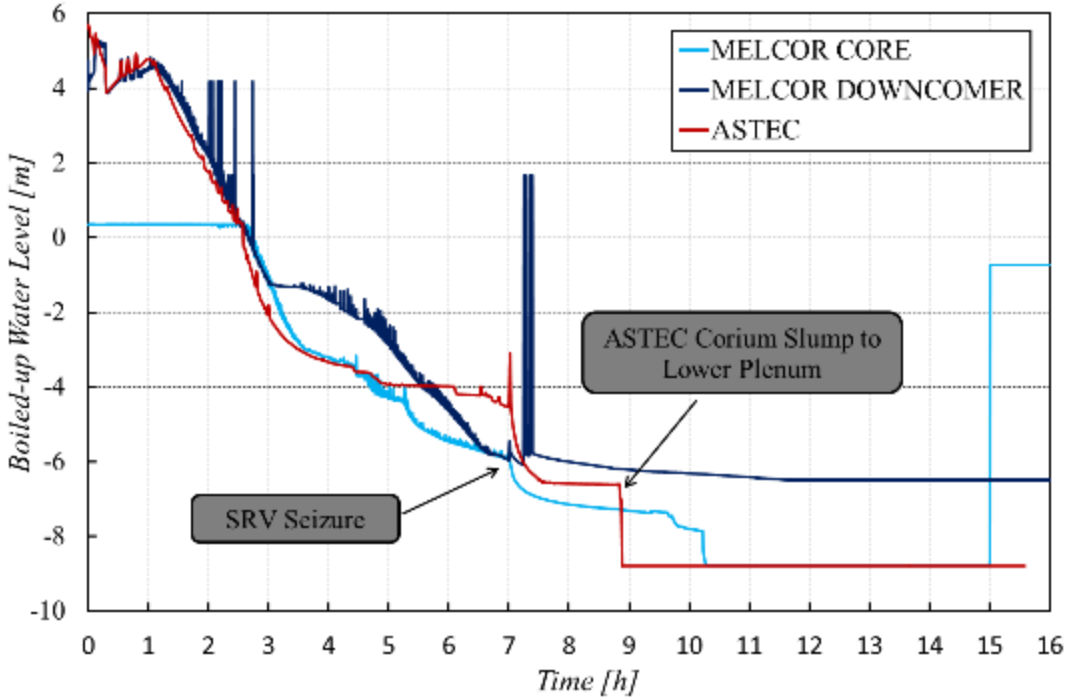

Figure 3-4 The MELCOR Core, MELCOR Downcomer, and ASTEC Core Water Level Transients

At 2.6 hours, both codes begin to model a decrease in the rate of water boiloff. This decrease in the rate is because of the contribution of steam cooling to convective heat transfer from the core. The water level decreases more slowly in MELCOR than in ASTEC. This difference is

likely attributable to the thermal hydraulic boiling models found within the two codes. The divergence in the RPV and downcomer water levels at 3.0 hours in MELCOR is from the RPV water level falling below the jet pumps.

Small fluctuations occur in the MELCOR downcomer and core water levels that are not seen in the ASTEC simulation. These fluctuations are likely to be an artifact of the numerical solution algorithm within MELCOR. ASTEC does not simulate debris formation except when a molten corium jet encounters water. In ASTEC simulation, the interaction between water and molten corium jet leads to debris formation in LP represented as 0D debris bed composed of spherical particles. It is important to underline that particulate debris beds are represented only in LP and not in the active core region. In contrast, MELCOR does simulate debris formation during fuel collapse. ASTEC does not employ a fuel failure model, but instead applies a continuum approach, which is discussed more in-depth in Chapter 5.

Both codes predict a rapid drop in water level at 7.0 hours as coolant flashes as a result of the drop in the system pressure. In both codes, the core water level consistently decreases as the corium relocates to the lower plenum. A key point of interest is that MELCOR predicts lower plenum dryout at 10.4 hours, whereas ASTEC predicts this at 8.9 hours, at the point when the corium relocates to the lower plenum.

3.5 Isolation Condenser Response

During the first hour of the accident, operators cycled IC operation to prevent the RPV pressure from reaching the SRV setpoint by cycling the IC and to limit the RPV cooldown rate to less than 100 °F/h. Because the IC behavior is a fixed boundary condition, both codes simulate identical heat removal behavior. This behavior can be seen in Figure 3-5.

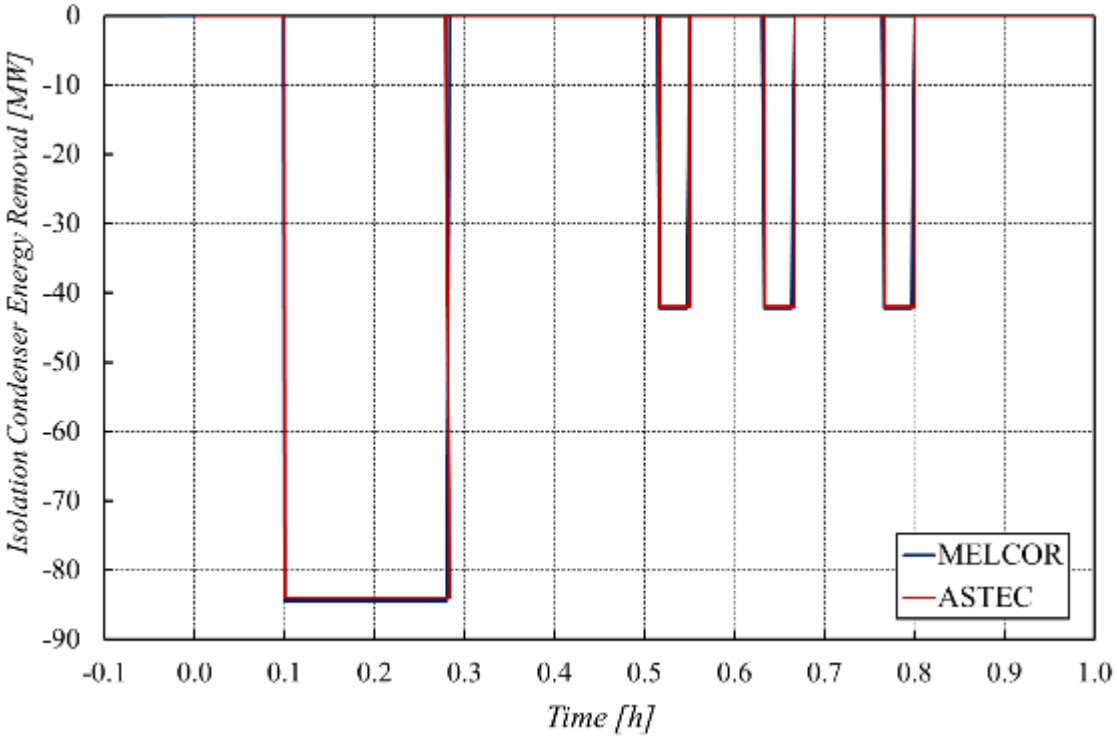

Figure 3-5 The Isolation Condenser Energy Removal

3.6 Containment Pressure

The containment pressure response can be seen in Figure 3-6; shown is the wetwell, drywell, and RPV pressure. Generally, both codes predict a pressure increase from 0.1 MPa to near 0.35 MPa at the point of vessel failure. During IC operation and periods of SRV discharge, both codes simulate a gradual increase in containment pressure as steam from the RPV condenses in the suppression pool. Both codes see a marked increase in pressure when runaway oxidation begins to occur in the core at near 4 hours in the simulations. This hydrogen then is discharged through the SRV, pressurizing the wetwell. Generally, ASTEC predicts a slightly higher containment pressure until just after the corium slump to the lower plenum. A small spike in the containment pressure is seen at this point from debris quenching and subsequent coolant evaporation. At this point hydrogen generation in ASTEC essentially stops, as does convective energy transfer from fuel debris.

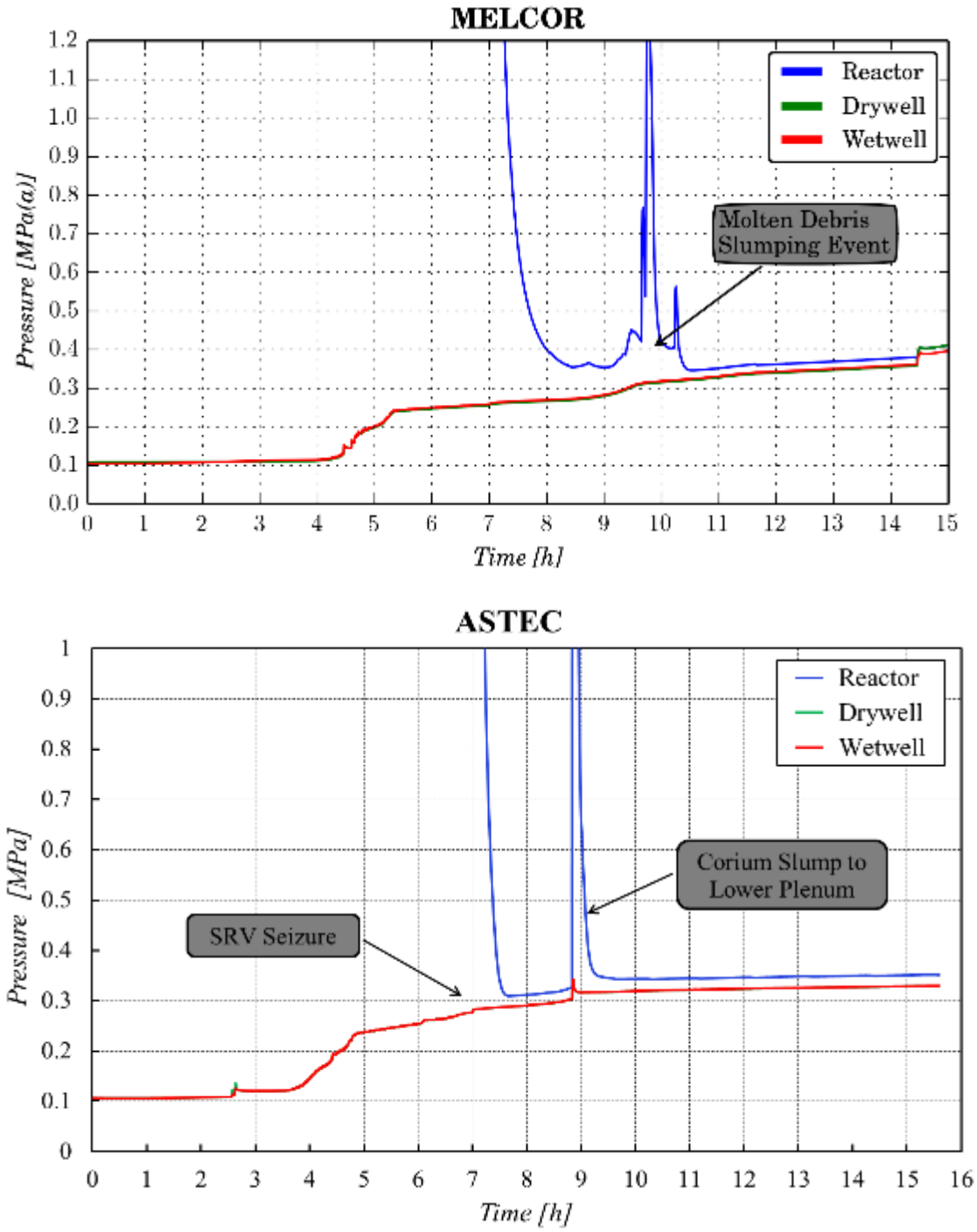

Figure 3-6 Containment Pressure Transient Plotted against RPV Pressure Transient

3.7 Wetwell Temperature

MELCOR and ASTEC wetwell water temperature and saturation temperature transients are shown in Figure 3-7. Both codes are in very close agreement until the energy removal rate from convective heat transfer begins to decrease in the ASTEC simulation near 5 hours into the scenario. Upon SRV seizure, ASTEC calculates a temperature increase of about 10 K, whereas MELCOR calculates a slightly higher temperature increase of approximately 13 K. Greater convective heat transfer from the degraded core in MELCOR could be responsible for the slightly higher wetwell temperature. MELCOR also consistently predicts a higher steam dome temperature, which is in line with this assertion. Additionally, this steam is vented to the wetwell by the SRV, so the temperature discrepancy is reasonable given the predicted steam dome temperature differences.

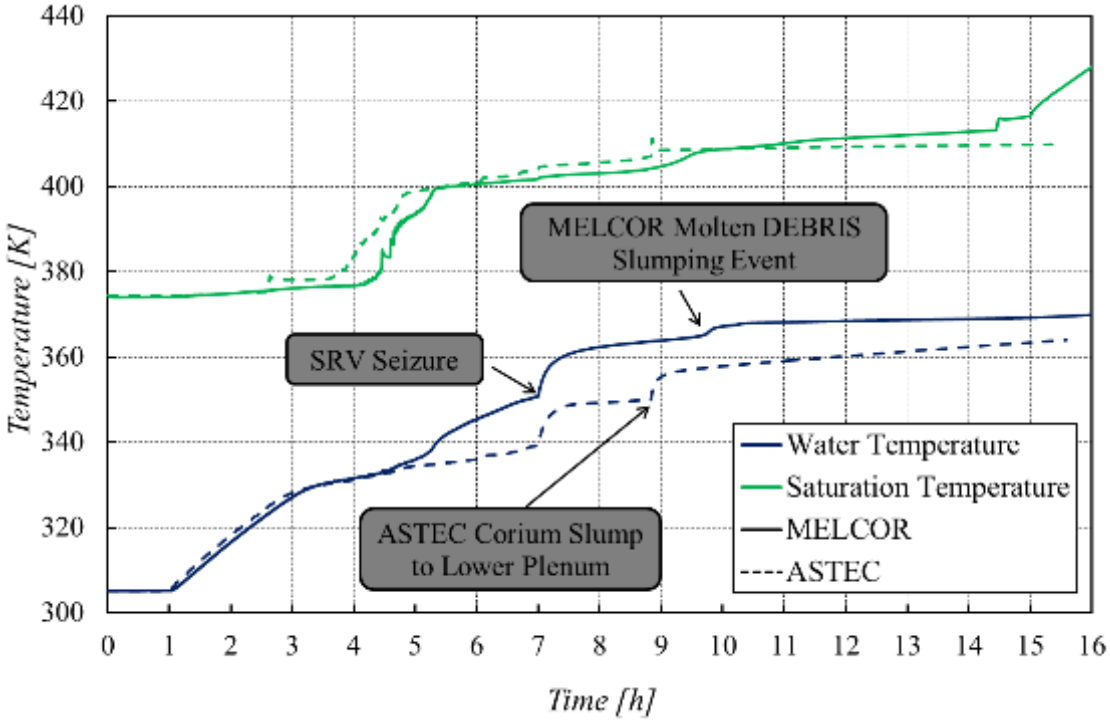

Figure 3-7 Wetwell Water and Saturation Temperature Transients

4 CORE DEGRADATION BEHAVIOR

This chapter provides a brief overview of the core degradation models for MELCOR and ASTEC. This brief description frames a presentation of the core degradation results for the stylized Fukushima Daiichi Unit 1 simulation presented in this paper. Oxidation phenomena, which are of key importance in modeling core degradation, are for the purpose of clarity presented only once in this report and are contained in the "Hydrogen and SRV Behavior Chapter."

4.1 Overview of MELCOR Core Component Degradation Representation and Models

A description of the most relevant MELCOR models and the codes overall view of core degradation and relocation are presented in this section. The majority of this information is taken from phenomenological descriptions found in the "Modular Accident Analysis Program (MAAP) – MELCOR Crosswalk: Phase I Study," and the "MELCOR Computer Code Manuals, Vol. 2: Reference Manual, Version 2.1.6840." A more complete description of each specific model is presented in this MELCOR manual. (Luxat, 2014) (Humphries, 2014)

4.1.1 MELCOR Degraded Core Components and Morphologies

MELCOR represents the core region in terms of both control volumes and core cells. A complete description of the plant model implemented can be found in Section 2.1. Within the core region, MELCOR models both core materials and components, similarly to ASTEC. The core cell materials are UO_2, Zicaloy, stainless steel, ZrO_2, stainless steel oxide, and B_4C. Each core cell is additionally portioned between the following components: (Humphries, 2014)

- Intact core components
    - Fuel
    - Fuel cladding
    - Fuel canister - portion not adjacent to control blade
    - Fuel canister - portion adjacent to control blade

- Particulate debris that results from the collapse of fuel rods or other core components
    - Inside the fuel channels
    - Inside the fuel channel bypass regions

- Structural components
    - Supporting - A structure that is capable of supporting components of the core (e.g., core plate)
    - Non-supporting - A structure that cannot support other core structures (e.g., a control blade)

- Oxide molten pool
    - Inside the fuel channel region
    - Inside the fuel channel bypass region

- Metallic molten pool
    - Inside the fuel channel region
    - Inside the fuel channel bypass region

MELCOR considers an additional field, which is termed conglomerate debris. This represents previous molten debris that has refrozen on an intact core structure. It is treated as part of the intact core structure on which it has solidified. (Humphries, 2014)

Particulate debris is formed from the failure of the embrittled core structures. MELCOR assumes that this can occur for fuel rods when:

- Fuel rods persist at elevated temperatures for such an extended period of time that creep failure would be likely.

- The fuel cladding metal thickness is reduced below a critical thickness by the effects of oxidation and melt erosion.

Non-fuel rod structures are assumed to collapse into a particulate debris bed when the remaining metal thickness (either Zircaloy or stainless steel) decreases below a critical thickness. As in the case of fuel cladding, the loss of metal thickness can occur due to oxidation and melt erosion.

For both fuel and non-fuel structures, the failure of a supporting structure will result in the supported structure collapsing into a particulate debris bed. Particulate debris in MELCOR is treated differently depending on whether or not it is located in channels or core bypasses, with different diameters and characteristics. (Humphries, 2014)

Debris that solidifies on failed solid debris forms part of the particulate debris bed. This has the effect of decreasing the free volume (i.e., porosity) of the solid debris bed. The resistance to fluid flow through particulate debris is thus calculated to increase with decreasing core node free volume. Within this MELCOR simulation, the particulate debris hydraulic diameter is 1.0 cm in the core region and 0.2 cm within the lower plenum. (Humphries, 2014)

MELCOR does not allow a particulate debris bed to become completely blocked to fluid flow. A limiting porosity is imposed in MELCOR calculations such that the free volume inside the particulate bed can never decrease below this limiting value. MELCOR assumes that flow through a particulate bed continues to occur. The default minimum porosity in a debris bed is 0.05 (or 5%).

This assumption in MELCOR also has the effect of maintaining heat transfer from core debris to fluids in the RPV (e.g., steam). Since a particulate debris bed has a large surface area, MELCOR calculates a significant amount of heat transfer between particulate debris and RPV fluids passing through the node.

MELCOR effectively models an incoherent melting of core debris around a ring. In this abstraction of the degraded core morphology, there will always be numerous paths through a particulate debris bed within a large ring for gas to continue to flow through the bed. RPV fluids will always be able to flow upward, to some extent, through a core ring, despite loss of free volume at an axial level. The diameter of particulate debris is not assumed to change with accumulation of debris in pores. However, MELCOR calculates a reduced surface area as conglomerate fills the interstitials between particulate debris, even though the particulate diameter does not change. (Humphries, 2014)

Table 4-1 Relevant MELCOR material melting temperature from defaults (a) or best practice (b) in (Humphries, 2014)

Material	Material Temperature (K)
Zircaloy	2098.0 (a)
Zirconium Oxide	2800.0 (b)
Uranium Dioxide	2800.0 (b)
Stainless Steel	1700.0 (a)
Stainless Steel Oxide	1870.0 (a)
Boron Carbide	2620.0 (a)
Carbon Steel	1810.9 (a)

4.1.3 Fuel Cladding Rupture

Fuel cladding rupture is responsible for early release of fission products, primarily the gap inventory. It also accelerates cladding oxidation by exposing internal cladding surfaces to steam and results in the relocation of molten U-Zr-O outside of the fuel clad where it subsequently candles down the fuel rod. (Humphries, 2014)

Within MELCOR, oxide layers can prevent relocation of molten U-Zr-O outside of the cladding. Molten material is assumed to be held up within an oxide shell when the thickness of the oxide shell is greater than a critical value, typically above the Zr melting temperature and when the component temperature is less than a critical value. When either of these conditions become violated, the oxide shell ruptures and the molten material inside is exposed and can candle down the fuel assembly. (Humphries, 2014)

4.1.4 Failure of Fuel Assembly Structures

MELCOR provides a user-specified time-to-failure model, with the time-to-fuel assembly failure specified at different assembly temperatures. The MELCOR simulations reported in this study use the time-to-failure model specified in Figure 4-1. This MELCOR model was developed based on insights from the VERCORS experimental program. (Pontillon, 2005) MELCOR also triggers the collapse of a fuel assembly if a lower core support structure fails (e.g., the core support plate). Alternatively, melting or collapse of a lower segment of a fuel support structure will trigger the collapse of all upper axial levels of the fuel assembly. (Humphries, 2014)

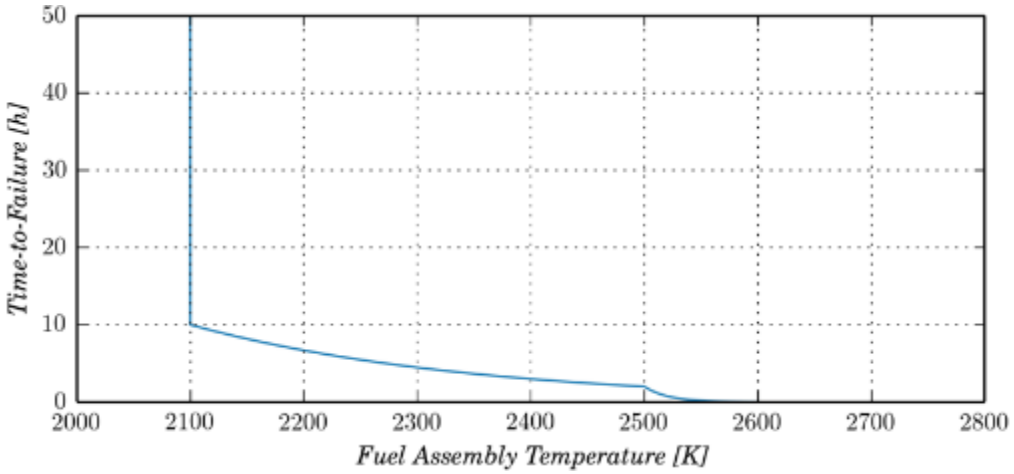

Figure 4-1 MELCOR Crosswalk Analysis Time-to-Failure Model

4.1.5 Mass Relocation Behavior

MELCOR assumes that molten material relocates downward through a candling process as long as fuel rings have not failed. The term candling refers to the downward flow of molten core materials and the subsequent refreezing of these materials as they transfer latent heat to cooler structures below. After fuel ring canisters fail, a significant amount of non-molten debris is generated. Both fuel debris and molten material will begin to redistribute radially based on a gravitational leveling algorithm. This becomes especially important in the distribution of material on the lower core plate and in the lower plenum in a MELCOR core degradation and relocation transient. (Humphries, 2014)

4.2 Overview of ASTEC Core Component Degradation and Relocation Abstractions and Models

Core degradation can easily be described in two distinct phases. The early phase corresponds to the first degradation phase of the accident, which covers the initial thermal-hydraulic phase (heatup phase before any material movement) as well as the first step of the loss of geometry phase (first control rod and fuel rod failures until the appearance of significant channel blockages). The late phase corresponds to an advanced degradation phase of the accident involving debris and possible molten pool and/or crust formation. (Chatelard, 2014)
Before core uncovery, ASTEC represents the vessel and core structures as a set of control volumes with an associated thermal inertia (heat capacity). From the core uncovery, the vessel domain is represented with 2D Eulerian meshing and core structures are discretized. Both early and late phases of degradation are represented with a continuous approach. Specific models (porous media for heat exchanges involving debris, radiation in cavities, debris relocation, etc.) are activated dynamically as the core degradation progresses. (Chatelard, 2014)

In the early phase, no relocation occurs. Thus, the core regions are represented by intact geometry. This representation allows one to represent not only fuel rods, but also shrouds, spacer grids, and core plates using a set of simple objects (cylindrical objects). During this phase, the thermal and thermomechanical interactions are computed by standard physical models (gap model, creep models, oxidation models, etc.). From here, the geometry evolves to a deformed geometry (mainly due to creep and dilatation, for instance ballooned rods). During the early phase, no debris is formed but some eutectics can lead to the formation of molten mixtures enclosed within the cladding. (Chatelard, 2014)

Material movement and relocation may occur at the end of this early phase. The treatment of melted materials in ASTEC requires that relocation occurs through the hydraulic channel (no axial relocation within rods). The field “magma” is dedicated to the description of core debris (solid particles and molten corium). The relocation is computed by a 2D transport model that is able to describe the behavior of candling on rods (when molten material fraction is not important) as the progression of an extended molten and its spreading over core plate. This behavior is described in the “Loss of Integrity Model” sub-section. (Chatelard, 2014)

The late stages of core degradation involve substantial melting and material relocation. Models in ASTEC deal with the dynamics of molten pool formation, its growth, and the progression of the melt inside the core, to be able to predict the amount of melt that is released into the lower plenum. A visualization of the interpretation of this treatment of core degradation can be seen in Figure 4-2. (Chatelard, 2014)

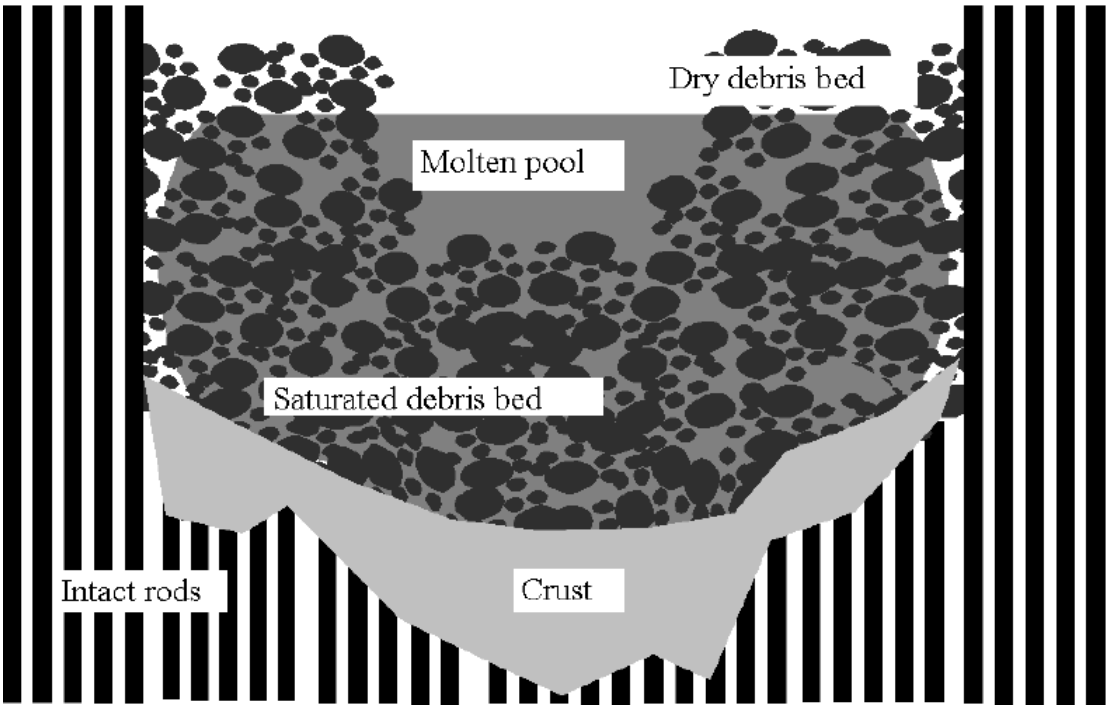

Figure 4-2 ASTEC Treatment of Core Degradation, based on TMI-2 Incident

4.2.1 ASTEC Degraded Core Components and Morphologies

ASTEC represents the core region in terms of macro components, super-macro components and a characteristic mesh. Super-macro components are a combination of two or more macro components. A complete description of the plant model implemented can be found in Section 2.1. Within the core region and the RPV, ASTEC models both core materials and components, similarly to MELCOR: (Chatelard, 2014)

- Core structures

- Cylindrical structures
    - UO_2, AgInCd or B_4C columns (rods/pellets)
    - Zr or stainless steel claddings (and associated oxides)
    - Core surrounding structures (e.g., shroud)
    - Spacer grids

- Horizontal structures
    - Horizontal plates
- Ellipsoidal structures
    - Lower head
- Degraded geometry
    - Relocated and relocating mixture – “magma”
- Lower plenum
- Fluids

The relocated and relocating mixture “magma” is a field to represent degraded structures which contains liquid or solid materials. When the volume fraction of “magma” is low within a core mesh, the component serves as a representation for candling behavior in which molten material runs down the side of a control rod. A schematic configuration of this “magma” candling configuration can be seen in Figure 4-3. (Chatelard, 2014)

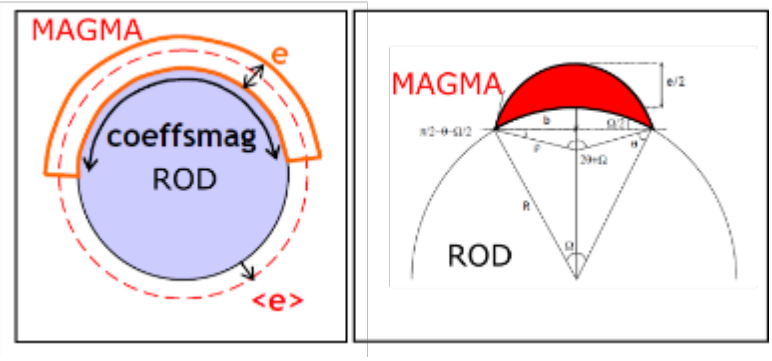

Figure 4-3 Schematic Configuration for MAGMA around a Rod for Low Volume Fraction of MAGMA (candling configuration)

As fuel rods continue to melt and degrade in a severe accident, the volume fraction of “magma” increases and the configuration no longer resembles candling behavior (as the films developing on neighboring rods coalesce). A description of this “magma” component can be seen in Figure 4-4 for later stages of core degradations. The molten/resolidified corium, solid debris, and degraded structures can be seen within the same “magma” meshing element. That is a significant difference with the approach retained in MELCOR, which preferentially forms particulate debris in BWR accident scenarios. (Chatelard, 2014)

Similarly to MELCOR, the porosity within the “magma” component is bounded by a minimum value, meaning that mesh can always have steam, water, or gas flowing through it. (Chatelard, 2014) This is a key difference in modeling compared to MAAP, which allows full channel blockage.

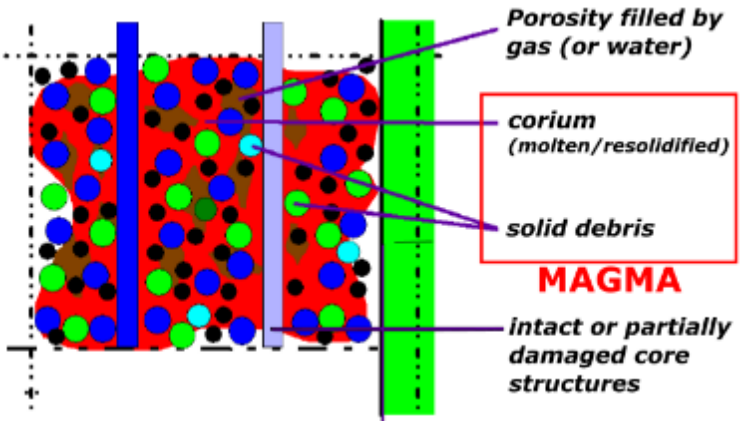

Figure 4-4 Description of a Core Mesh in ASTEC V2.0

The representation inside the lower plenum is different from the one in the core domain. The lower plenum is represented by a single control volume in which up to three corium layers and two debris beds can be represented (their formation and mixing is computed dynamically according to a fragmentation and thermochemical phase separation model). The slump of overheated corium (magma in core domain) into water is predicted using an analytical model and leads to form a debris bed into the lower plenum with an imposed debris size. A schematic for how this particulate debris is formed is shown in Figure 4-5. Debris is represented as a set of spherical particles, characterized by a representative geometry that includes internal and external diameter, axial extension, and particle size distribution. The “debris” is used to represent the formation of debris beds within the lower plenum. (Chatelard, 2014)

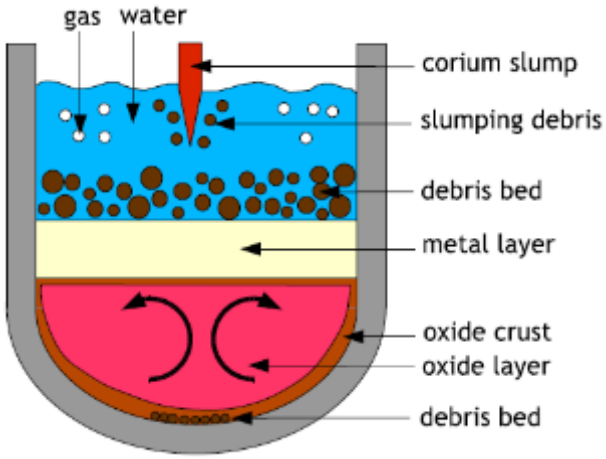

Figure 4-5 Representation of Particulate Debris Formation in ASTEC from a Jet of Molten Corium Entering a Pool within the Lower Plenum

4.2.2 Loss of Integrity Model

Within the ASTEC ICARE module many physical phenomena (ballooning, creep and, finally, burst) are described in a mechanistic way by special models, such as creep models for fuel and control rods. However, such models do not deal with the failure of the solid zirconia shell that may occur at temperatures lower than the ZrO_2 solidus temperature. This phenomenon can have an impact on the whole core degradation process if solid fuel pellet fragments can relocate in such a situation. The possibility of such relocation remains a subject of discussion after the interpretation of experiments such as Phébus-PF. Upon failure of this outer layer, candling (axial

relocation via “magma”) is now enabled within the code and molten materials are able to relocate downwards in the bundle. (Chatelard, 2014)
The management of this phenomenon is treated in the "loss of integrity" model. Additionally, this model also treats the mechanical failure of specific components for which creep models cannot be applied (e.g. spacer grids). Generally, the loss of integrity model is applied to the following phenomena, with associated failure conditions: (Chatelard, 2014)

- Absorber rods in order to allow candling and relocation of B4C and steel cladding on the external side of the guide tube
    - Condition: TGT > 1730 K
    - All layers of the absorber rod guide tubes are assumed to lose integrity and are replaced with a mixture of B4C and the guide tube materials.

- Fuel rods in order to allow the molten U-Zr-O alloy to flow down on the external side of the cladding before melting of the zirconia layer
    - Condition 1: TC > 2250 K and ZrO2 thickness > 300 μm
    - Condition 2: TC > 2500 K
    - The outer zirconia layer of the fuel rod component is assumed to fail and is replaced with a mixture of U-Zr-O.

- Zircaloy spacer grids in order to allow downwards movement and relocation of grid materials before melting of the zirconia layer
    - Conditions and loss of integrity modeling same as fuel rod model

The layered treatment of the fuel rods can be seen in Figure 4-6. Per the above explanation, the outermost ZrO_2 layer of this component transforms to a U-Zr-O mixture when the loss of integrity conditions are met. (Chatelard, 2014)

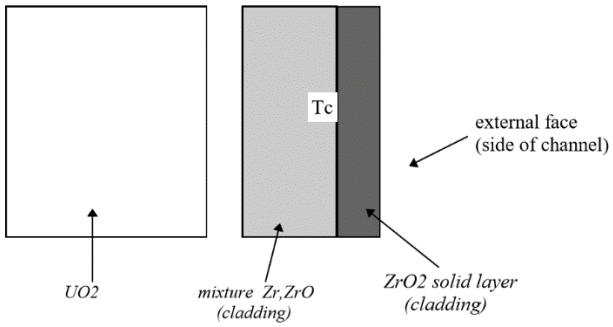

Figure 4-6 Fuel Rod Modeling within the ASTEC ICARE Module

In addition, recall that the mixture (U, O, Zr) and its chemical behavior is estimated according to a specific model that is based on a “simplified” ternary phase diagram. (Chatelard, 2014)

4.2.3 Creep and Burst Models

In order to capture the burst of the cladding leading to first FPs release, the deformation behavior of fuel rods at high temperatures and stresses is computed according to cladding creep velocity and burst models. The approach to predict creep is simplified and dealt with 2D configuration without taking care of the contact and blockage due to ballooning (a 3D approach was developed specifically in the IRSN DRACCAR code for LOCA conditions). Accordingly, only the Δ-Zr layer of the cladding is considered in the model. This means that the αZr(-O) and ZrO_2

layers are assumed to have no mechanical resistance. However, in interpreting the absence of these layers in the creep treatment it is important to keep in mind the fact that they are highly brittle. Upon reaching the conditions for burst, which are either temperature or stress/strain dependent, the cladding rupture can occur, exposing the inner UO_2 layers to water and high temperature gasses. (Chatelard, 2014)

4.2.4 Material Melting and Eutectic Behavior

ASTEC informs solidus and liquidus temperatures for structural and core materials from relevant binary and ternary phase diagrams. The values within the code for relevant pure materials and eutectics can be seen in Table 4-2. The implementation of these phase diagrams allows gradual changes in melting temperatures (based on composition) for eutectics and "pure" materials commonly found within a reactor environment. A simplified U-Zr-O ternary phase diagram addresses the eutectic formed by UO_2 and ZrO_2 and is used to predict chemical behavior of the three-compounds mixture in steam atmosphere. Other chemical interactions in corium are neglected in ASTEC code. (Chatelard, 2014)

Table 4-2 Pure Material and Eutectic Solidus and Liquidus Temperatures in ASTEC

Material Pairs		Molar Ratio	Solidus Temperature (K)	Liquidus Temperature (K)
SS	-	-	1671	1727
UO_2	-	-	3085	3130
Zr	-	-		
ZrO_2	-	-	2973	2974
B_4C	-	-		
SS	ZrO_2	0.1/0.9	1671	2973
SS	ZrO_2	0.9/0.1	1671	1973
UO_2	ZrO_2	0.1/0.9	2911.1	2933.2
UO_2	ZrO_2	0.9/0.1	2936.3	3076.2

Additionally, intact structures can undergo liquefaction and dissolution utilizing unique models for each material pair. Relevant dissolution and liquefaction models implemented into ICARE include: (Chatelard, 2014)

- UO_2 liquefaction by Zircaloy
- UO_2 and ZrO_2 dissolution by molten Zircaloy
- Zircaloy liquefaction by solid stainless steel
- Stainless steel liquefaction by solid boron carbide
- Liquefaction of the Zircaloy cladding tube by spacer grid materials

As in MELCOR modelling, ASTEC assumes that an oxide layer can prevent a molten mixture (such as U, O, Zr or molten steel) from leaking into core flow channels and to instead relocate. As soon as criteria integrity are reached or interactions (melting, liquefaction, dissolution) lead to dislocation of the oxide shell, the mixture located within the core structures feeds the "magma" field. The magma field holds the corium transport in the core domain. (Chatelard, 2014)

4.2.5 In-Core Material and Debris Movement

ASTEC models the relocation and movement of degraded core materials through the 2D movement/relocation model. The decanting model moves material from “macro” components (such as fuel rods, spacer grids and control blades), which are not able to move axially, to other “macro” components that are permitted to move axially (e.g. “magma” or debris). (Chatelard, 2014)

The relocation of molten material is calculated from momentum conservation equations for the liquid phase. All of the species are supposed to move at the same velocity; the possible stratification or relative diffusion of species in the corium is not modelled. Additionally, “magma” is considered to have a minimum porosity, which means that gas and steam/water can always flow through this component. (Chatelard, 2014)

4.3 Debris Mass Distribution

The debris mass distribution for both MELCOR and ASTEC during the accident simulation is shown in Figure 4-7. It shows the amount of total core debris within both the core region and the lower plenum. The timings of initial core plate failure can be seen in both of the codes. In MELCOR, a portion of the core plate fails relatively early - 5.0 hours - into the transient, whereas in ASTEC the core plate melts gradually, beginning at 6.0 hours.

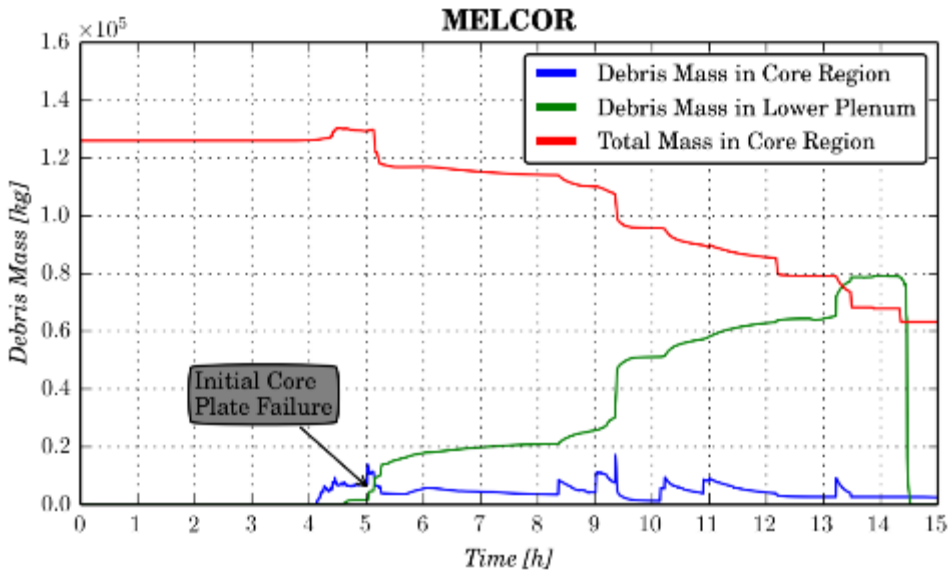

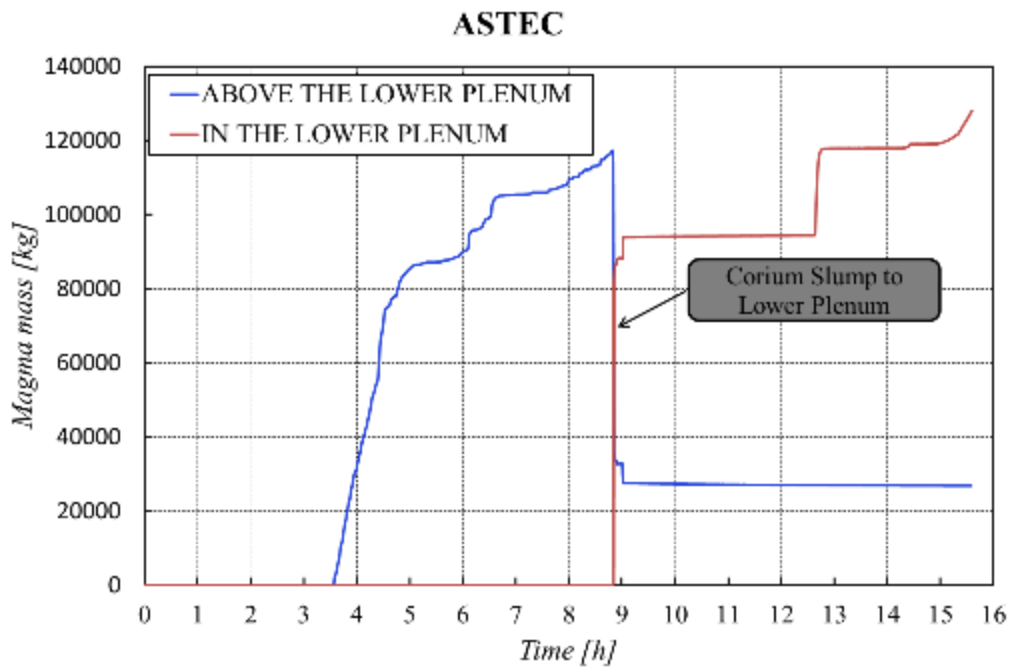

Figure 4-7 Debris Distribution during both within the Core Region and within the Lower Plenum

ASTEC forms a crusted “magma” pool in the central region of the core, which then progresses downward through the primary containment valve (PCV) as the simulation progresses. This means that the core plate does not see significant heatup until just before failure when the molten pool nears it. However, this also means that the failure of the lower core plate is much more drastic when it does occur. The timing of this large relocation of corium mass to the lower plenum in the ASTEC simulation corresponds to a large spike in RPV pressure to near 7.0 MPa from a depressurized value near 0.3 MPa. Compared to MELCOR, ASTEC produces corium/debris at a much higher rate than MELCOR. This can especially be seen between hours 3.0 and 6.0 in the simulation. By 6.0 hours more than half of the core has been dislocated into “magma,” whereas in MELCOR less than twenty percent of the core has failed.

MELCOR, which preferentially forms particulate debris and not molten pools like ASTEC and MAAP, relocates this particulate debris to the lower plate and causes it to fail relatively early in the simulation. As the simulation progresses from this point of initial core plate failure, there are many minor relocations of debris from the core region to the lower plenum, on top of the lower head. A large slumping event near 9.4 hours into the simulation causes a much smaller spike in RPV pressure compared to ASTEC, since a much smaller amount of corium mass slumped compared to ASTEC.

4.4 Fuel Temperature Transient

Within this section the fuel temperature transient is presented first for MELCOR and then for ASTEC. Additionally, the mesh average temperature for the core region is also presented for ASTEC. MELCOR does not have such a representation and thus no figure is presented.

4.4.1 MELCOR

The fuel temperature transient for MELCOR from 4.0 hours to 8.75 hours is presented in Figure 4-8. The fuel temperature shown is taken from intact fuel only. Failed assemblies are represented with the dark blue blocks from 5.25 hours onwards. (Luxat, 2014)

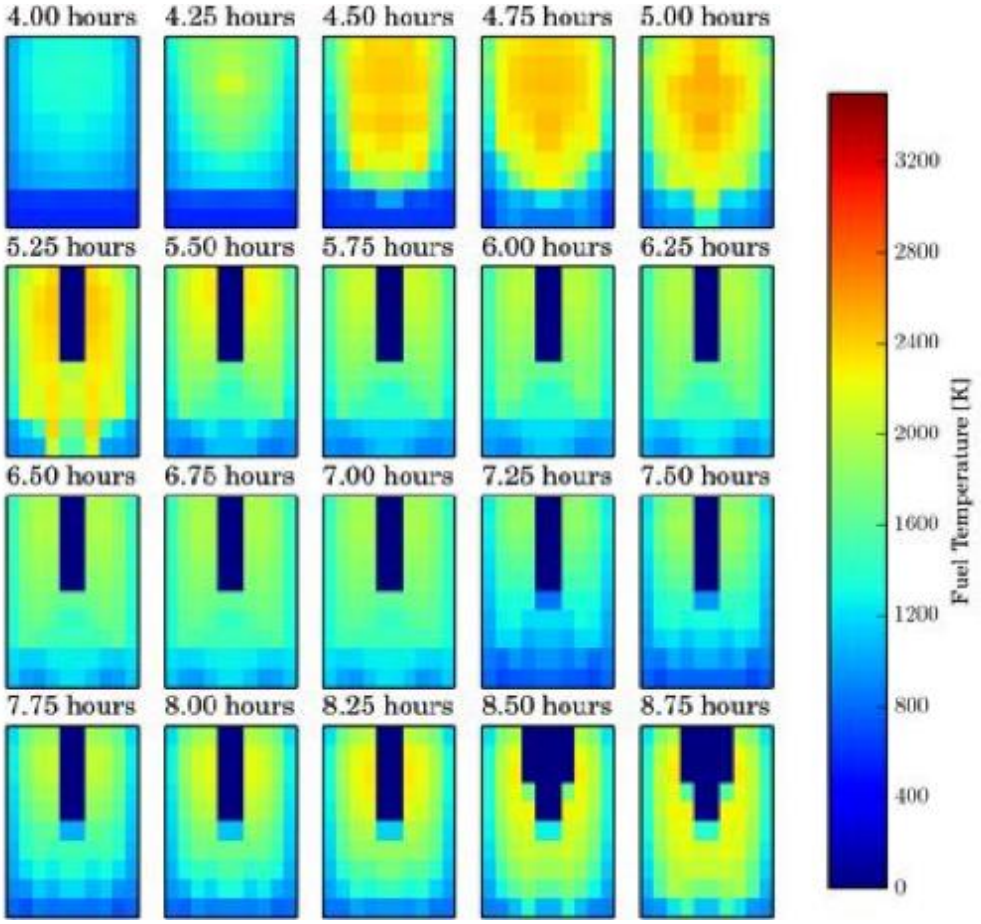

Figure 4-8 Distribution of Active Core Region Fuel Temperatures from Hours 4.0 to 8.75 from the MELCOR Simulation. (Luxat, 2014)

It can be seen that the first assembly failure occurs within MELCOR just after 5.0 hours. Upon failure, particulate debris builds up on the core plate, eventually failing it. The core plate takes into account both thermal and mechanical challenges to its integrity. These assembly failures are only within the innermost ring of the core; the four outer rings remain intact until 8.4 hours when the 2nd inner ring sees failure near the top of the core. When a portion of an assembly fails within MELCOR, all of the assembly above the failed region is also considered to have failed. The fuel temperature transient is shown from 6.0 hours to 15.0 hours in Figure 4-9.

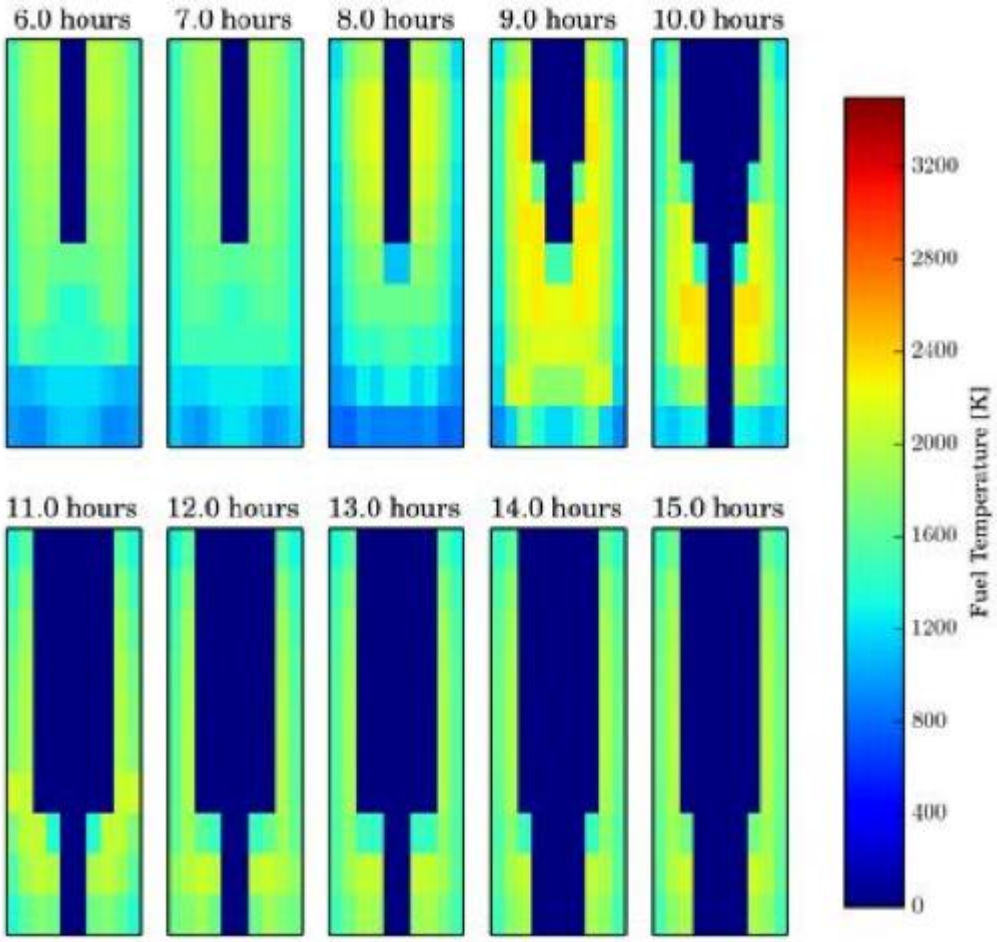

Figure 4-9 Distribution of Active Core Region Fuel Temperatures from Hours 6.0 to 15.0 from the MELCOR Simulation. (Luxat, 2014)

The initial collapse of the third ring of the core occurs just after 9.0 hours. Between 9.0 and 10.0 hours the entire inner ring of fuel assemblies has failed. As the transient progresses from 10.0 hours to 15.0 hours the remainder of the fuel assemblies within the 2nd innermost rings of the core have collapsed and the 3rd innermost ring continues to degrade. However, by 15.0 hours into the event neither the 4th or 5th innermost rings have collapsed. The Fukushima Unit 1 Uncertainty analysis indicated that in a majority of cases, these rings do in fact eventually collapse/fail. Before the failure in rings 1, 2 and 3 it can be seen that the temperature builds up in the immediate vicinity of the failure to values above 2100 K, which is the minimum temperature for assembly failure in this simulation.

4.4.2 ASTEC

The fuel temperature transient for ASTEC from 3.25 hours to 8.75 hours is presented in Figure 4-10. Failed fuel, which has relocated from the rod component to the “magma” component, is represented in the figure as black. Black color does not mean that the mesh is empty as it can be full of debris (MAGMA). For understanding, it is noted that in the V2.0rev3 of the ASTEC code, the only loss of integrity leading to mass transfer from rod to MAGMA field (debris) is the melting. It can be easily seen that unlike MELCOR there is no assembly/rod collapse model. Fuel rod failure in ASTEC is a result of material melting. This divergence in modeling approach is a key difference.

Another key difference is the global overheating of the core, which diffuses radially to all the core rings. The radial thermal gradients are lower in ASTEC simulation than in MELCOR even at the beginning of the core degradation. Due to the lack of the collapse model, intact fuel rods can remain above a pool of molten corium. Fuel failures within ASTEC begin at the top of the core near 3.625 hours and then occur within the top half of the core until 4.0 hours. After 4.0 hours, fuel failures begin to occur in half of the reactor core with nearly all fuel in the lower half of the core becoming failed by 6.25 hours into the transient. At the time of relocation to the lower plenum at 8.8 hours there is still a significant portion of fuel remaining in the topmost region of the core, which then fails later in the transient.

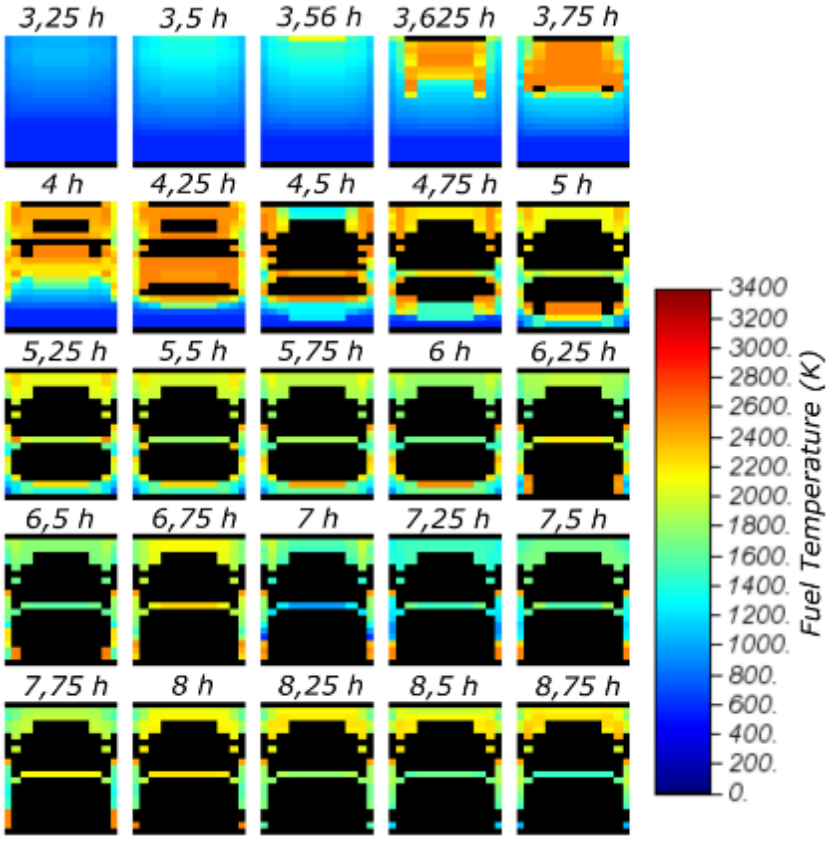

Figure 4-10 Distribution of Active Core Region Fuel Temperatures from Hours 3.25 to 8.75 Hours from the ASTEC Simulation

A second plot of temperature in the core region through 9.0 hours of simulation time is shown in Figure 4-11, which shows the mesh average temperature in the core region from 3.25 hours to 9.0 hours. The plotted domain extends from the top of bottom head to the top face of upper core plate. Consequently, the upper half of the plotted domain corresponds to the active region of the core. The mesh average temperature here incorporates both to all components within the mesh (rods, “magma,” control blades, etc.) and fluid channel temperatures. In the 5th ring, the core shroud is not accounted for in the average temperature. For each core ring and for each mesh, the average temperature is evaluated using Equation 4-1. (Chatelard, 2014)

$$T_{average} = \frac{\sum_{wall} \dot{M} \times Cp \times T + M_{water} \times Cp_{water} \times T_{water} + M_{gas} \times Cp_{gas} \times T_{gas}}{\sum_{wall} M \times Cp + M_{water} \times Cp_{water} + M_{gas} \times Cp_{gas}} \quad (4\text{-}1)$$

From 3.56 hours to 5.0 hours the core degradation progresses in the active core region. One can see that the hot spot located at the top of the core in the inner rings triggered the oxidation processes and progressively the overheated zone extends radially. From 3.6 hours, the overheating of the core is sufficient to reach melting temperature of structures (2550K for the ASTEC simulation) and then relocation of material starts and leads to the formation of a molten pool that will progress downward. As it progresses downwards, this molten pool refreezes on colder structures or in contact with the water level and then reheats and continues flowing. At 4.5 hours, the upper region of the core in all the core rings is overheated.

The behavior in the 5th ring changes rapidly from 4.25 hours to 4.5 hours. This is a result of overheating in the 5th ring itself and not of molten material flowing outward from the 4th ring, causing a flow restriction and subsequent oxidation. Near 4.0 hours the core shroud starts to melt in the upper half of the core due to high gases that heat it above 1730K. Close to 5.0 hours, a significant amount of molten material forms a molten pool above the core support plate. The crust that was formed progressively heats up and the core support plate is melted in its center close to 6.0 hours. Then molten material progresses downward, slowed down by water and alternating refreezing of the crust with melt and flow down. At close to 8.8 hours the corium pool reaches the bottom head.

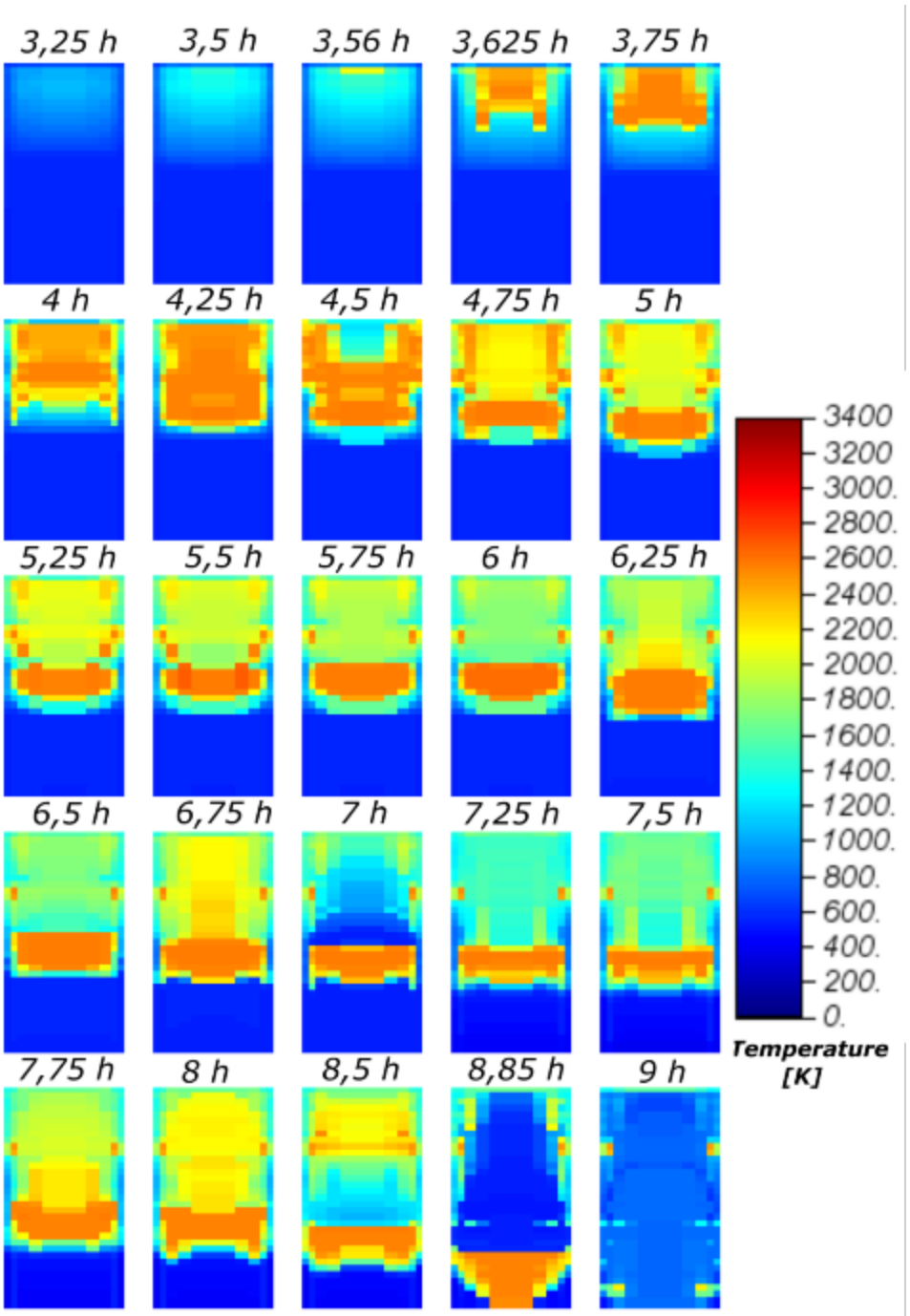

Figure 4-11 Distribution of Core Region Mesh-Average Temperatures from Hours 3.25 to 9.0 Hours from the ASTEC Simulation

4.4.3 Comparison of Degradation Transients

The delay of close to half an hour or one hour between the ASTEC and MELCOR simulations in the heatup of the core is not discussed, as it is related to the timing of severe accident simulation; additionally, discussion of thermal-hydraulic behavior covers this difference in onset timing.

The temperature field at 4.0 hours for the MELCOR simulation is close to the one at 3.5 hours for the ASTEC simulation at the top of the core (close to 1200 K - 1400 K). The bottom parts of the fuel rods are at saturation temperature. The axial temperature gradients are higher in the MELCOR simulation.

In the first minutes of heatup, both codes predict that heatup progresses from top to bottom. The initial hottest spot is located in the center of the core (1st ring) and in the top half part of the core (seen at 3.56 hours for ASTEC and at 4.25 hours for MELCOR). The degradation starts at the top of the active zone in both MAAP and ASTEC simulations, whereas MELCOR predicts it in the middle of the core region. A possible explanation for the difference in location of the initial hottest spot is that the ASTEC domain over the core upper plate is adiabatic, with the exception of steam exhaust from the area. There is no radiative heat transfer over the upper core plate in ASTEC.

In the uncovered part of the core, the increase in temperature is strongly driven by oxidation of Zircaloy. Accounting for the melt-down or the collapse of fuel rods has a significant impact on the calculation of temperatures. Therefore, ASTEC and MELCOR temperature fields are strongly different during core degradation. From the timing of 4.55 hours to 5.25 hours for MELCOR, one notes that the fuel heats up from top to bottom and that temperature in the 5th core ring remains below 2000K, whereas from 3.625 hours to 4.25 hours for ASTEC, the core heats up in the upper half and temperature increases rapidly in all core rings. After 4.0 hours, the fuel temperature in the 5th ring is above 2000 K for most of the uncovered elements. As a consequence, for the ASTEC simulation fuel melting occurs also in the 5th ring.

4.5 Core Degradation Transient

This section presents the core degradation transient for both the MELCOR and ASTEC simulations. Both the ASTEC and MELCOR figures (Figures 4-12 through 4-16) present the core from the bottom of the lower plenum to the top of the active core region. For the MELCOR simulation, snapshots of the status of the RPV are shown from 2.0 hours to 14.0 hours. For the ASTEC simulations, snapshots are shown from 2.6 hours to 15.6 hours.

4.5.1 MELCOR

Snapshots of the stratus of the RPV within MELCOR can be seen from 2.0 hours to 14.0 hours in Figure 4-12 and Figure 4-13. Within the figure the following fields are shown: water (blue), support structures (yellow), particulate debris (green), and fuel (pink/purple). Note that these images do not show particulate debris that may be trapped within the bypass region. The water level is shown decreasing from the top of the core region at 2.0 hours, to boiling off completely just after 10.0 hours. Fuel assembly collapse timings are also shown as they occur progressively within the simulation. The first such event occurs between 4.0 and 6.0 hours. By 10.0 hours, the inner ring of fuel has completely failed and by 14.0 hours the inner two rings have completely relocated to the lower plenum. Core support plate inner ring degradation and failure occurs between 4.0 and 6.0 hours. Additionally, the location and amount of particulate debris, first held up on the core plate then relocated to the lower plenum, can be well tracked. Within this MELCOR simulation this particulate debris has a constant downward velocity of 0.01 m/s for gravitational settling; this can be a user-specified value within the code.

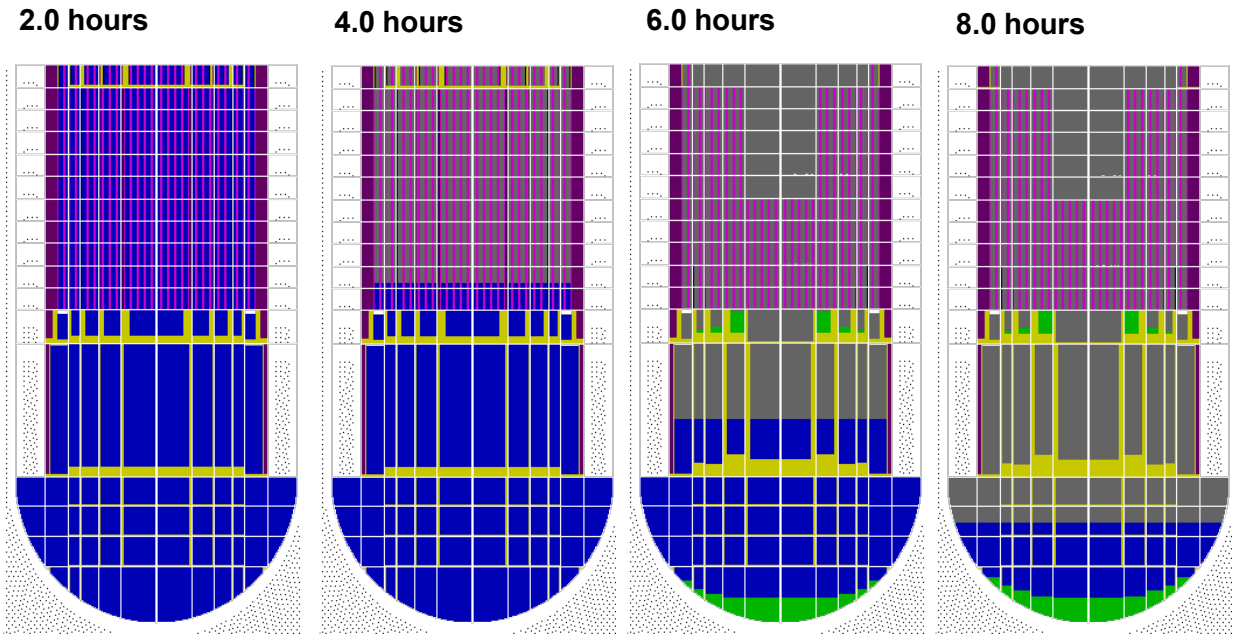

Figure 4-12 Core Degradation Transient, Showing Debris Type within the RPV from 2.0 h to 8.0 h for the MELCOR simulation

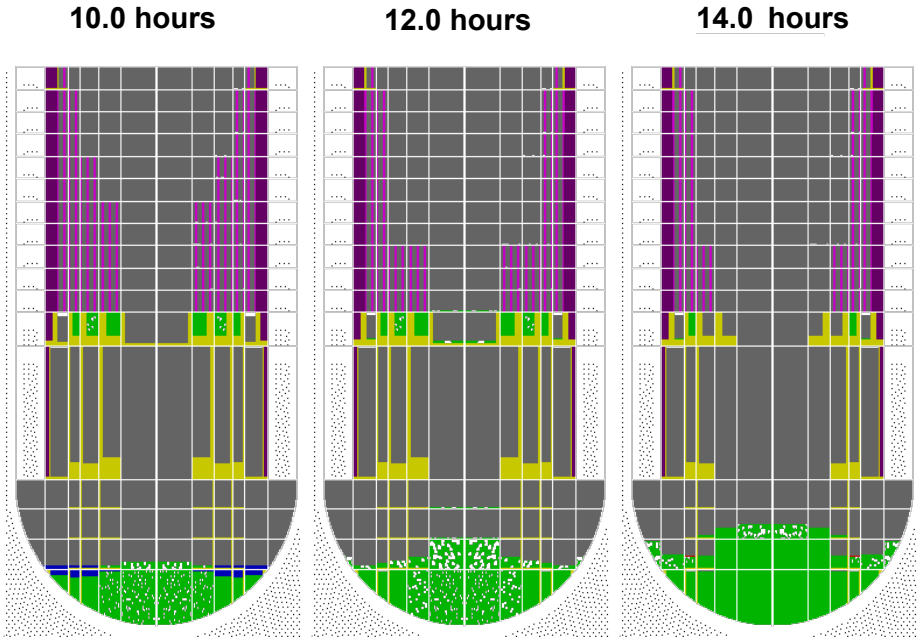

Figure 4-13 Core Degradation Transient, Showing Debris Type within the RPV from 10.0 h to 14.0 h for the MELCOR Simulation

4.5.2 ASTEC

The core degradation transient for the ASTEC simulations from 2.6 hours to 4.0 hours is shown in Figure 4-14. The boildown of water through the core can be well seen. Its cooling effect on adjacent fuel is also well shown with fuel components next to water being maintained at relatively low temperatures. Heatup of fuel components can be seen to begin at the top of the core and progress downwards from there. The beginnings of the heatup can be seen at just 3.0 hours into the simulation. Higher fuel temperatures are then seen at 3.5 hours and fuel melting begins to occur by 4.0 hours. At the 4.0 hours snapshot, the molten pool (yellow) can be seen in the middle of the core.

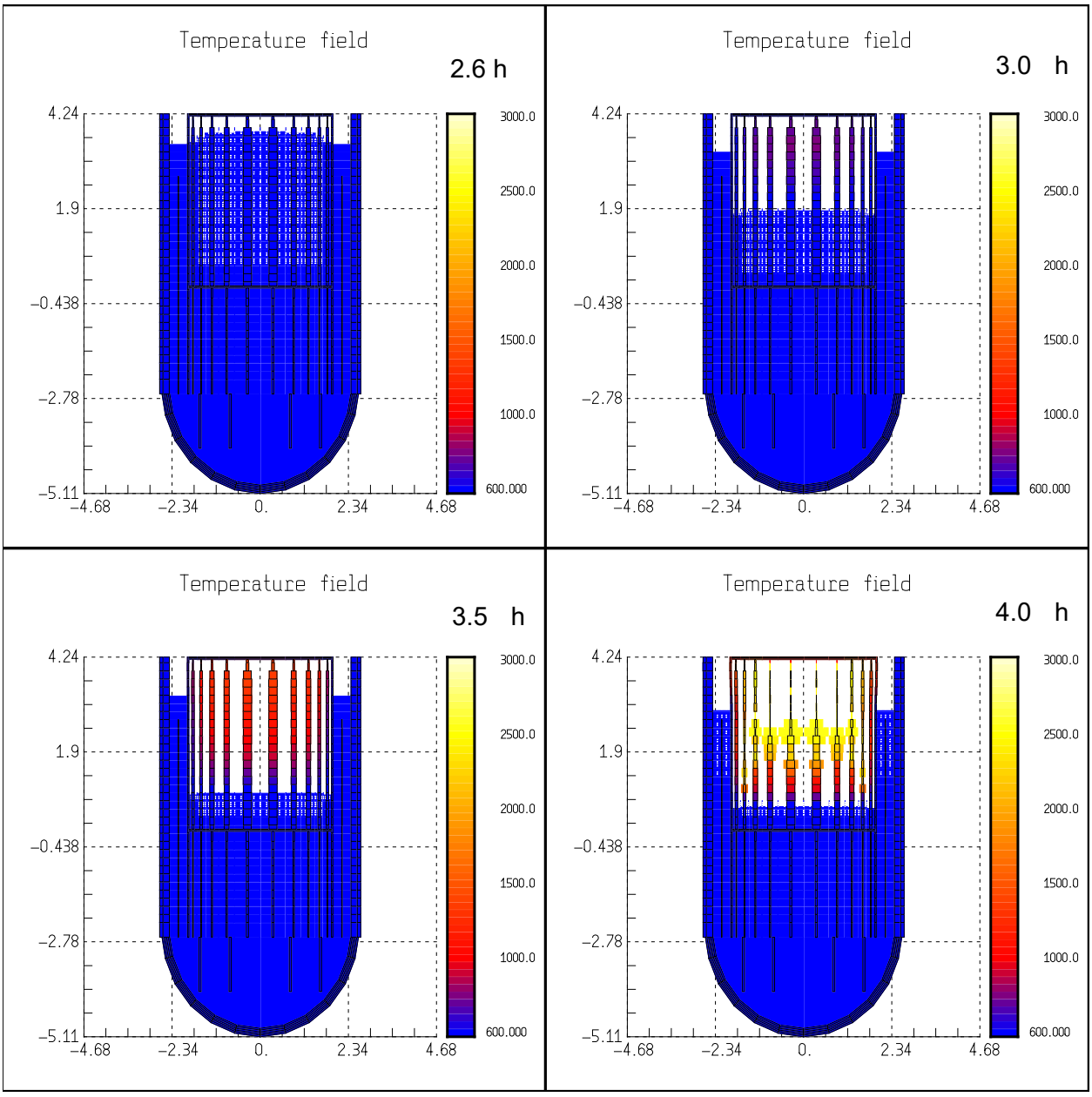

Figure 4-14 Core Degradation Transient, Showing Temperature Field in the RPV from 2.6 h to 4.0 h for the ASTEC Simulation

Core degradation transient snapshots for the ASTEC simulation are shown from 4.5 hours to 8.8 hours in Figure 4-15. The progression of the molten pool through the core region can be well seen, beginning at 4.5 hours just below the midpoint of the core and progressing to the core support plate. The crust on the bottom portion of the molten pool can clearly be seen: the bottom of the pool has a temperature near 1500 K, as opposed to the temperatures above 2500 K found in the middle of the molten pool. The core support plate then melts near 6.0 hours into the simulation, however, molten material is held up as it refreezes to other support structures. Full relocation to the lower plenum occurs near 8.8 hours. Buildup of molten material on the lower head is also evident at this time.

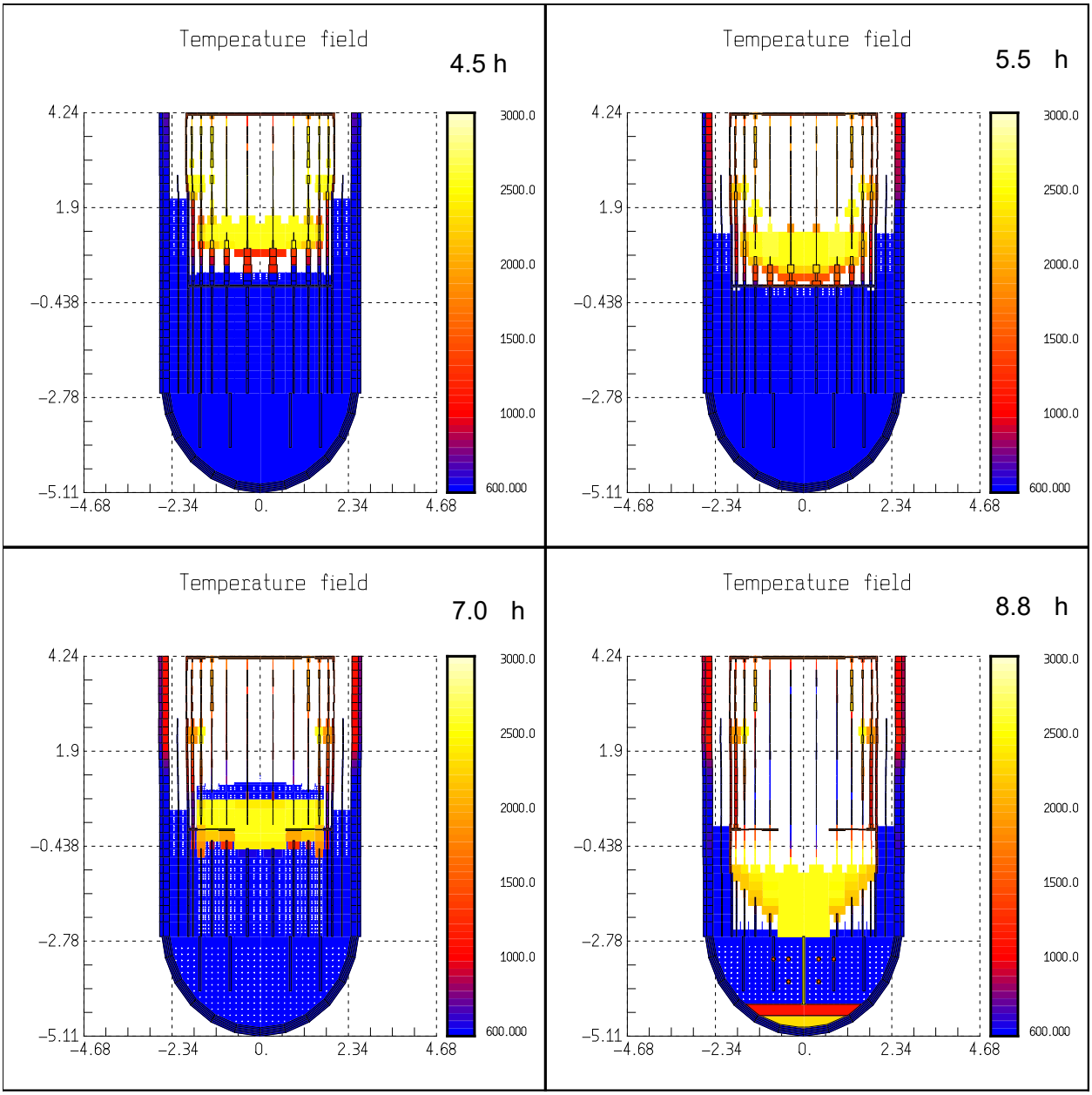

Figure 4-15 Core Degradation Transient, Showing Temperature Field in the RPV from 4.5 h to 8.8 h for the ASTEC Simulation

Degradation transient snapshots from 10.0 hours to 15.6 hours are shown in Figure 4-16. The distribution of temperature within debris built up within the lower plenum can be seen, with higher temperatures in the bottom of the lower plenum and lower temperatures above. These temperature distributions are a result of the lower plenum layer model found in ASTEC. At 15.6 hours into the simulation, the failure of the RPV can be seen to occur along the side of the RPV, at the highest portion of the lower head of the vessel.

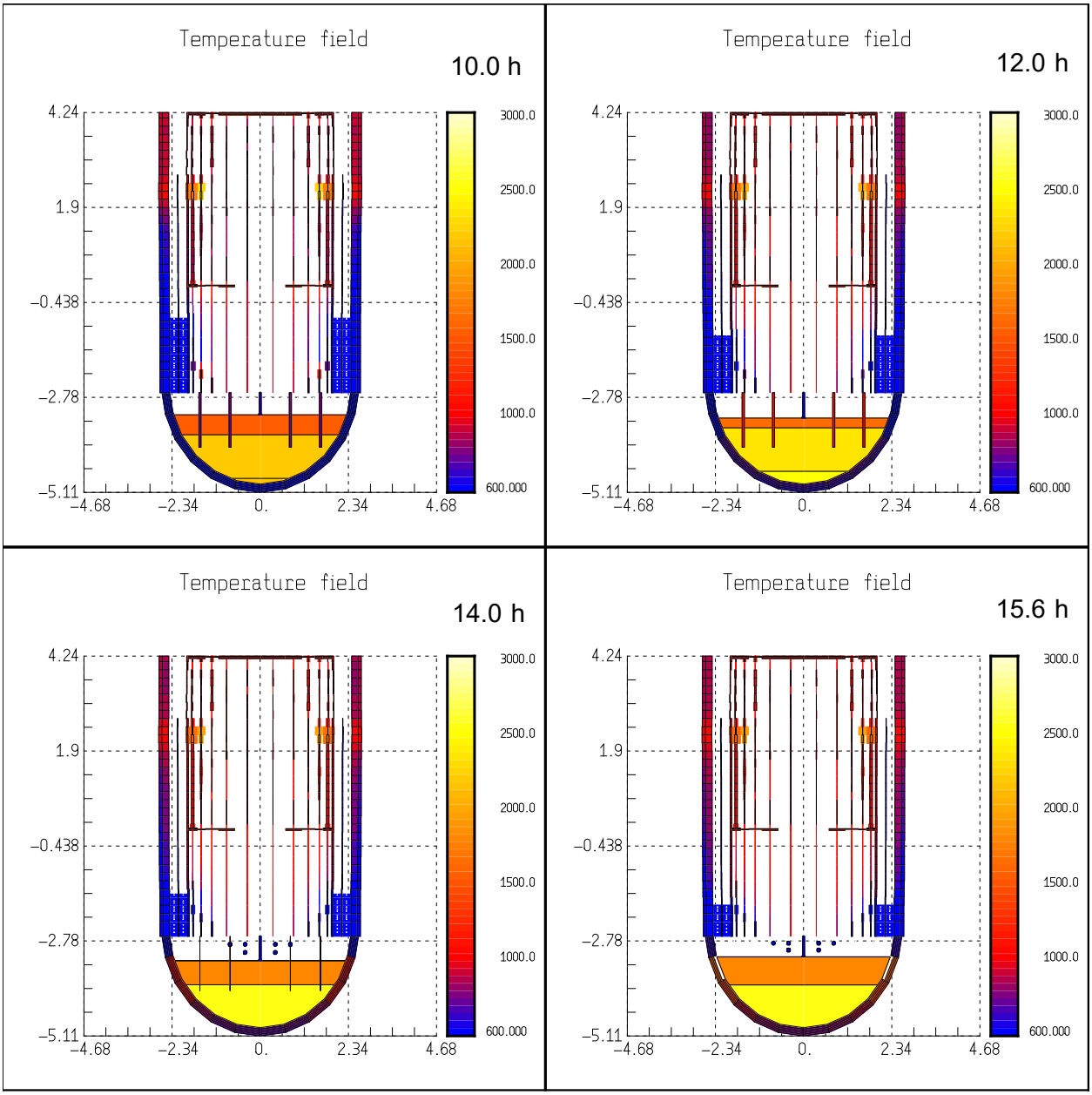

Figure 4-16 Core Degradation Transient, Showing Temperature Field in the RPV from 10.0 h to 15.6 h for the ASTEC Simulation

4.6 Cladding Temperature Transient

The cladding temperature transients for both MELCOR and ASTEC for all core regions are shown in Figure 4-17 and Figure 4-18. It can be seen that there is a hard cutoff for melting and dislocation of cladding in the ASTEC simulation just above 2500 K. It can also be seen that if this melting temperature is reached then the cladding immediately dislocates and become part of the “magma” field. The MELCOR simulation on the other hand does not see many cladding failures as a result of solely melting, though some may occur just after 5.0 hours into the simulation. The majority of the failures of cladding are a result of time-at-temperature failures. The curve for assembly failures using this model can be found in Figure 4-1.
Comparatively, the ASTEC simulation sees a significantly higher number of cladding failures, due to elevated temperatures in the ASTEC simulations. If assemblies in the MELCOR simulation would have seen temperatures as high as those predicted by ASTEC, they would also have failed. This indicates that less heat is removed from the fuel rods in the ASTEC simulation. It can also be seen that the increase in temperature in MELCOR is more gradual than ASTEC. From the onset of heatup in MELCOR, it takes nearly 2.0 hours to reach temperatures near 2500 K. However, in ASTEC it only takes ~1.2 hours to reach temperatures above 2500 K. This heatup rate difference is a result of different fuel loss of integrity models and fuel relocation models.

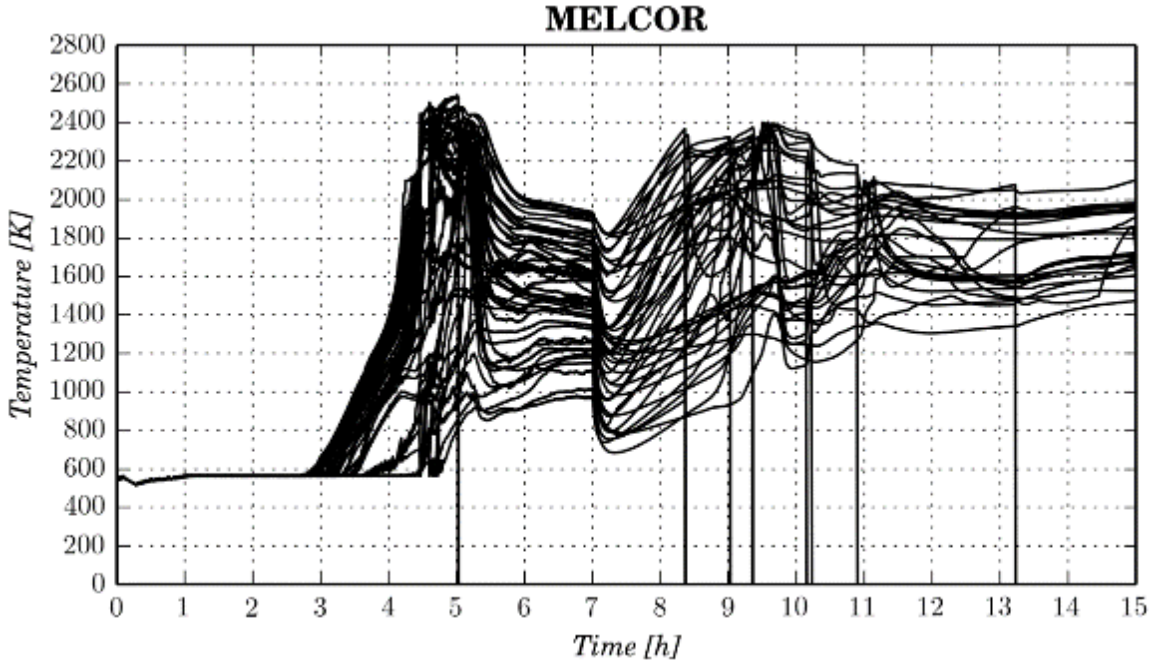

Figure 4-17 Cladding Temperature Transient, Showing all Different MELCOR Nodal Locations within the Core Region

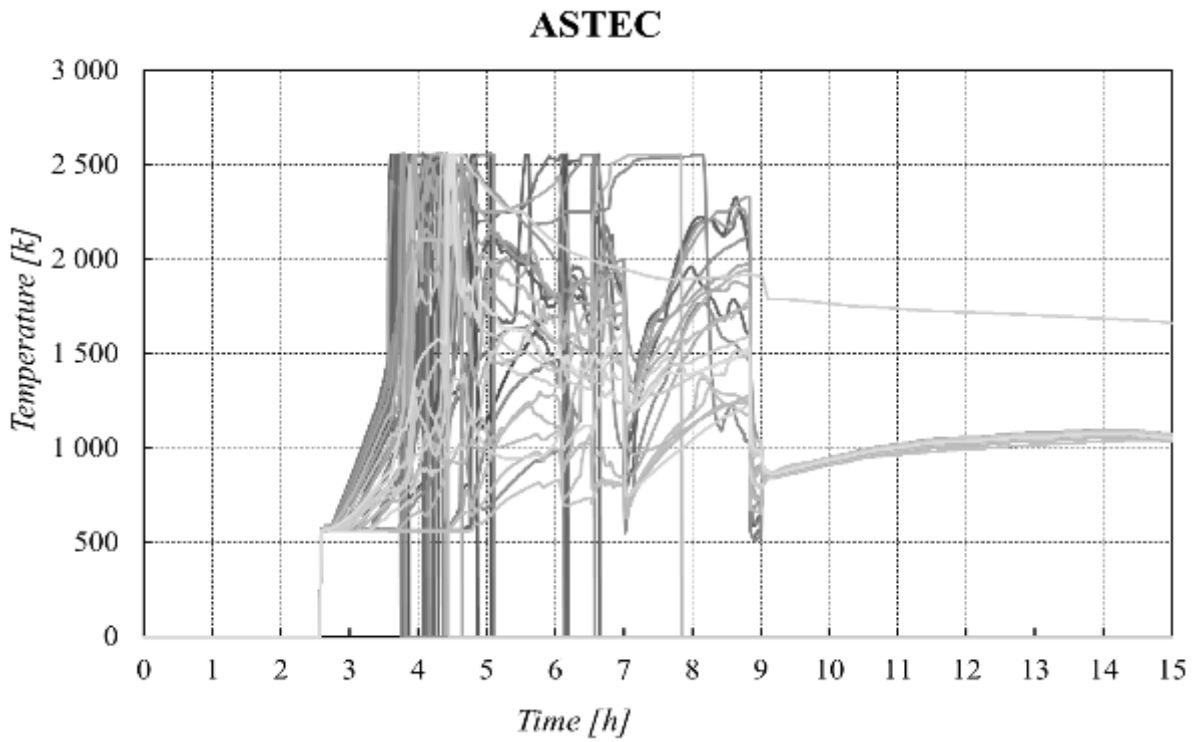

Figure 4-18 Cladding Temperature Transient, Showing all Different ASTEC Mesh Locations within the Core Region

4.7 Debris Morphology and Porosity

In the ASTEC simulation, the porosity, shown in Figure 4-19, is calculated for each mesh and corresponds to available volume for fluid over volume of the mesh. It is displayed in each core ring and meshes of the core region (both active and passive). The bottom head region, corresponding to a simplified lower plenum control volume (CV), is not presented.
The porosity field highlights the relocation of molten material. One can see that ASTEC predicts formation of a dense molten pool that is formed during core degradation. It can be seen that the minimum porosity (0.1) is reached when molten material is relocated. In ASTEC, a minimal flow area is kept in molten pool regions so that heat exchanges and chemical interactions still apply. Considering the porosity at 4.25 hours, it is noted that there is some relocated material that reduces the flow area in the 5th core ring close to the core support plate. This reduction in flow area results from oxidation and subsequent melting in the ring.

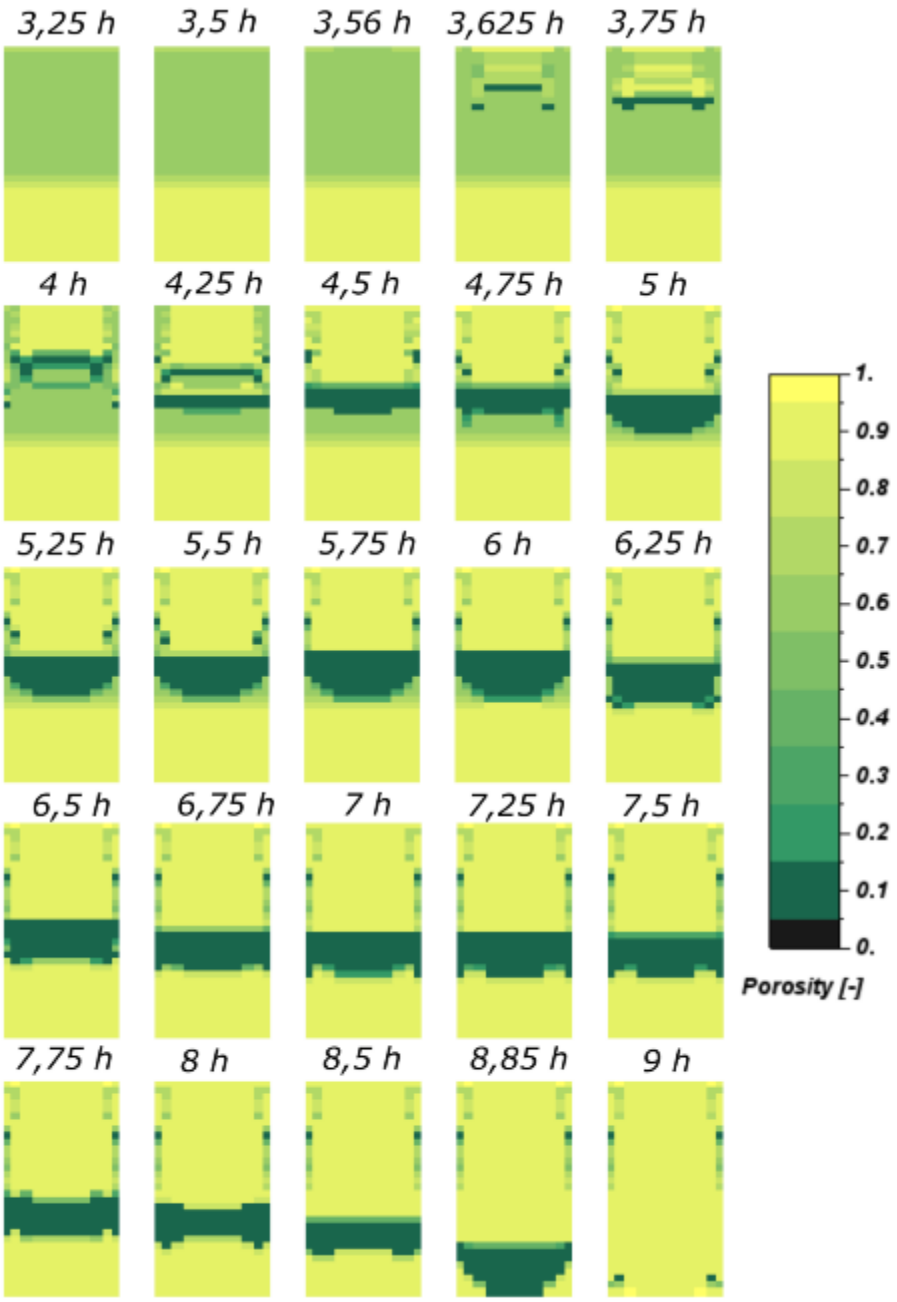

Figure 4-19 Mesh Porosity Distribution within the Core Region for the ASTEC Simulation

The morphology of the MELCOR simulation can be inferred from Figure 4-20 and Figure 4-21. Figure 4-20 presents the total amount of intact fuel and mass of molten material, whereas Figure 4-21 presents the debris mass within the core and in the lower plenum. Both plots show the total amount of mass in the core, which begins to decrease after 5.1 hours when the first fuel plate failure occurs in MELCOR. Molten mass begins to accumulate in the core region after 4.2 hours. However, after 6.0 hours there is no significant amount of molten mass present. This is in stark contrast to the ASTEC code. The majority of debris in the MELCOR simulation is higher porosity particulate debris. This debris can be found in both the core region, held up on

the core support plate, and in the lower plenum. Figures 4-12 through 4-16 in the “Core Degradation Transient” section present snapshots showing the locations of this particulate debris.

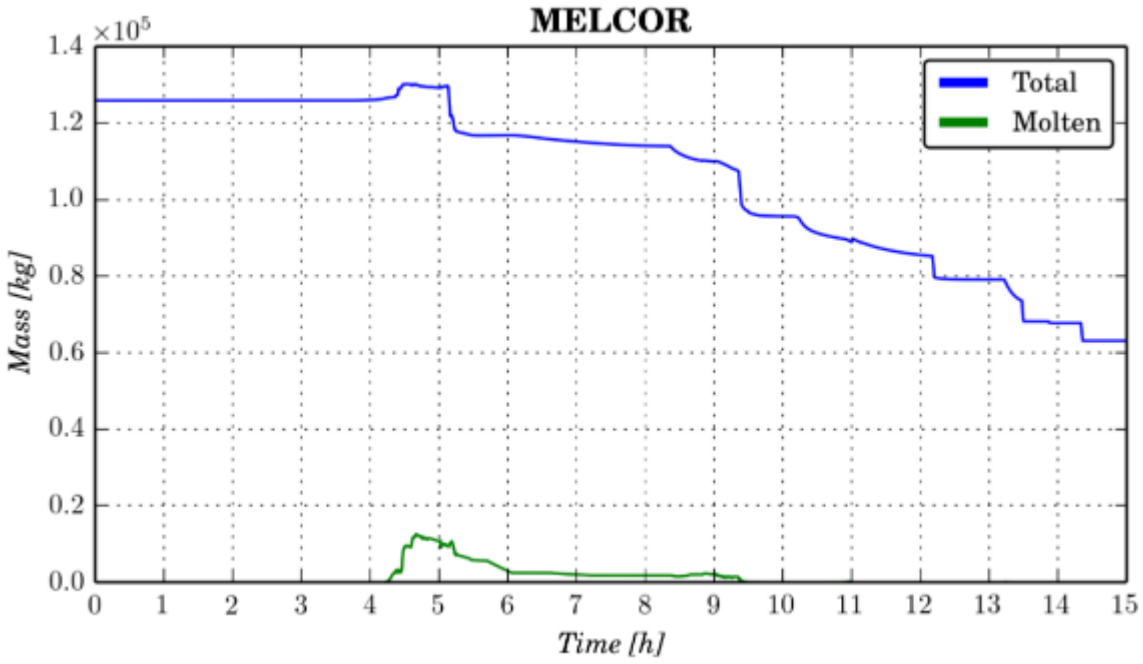

Figure 4-20 Core Degradation Transient within the MELCOR Simulation, Showing the Total Amount of Intact Fuel and Structures and the Amount of Molten Material

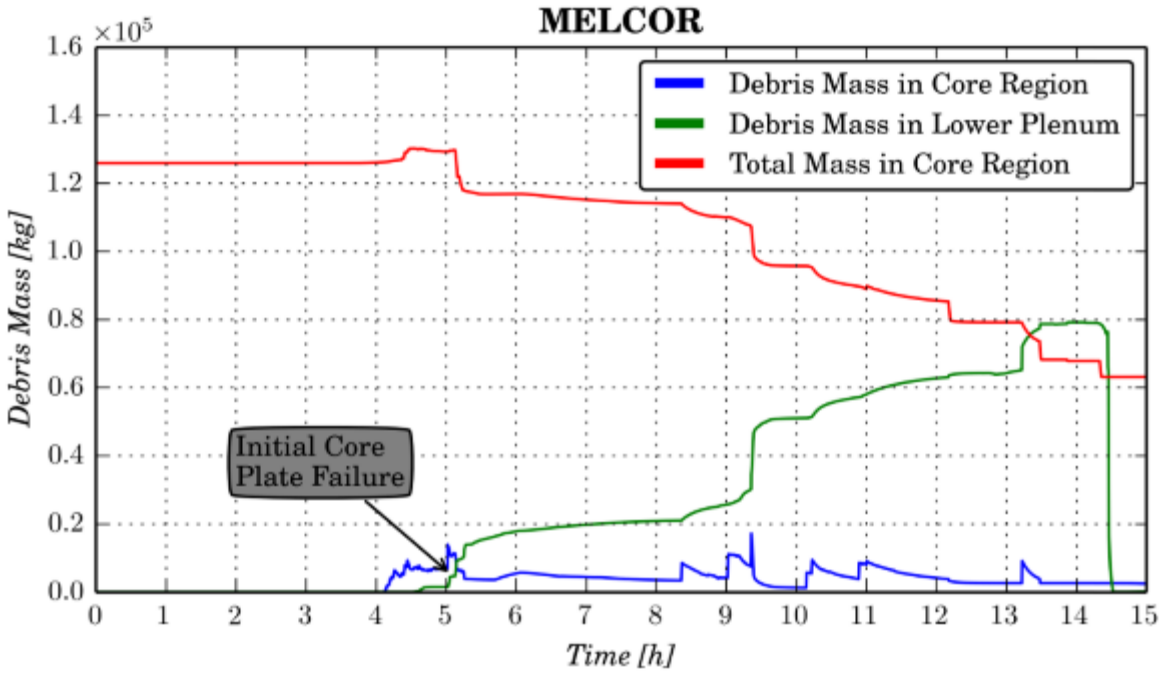

Figure 4-21 Debris Mass within the Core and Lower Plenum for the MELCOR Simulation

4.8 Flow Channel Blockage

As core damage progresses, and during the accident transient, vertical flow through the core region decreases as the fuel fails and becomes relocated to the flow channel. Figure 4-22 shows the minimum ratio of vertical flow area to initial vertical flow area for each ring in the core. Fuel and other failed structures that are relocated to the flow channels in MELCOR can be in the form of either particulate or molten debris, whereas ASTEC uses a single field “magma” that represents particulate debris, molten corium, and associated porosity. Overall, it can be seen that there is more flow blockage in ASTEC than there is in MELCOR. This especially becomes the case after 4.0 hours when ASTEC approaches the minimum porosity allowed by the “magma” field.

For inner rings 1, 2 and 3 in the ASTEC scenario, the total available flow fractional area for steam and gasses decreases from 1.0 to 0.15 between hours 3.5 and 3.75 in the simulation. For ring 4, the flow area becomes significantly degraded after 3.7 hours, dropping to less than 0.3 fractional flow area by 4.0 hours and 0.15 by 4.3 hours. Rings 1, 2, 3, and 4 remain at 0.15 until the end of the simulation. For ring 5, the fractional flow area drops quickly to 0.15 after fuel begins to fail in the outermost ring just after 4.4 hours, then increases slightly to remain at 0.17 until the end of the simulation.

Except for Ring 1, the minimal flow area fraction in MELCOR is typically greater than 0.4. There is never any total blockage of flow channels. The variability in open flow area comes from debris relocation, melting and re-solidification. As the fuel assemblies completely fail during the transient, the flow area returns to its nominal value, indicating that a significant flow area exists through this area of the core.

The main takeaway from these plots is that the flow through the ASTEC core is significantly inhibited compared to MELCOR after 3.5 hours into the simulation. This decrease in available flow area clearly has an impact on the total amount of decay heat that can be removed from degraded and intact fuel material via convective cooling. Figure 3-1 demonstrates that the rate of convective heat transfer decreases after these flow channels in the active core region begin to become blocked. This decrease in convective heat removal leads the cladding temperature to become hotter and thus leads to more Zr oxidation and associated energy release, further fueling the degradation process.

However, if we look at Figure 5-1 in the following Chapter, we can see that the amount of hydrogen generation in ASTEC is unaffected by this reduction in flow area. This indicates that the total flow area remaining after core degradation begins is sufficient to fuel the zirconium oxidation reaction.

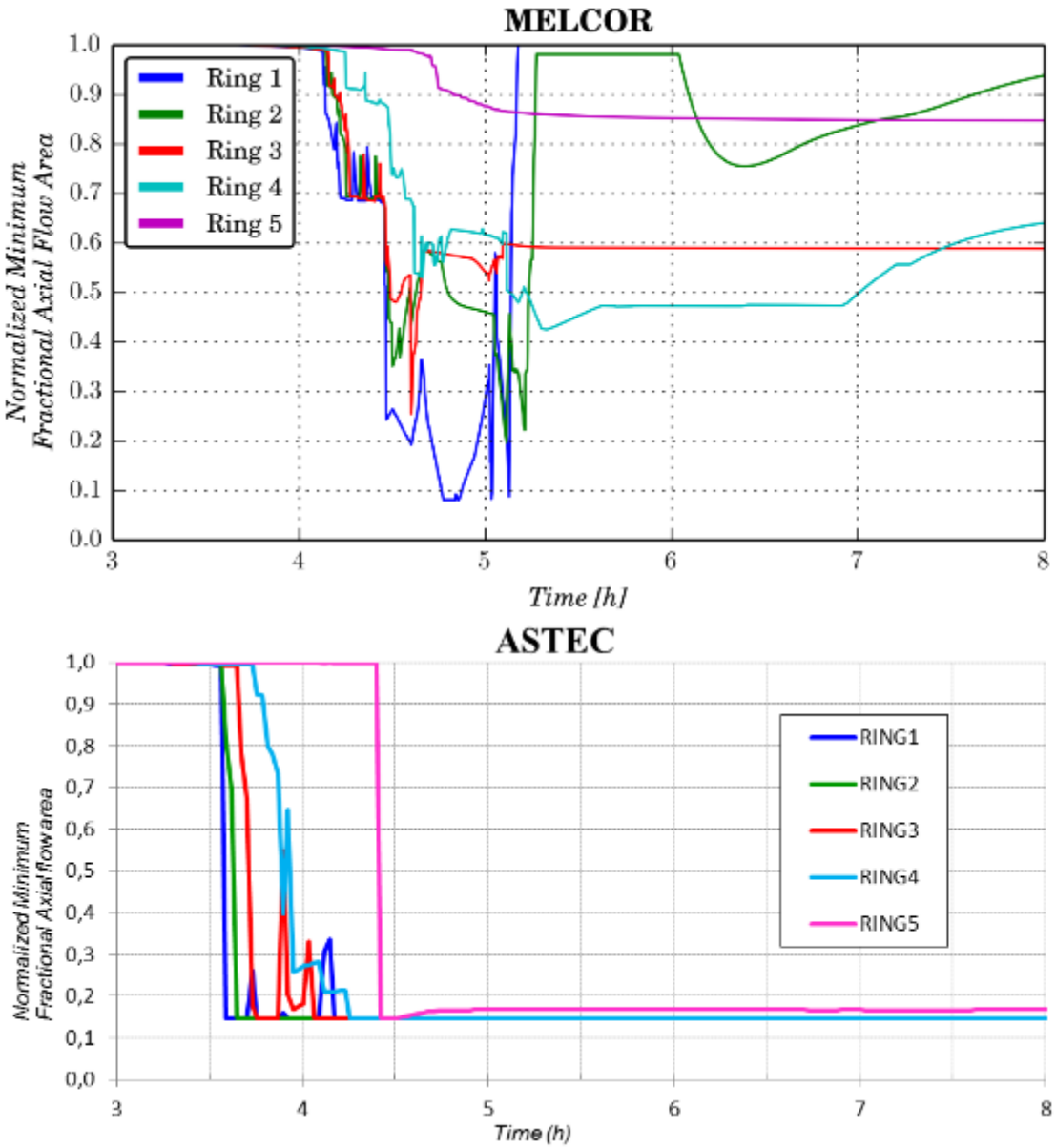

Figure 4-22 Normalized Minimal Fractional Flow Area on a per Ring Basis during the Core Relocation Period of the Accident Scenario (Plots are for Vertical Flow within the Active Core Region)

4.9 Wall to Fluid Exchange Surface

The discussion on flow channel blockage and porosity highlighted significant differences in the flow path for the steam. Another important parameter is the wall-to-fluid surface area for convective heat exchanges and oxidation. In the ASTEC code, each wall (rods, grids, debris) has its own contact surface with fluid. Accounting for degradation, the choice of modelling can greatly affect that surface area and then the physical processes occurring on it. It can have an impact on the possible cooling of debris or the oxidation processes triggered by high temperatures.

The convective surface is represented in a field for the entire core domain (active and passive) except the simplified lower plenum CV (hemispherical part of the lower plenum). To maintain a comparable order of magnitude of the volumetric surface in each ring, the choice was made to express the total convective surface with fluid in a mesh over the volume of mesh (geometrical volume and not fluid volume). That parameter corresponding to a volumetric surface area is expressed in [m^{-1}].

One can see that the wall-to-fluid exchange surface per unit volume varies from 150 m^{-1} to less than 10^{-3} m^{-1}. The choice of modelling used for the debris in ASTEC is presented in Section 4.2.1. The evolution of this surface area per unit volume can be seen in Figure 4-23. At 3.5 hours, the core is divided into two parts: the top part where the volumetric surface area is around 150 m^{-1} corresponding to the active core region, and the bottom zone with a volumetric convective surface around 10 m^{-1} corresponding to the lower plenum.

Concerning the evolution of the volumetric surface area, it is clearly linked to the degradation stage of the fuel rods and the presence or the relocation of debris. Since ASTEC represents a small amount of corium as a film partially covering the intact core structures in a given mesh, the total wall-area-to-volume ratio increases slightly compared to the same configuration without magma. In the meantime, the available volume for the fluid (water and gas) reduces. For an advanced stage of core degradation, meshes in which debris is relocated form a dense zone in which this ratio decreases. It is clearly highlighted on Figure 4-23 from 5.0 hours to the relocation to the lower plenum.

One can see that there is not a direct agreement of the porosity field and the wall to fluid interaction surface field. This is particularly visible at 4.5 hours and 8 hours in the dense portion of the active core region. This is clearly linked to the choice of modelling made in ASTEC and the threshold effect that appears in the transition phase. For instance, when both core structures and debris are present in a mesh and suddenly, due to relocation or melting, only debris or only partial degraded structures remain in the mesh.

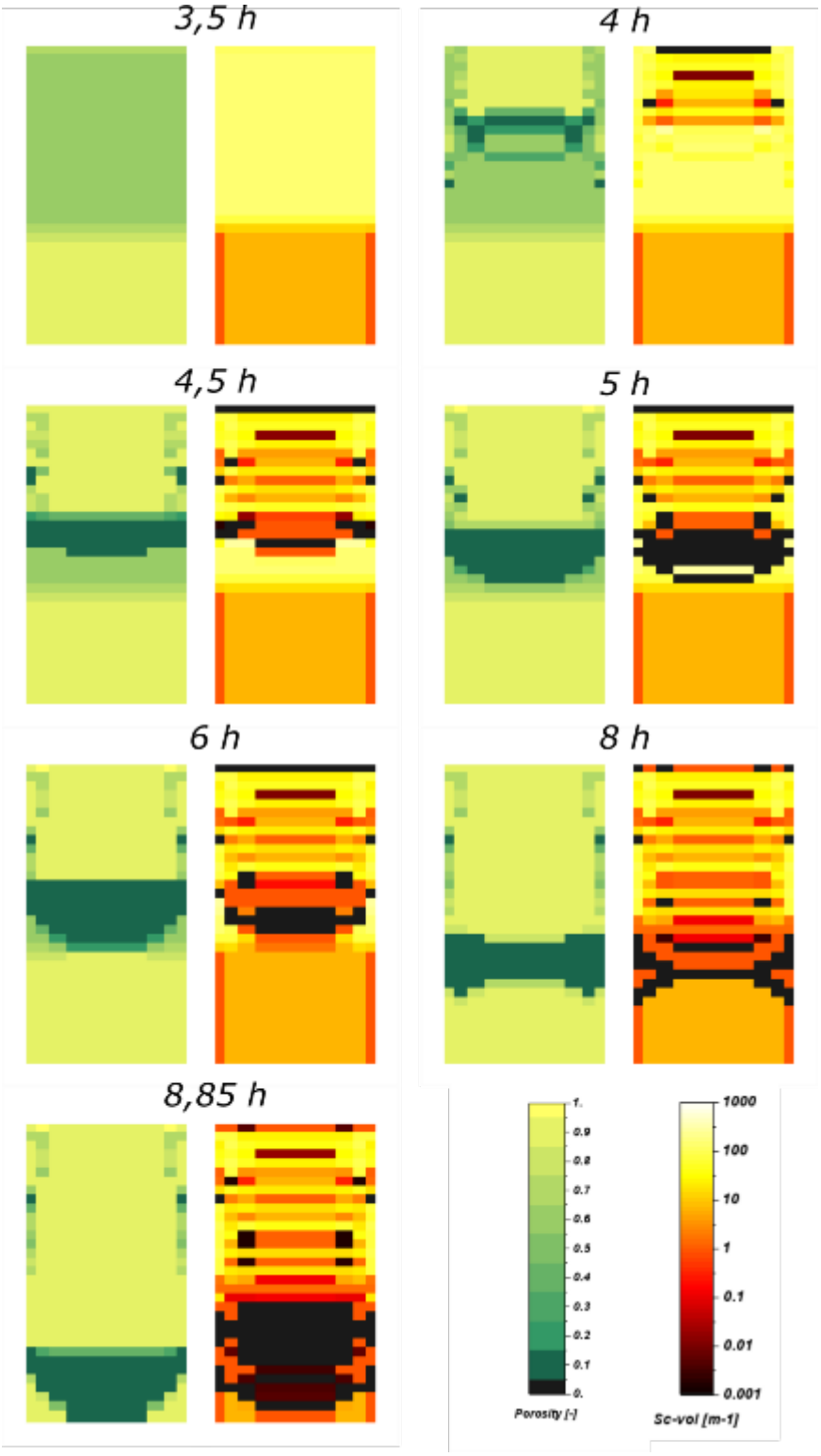

Figure 4-23 Porosity and Wall-to-Fluid Volumetric Surface in Each Mesh of the Core Domain (active + passive) for ASTEC Simulation

5 HYDROGEN, SAFETY RELIEF VALVE AND LOWER PLENUM BEHAVIOR

Hydrogen generation during a severe reactor accident poses significant risks. Reactor containments can be inerted with nitrogen to inhibit any hydrogen combustion. Even if the hydrogen does not combust, the additional partial pressure can over-pressurize the RPV or containment. Because of its gaseous nature, nominal leakage or pressure induced leaks (e.g., drywell head flange failure) can allow hydrogen to seep into the reactor building and accumulate. As evidenced by the explosions in the Fukushima Daiichi Units 1, 3, and 4, this can lead to catastrophic and dangerous consequences. Along with injuring workers, hydrogen combustion can damage reactor building structures, creating release pathways for radiation to leak into the environment. For these reasons, it is important to model hydrogen production when analyzing a severe accident scenario to develop hydrogen build-up mitigation strategies.

Before the reactor pressure vessel is breached, hydrogen is predominately generated by the oxidation of core materials by steam. Zircaloy cladding oxidation produces the majority of the hydrogen during a severe accident. Stainless steel and control rod poison (B_4C) will also oxidize; the hydrogen production from these reactions is important but fractional compared to the amount from Zircaloy oxidation. Because the oxidation reaction is dependent on steam availability, the treatment of steam flow through the core can affect both hydrogen generation rates and the net hydrogen produced. Therefore, debris formation and blockage models as well as core porosity can greatly influence in-core hydrogen generation.

The purpose of this chapter is to discuss the hydrogen production transients observed in MELCOR and ASTEC simulations. Fundamentally, MELCOR and ASTEC use similar approaches to model oxidation. Both codes implement parabolic reaction rate models based on oxidation reaction rates, oxygen diffusion, steam availability, and un-oxidized material availability. Oxidation rates are based on parabolic correlations with constants determined by experimentally derived correlations. However, differences arise in the choice and application of said correlations. (Chatelard, 2014) (Humphries, 2014)

MELCOR and ASTEC both consider the oxidation of Zircaloy structures (cladding, shrouds, and spacer grids), B_4C, stainless steel, and particulate debris. MELCOR also models the oxidation of BWR canisters; no equivalent model exists in ASTEC. (Chatelard, 2014) (Humphries, 2014)

5.1 Overview of Hydrogen Generation in ASTEC

5.1.1 Zr Oxidation

ASTEC employs, for PWR cladding applications, the Cathcart-Pawl, Urbanic-Heidrick, and Prater-Courtright correlations to evaluate oxidation layer growth. Specifically, the correlations specify rate constants for the total oxygen mass gain and ZrO_2 layer thickness. (Chatelard, 2014)

To better allow “best-estimate” PWR studies, IRSN has also created a self-described “homemade” correlation to account for the transition of oxidation rates from 1880 K to 1900 K. The “best-estimate” correlation was developed by re-evaluating available experimental data on the basis of diffusion theory accounting for temperature drops in the oxide layer. (Chatelard, 2014)

A key feature of ASTEC's oxidation package is its detailed, three-layer Zr oxidation model. The three-layer model accounts for the layer thickness of β-Zr, α-Zr(O), and ZrO_2 layers. ASTEC uses mass and layer thickness correlations to evaluate the growth of α-Zr(O), and ZrO_2 layers. Layer growth plays a key role in oxidation rate calculations as it can limit oxygen diffusion into the Zr layers. (Chatelard, 2014)

5.1.2 Stainless Steel Oxidation

Compared to Zr oxidation, stainless steel oxidation is a complicated process. This is a result of the presence of a number of auxiliary elements found in stainless steel (e.g. Mn, Mo, Ti, Si, Nb) in conjunction with the basic alloying elements of Cr and Ni. The presence of these auxiliary elements leads to complex oxide layers. Thus, ASTEC does not use a multi-layer system for stainless steel oxidation. To simplify these reactions, ASTEC treats stainless steel as an alloy composed solely of Fe, Cr, and Ni with fixed mass fractions and solves four stoichiometric oxidation reactions involving said elements. (Chatelard, 2014)

While stainless steel oxidation has some complexity, the fundamental oxidation process is still governed by parabolic rate kinetics using a classical Arrhenius formulation with constants determined by the mass composition of the stainless steel. Depending on the type of stainless steel (i.e., austenitic or ferritic), ASTEC uses data from White or Leistikov. (Chatelard, 2014)

5.1.3 B_4C Oxidation

B_4C oxidation in ASTEC is a straightforward process. B_4C oxidation rates are governed by an Arrhenius type relationship that incorporates the traditional Arrhenius formula in addition to two pressure terms. Based on experimental observations, the partial pressure of steam and total system pressure influence B_4C oxidation rates, hence the additional pressure terms. Coefficients for B_4C oxidation rate are temperature-dependent and were derived from IRSN experiments conducted in 2006. ASTEC does not allow B_4C oxidation until either the control rod cladding totally dissolves from B_4C/stainless steel interactions or the guide tube temperature exceeds a set threshold. (Chatelard, 2014)

5.1.4 MAGMA Oxidation

"Magma", a combination of U, Zr, and O, can also oxidize. "Magma" is formed as cladding and fuel melt and subsequently freezes along core structures. "Magma" contains Zr that can be oxidized in the core for the V2.0 version. "Magma" oxidation is governed by oxygen diffusion through the outer crust layer. (Chatelard, 2014)

5.2 Overview of Hydrogen Generation in MELCOR

MELCOR models oxidation as part of COR package calculations. Like ASTEC, MELCOR employs parabolic rate kinetics in the form of an Arrhenius style equation to solve for oxidation rates. However, there are differences in the correlations used to determine the oxidation rate constants. Zircaloy oxidation is calculated for cladding, for both canister components, and for control rod guide tubes; steel oxidation is calculated for the other structure (SS or NS) components. Both Zircaloy and steel oxidation are calculated for particulate debris. For BWR cores, oxidation of both sides of the canister walls (which may be exposed to differing environments) is modeled. Within MELCOR, there is a minimum oxidation cutoff temperature of 1100 K. (Humphries, 2014)

5.2.1 B_4C Oxidation

There are two options within MELCOR for modeling the reactions of B_4C. The default model, used in this analysis, developed by ORNL for the MARCON 2.1B code (Humphries, 2015) treats only oxidation by H_2O. Irrespective of the modeling option, the B_4C reaction will not begin until the steel control blade sheaths have failed (B_4C is not exposed to steam until failure occurs). Failure is assumed to occur when the mass of intact steel in the control blade component falls below a user-specified fraction of its initial value. The intact steel is consumed by both steel oxidation and dissolution/melting. (Humphries, 2014)

Following failure of the steel, the reaction is permitted to begin if steam or oxygen is available and the B_4C component temperature is above a threshold of 1500 K. MELCOR also limits the fraction of the initial mass of B_4C that is permitted to react. The default maximum reaction consumption fraction of 0.02, which is used in this analysis, was chosen on the basis of experimental observations. This number is significantly lower than what is allowed by ASTEC. (Humphries, 2014)

5.2.2 Zr Oxidation

For Zr-H_2O oxidation, MELCOR solves for the oxidation rate constant using the Urbanic-Heidrick correlations. For the Zr-O_2 reaction, MELCOR evaluates the rate constant using a correlation described in “Spent Fuel Heatup Following Loss of Water During Storage”. (Nourbakhsh, 2002) If both H_2O and O_2 are present, MELCOR maximizes the total oxidation rate (i.e., all oxidation is assumed to be from the gases that would give the highest oxidation rate). Unlike ASTEC, MELCOR does not model oxidation layer growth; however, unoxidized material availability is considered as part of the oxidation rate calculations. (Humphries, 2014)

5.2.3 Stainless Steel Oxidation

Like ASTEC, MELCOR also treats stainless steel as a simplified mixture for oxidation purposes. However, MELCOR only considers oxidation energy from Fe and Cr reactions. Oxidation energy release is governed by weighting the Fe and Cr reaction energies by the relative masses of the components in the steel. The other chemical components of the stainless steel are ignored. MELCOR evaluates the stainless steel oxidation with O_2 using constants from the study: “Fifth Annual Report – High Temperature Material Programs, Part A.” For stainless steel/H_2O oxidation reactions, MELCOR uses White’s parabolic rate law to determine reaction rate constants. (Humphries, 2014)

5.3 Hydrogen Production During Core Melt

While hydrogen generation through an intact core is relatively straightforward, the relocation of core material and flow path availability introduces both complexity and uncertainty into oxidation rate calculations during core melt. Specifically, debris relocation and channel blockage can greatly limit steam availability. So, even if MELCOR and ASTEC model oxidation in a similar fashion, the total oxidation can significantly vary due to core degradation and thermal-hydraulic treatment within each code. (Humphries, 2014) (Chatelard, 2014)

5.3.1 Increased Oxidation Area from Material Failure

For cladding and BWR canisters, all oxidation initially occurs on the outer surfaces as steam cannot reach the inner Zr. Because of the high temperatures and pressures during a severe accident, cladding and canisters can and will fail through processes such as ballooning. When this occurs, the inner surfaces are exposed to steam, pending availability, and will begin to oxidize as well. Failure to account for this oxidation process can lead to lower oxidation energy and hydrogen mass predictions.

While MELCOR does not have an explicit shattering model, it does consider increased oxidation surface area from candling and canister failure. The oxidation surface area is equated to the heat transfer area at a given node. The new heat transfer area is calculated based on the volume of conglomerate debris (e.g., frozen debris from candling) within a flow channel. MELCOR assumes that there is always some flow through debris though. This modeling practice is in line with ASTEC. (Humphries, 2014) (Chatelard, 2014)

5.3.2 Particulate Debris

During a severe accident, debris beds from failed material can accumulate in the lower plenum, in bypass channels, and on core support structures. If steam can flow through these debris beds, debris oxidation can occur. Debris in the lower plenum can also oxidize from quenching if some pool is available. MELCOR and ASTEC both model particulate debris oxidation. (Humphries, 2014) (Chatelard, 2014)

MELCOR treats debris oxidation using the same parabolic kinetic principles and numerical algorithms as they do for cladding. Both codes treat particulate debris as spheres and solve the parabolic rate equations with respect to a spherical geometry (as opposed to a cylinder for cladding). For this simulation, ASTEC does not model particulate debris or its oxidation in the core region. For the debris beds formed in the lower plenum, no chemical interaction is computed. (Humphries, 2014) (Chatelard, 2014)

In ASTEC, particulate debris only forms if a molten jet interacts with a pool. That is, no debris forms in the core region. This implies that debris oxidation in ASTEC only occurs in the lower plenum from quenching. However, oxidation of “magma” in the core region also occurs. There are a number of possible effects that may arise from this. Conversely, because MELCOR allows debris oxidation in the core region, there could be less debris oxidation in ASTEC. This is discussed further in Section 5.2. (Humphries, 2014) (Chatelard, 2014)

5.3.3 Post-Slump Oxidation

Debris quenching in the lower plenum pool can also lead to oxidation. Much like debris oxidation, the core degradation models in ASTEC and MELCOR directly impact the amount of debris in the lower plenum and, by association, the amount of debris oxidation. Core degradation models are presented in Chapter 4. MELCOR models debris formation in the fuel region from candling and fuel assembly collapse. Using its relocation physics model, based on physical parameters such as debris falling velocity, MELCOR allows debris to relocate downwards where it can gather on core support structures or in the lower plenum. MELCOR allows debris in either location to oxidize. Since MELCOR does model core support failure, this debris can also drop into the lower plenum if the support structures fail. ASTEC does not model particulate debris formation unless molten core material interacts with water. Thus, all debris created in ASTEC is assumed to be in the lower plenum. (Humphries, 2014) (Chatelard, 2014)

5.4 Total In-Core Hydrogen Generation

The total hydrogen mass produced by both ASTEC and MELCOR is shown in Figure 5-1. Included are the individual materials that are oxidized, including B_4C, zirconium, and stainless steel.

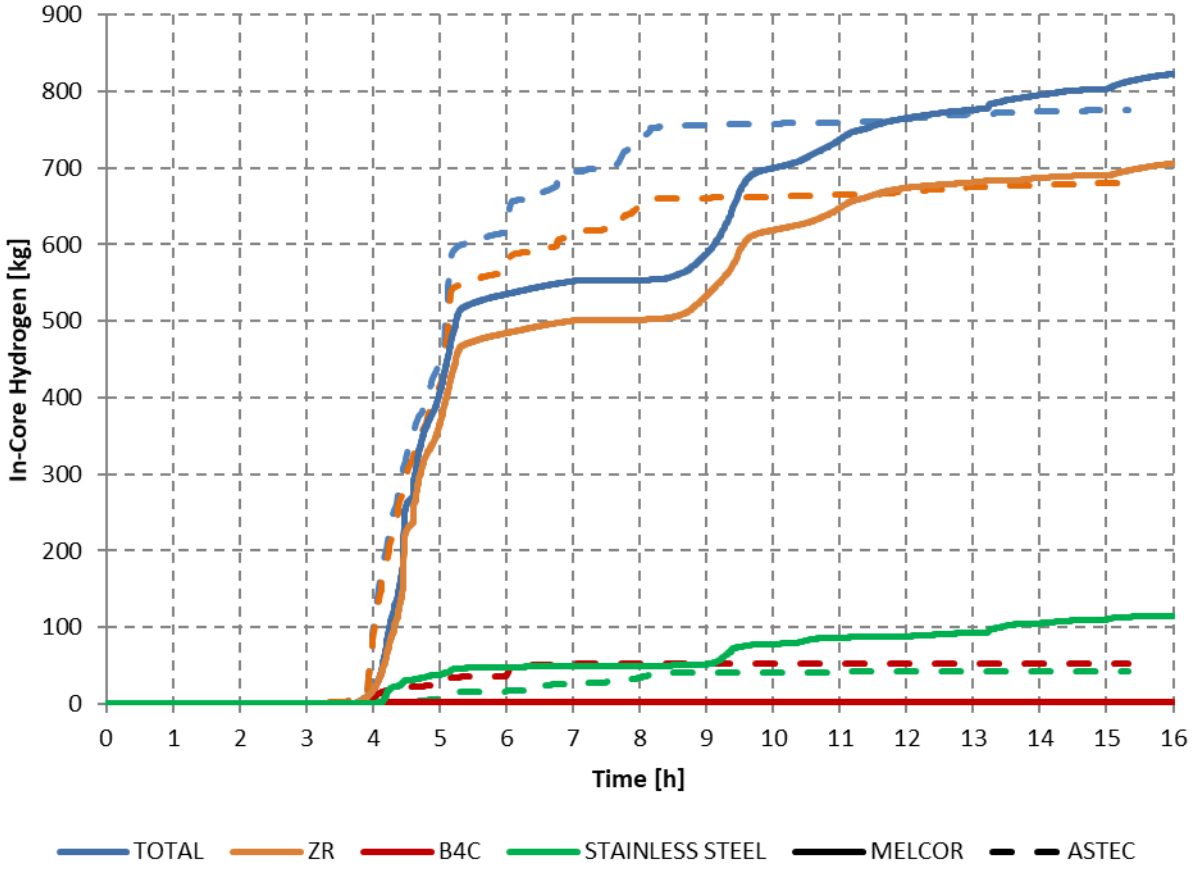

Figure 5-1 Total and Constituent Hydrogen Generation in Both ASTEC and MELCOR

5.4.1 ASTEC Transient

As seen in Figure 5-1, the onset of oxidation occurs at 2.8 hours in ASTEC. At 2.6 hours, the RPV water level predicted by ASTEC drops sharply, leading to rapid fuel uncovery. Compared to MELCOR, the ASTEC fuel temperatures increase faster, initiating the oxidation reaction at an earlier time.

From 5.0 hours onwards, MELCOR and ASTEC significantly diverge in their predictions. Between 5.0 to 5.2 hours, ASTEC predicts a sharp rise in the hydrogen mass. Then, ASTEC models a relatively linear increase in hydrogen inventory until 8.3 hours with a two-step increase at 6.0 hours and 7.6 hours. From 8.3 hours to the end of the simulation, ASTEC predicts a modest increase of 19 kg hydrogen. Overall, a total of 776 kg is produced in the ASTEC simulation.

The bulk of hydrogen production in the ASTEC accident sequence occurs from roughly 3.7 hours to 5.2 hours. During this time, there is significant melting of fuel which leads to “magma” formation. Also, the fuel temperatures during this time rise sharply from around 525 K to 2500 K. ASTEC does not represent any mechanical loss of integrity of the fuel rod; the fuel rods are maintained in meshes until their temperatures reach the melting temperature of oxides (UO_2-ZrO_2) reduced according to ASTEC recommendations to 2500K. That temperature acts as a criterion for the loss of integrity of rods. As a consequence, it leads to significant differences compared to the MELCOR simulation. In MELCOR, the fuel rods lose their integrity based on a time and temperature criterion. Then, rods are fragmented into particulate debris which is drained to the bottom. This allows overheated metallic material (cladding) to leave the hot spot in the core and limits oxidation. In the ASTEC code, the fuel and cladding are overheated up to 2500K before leaking. As a consequence, the Zr cladding is maintained in a hot atmosphere and this leads to a sharper oxidation rate compared to the one seen in MELCOR simulation.

There are two noticeable transients in hydrogen production from 5.2 to 8.3 hours. The first occurs at 6.0 hours. This transient corresponds to increased “magma” formation and fuel failure. Also, the molten pool begins to migrate downwards around this time. Given that the hydrogen increase is primarily from Zr and B_4C oxidation, this suggests that additional fuel failure, possibly at a lower core elevation, is responsible for this transient. The second jump in hydrogen production is around 7.6 hours. The amount of “magma” begins to increase at 7.5 hours.

The SRV seizure at 7.0 hours and core slump at 8.9 hours both significantly impact hydrogen production in ASTEC. As expected, oxidation slows down after the SRV seizure as the RPV rapidly depressurizes. Oxidation resumes as steam builds up in the RPV. Following the core slump, oxidation essentially halts; only 23 kg of hydrogen is produced for the remainder of the accident (approximately 7.5 hours). ASTEC does not model oxidation within the hemispherical portion of the lower head, therefore this additional hydrogen is due to remaining structures still held up within the RPV being oxidized by water still trapped within the downcomer region.

Stainless steel oxidizes in ASTEC in a gradual but persistent manner. Stainless steel oxidation begins around 4.5 hours and proceeds with a linear fashion. Notably, the stainless steel oxidation rate appears to increase just before the core slumps. As core support plate failure causes core slumping, the increase of stainless steel oxidation is from core support plate and other supporting structures. Stainless steel oxidation ceases post core slump. As Zr oxidation continues, this implies that the lack of stainless steel oxidation is from material unavailability.

The B_4C oxidation trend is relatively straightforward. After the onset of B_4C oxidation at 3.9 hours, B_4C steadily oxidizes with brief jumps at 5.1 and 6.1 hours. Since these jumps occur at the same time the Zr oxidation rate increases, it is likely that they share similar underlying causes. After 6.1 hours, B_4C oxidation halts. Like stainless steel, continued Zr oxidation suggests that the discontinuation of B_4C oxidation is from a lack of unoxidized material.

5.4.2 MELCOR Transient

Oxidation begins in the MELCOR simulation at 3.6 hours and continues steadily until 5.2 hours. After 5.2 hours, hydrogen production slows and eventually plateaus when the SRV seizes at 7.0 hours. Unlike ASTEC though, oxidation does not resume in MELCOR until 1.5 hours after the SRV seizes. When oxidation does resume, it follows the same pattern seen from 3.6 hours to 7.0 hours. There is exponential hydrogen production from 8.5 hours to 9.6 hours followed by a steady linear increase until the simulation terminates.

There are three points of interest in the hydrogen production plot for MELCOR at 5.2 hours, 8.4 hours, and 9.5 hours respectively. A brief discussion on these points follows. The inflection points at 5.2 and 9.5 hours relate to fuel assembly collapse in ring 1 and core slumping respectively. At these points, oxidation slows from exponential to linear growth. At 8.4 hours, fuel assemblies in ring 2 collapse. Unlike the collapse of ring 1 fuel, assembly collapse in ring 2 spurs oxidation, leading to an hour-long period of exponential hydrogen generation. While it is unclear as to what induces these responses, a key takeaway is that core degradation and material relocation have strong impacts on MELCOR oxidation calculations. It is interesting to note however that the oxidation of stainless steel becomes quite rapid as the melting point of the steel is approached.

Although MELCOR oxidizes supporting and non-supporting stainless steel (definitions available in MELCOR literature), stainless steel oxidation in MELCOR is coupled to support plate degradation. The onset of stainless steel oxidation occurs at 4.2 hours when the upper tie plate initially fails. Stainless steel oxidation steadily progresses until 5.2 hours. After 5.2 hours, stainless steel oxidation essentially stops. Oxidation resumes at 9.3 hours, or just before the core slumps. The rise in stainless steel oxidation could be from debris quenching as the support plate fails, debris created from the failing support plate, or from the support plate itself oxidizing as unoxidized material is exposed. A similar transient occurs at 13.3 hours when more fuel collapses in Ring 2. Much like Zr, core degradation appears to primarily influence stainless steel oxidation.

MELCOR predicts virtually no H_2 production from B_4C oxidation. This is because the MELCOR default is to allow only 2% of initial B_4C melt to be oxidized, reflecting the expected behavior in BWR control blades where the B_4C-Fe eutectic results in blade liquefaction at about 200K below the normal stainless steel melting point. Oxidizing B_4C would be relocated to cooler regions as the blade temperature approaches about 1500K, thereby limiting the total about of boron carbide that can oxidize.

5.5 Hydrogen Generation by Radial Ring

The amount of in-core hydrogen generated in each radial ring in both MELCOR and ASTEC is presented in Figure 5-2. It can be seen that in both MELCOR and ASTEC, the ring with the least amount of hydrogen generation is the innermost ring: ring 1. Additionally, both codes predict the highest amount of hydrogen generation in the 3rd ring of the core. In both ASTEC and MELCOR, the second and fourth rings track one another. However, the total hydrogen generated in ASTEC is near 180 kg per ring, while in MELCOR 145 kg per ring is generated. The ASTEC hydrogen generation plots plateau after relocation to the lower plenum. SRV discharge significantly decreases and hydrogen generation ceases. ASTEC V2.0 does not model oxidation in the lower plenum.

Clearly divergent behavior can be seen in the fifth ring of the core. Just after 4.0 hours into the simulation, hydrogen generation increases rapidly in the ASTEC simulation. Then the generation rate plateaus within thirty minutes. MELCOR shows a hydrogen generation rate, also beginning just after 4.0 hours. At 7.0 hours, the hydrogen generation rate plateaus before again resuming just before 9.0 hours. This timing corresponds to the initial fuel assembly failure timings in both the third and fourth rings in MELCOR. It is postulated that the relocation of debris from these assemblies and subsequent quenching generated enough steam to start oxidation once again. After ~10.3 hours the water in the lower plenum is completely evaporated in the MELCOR simulation. After this point, subsequent oxidation does not result from additional

steam generation. In fact, SRV discharge plateaus after this point. Residual steam may be present in the RPV, fueling the reaction of remaining core structures.

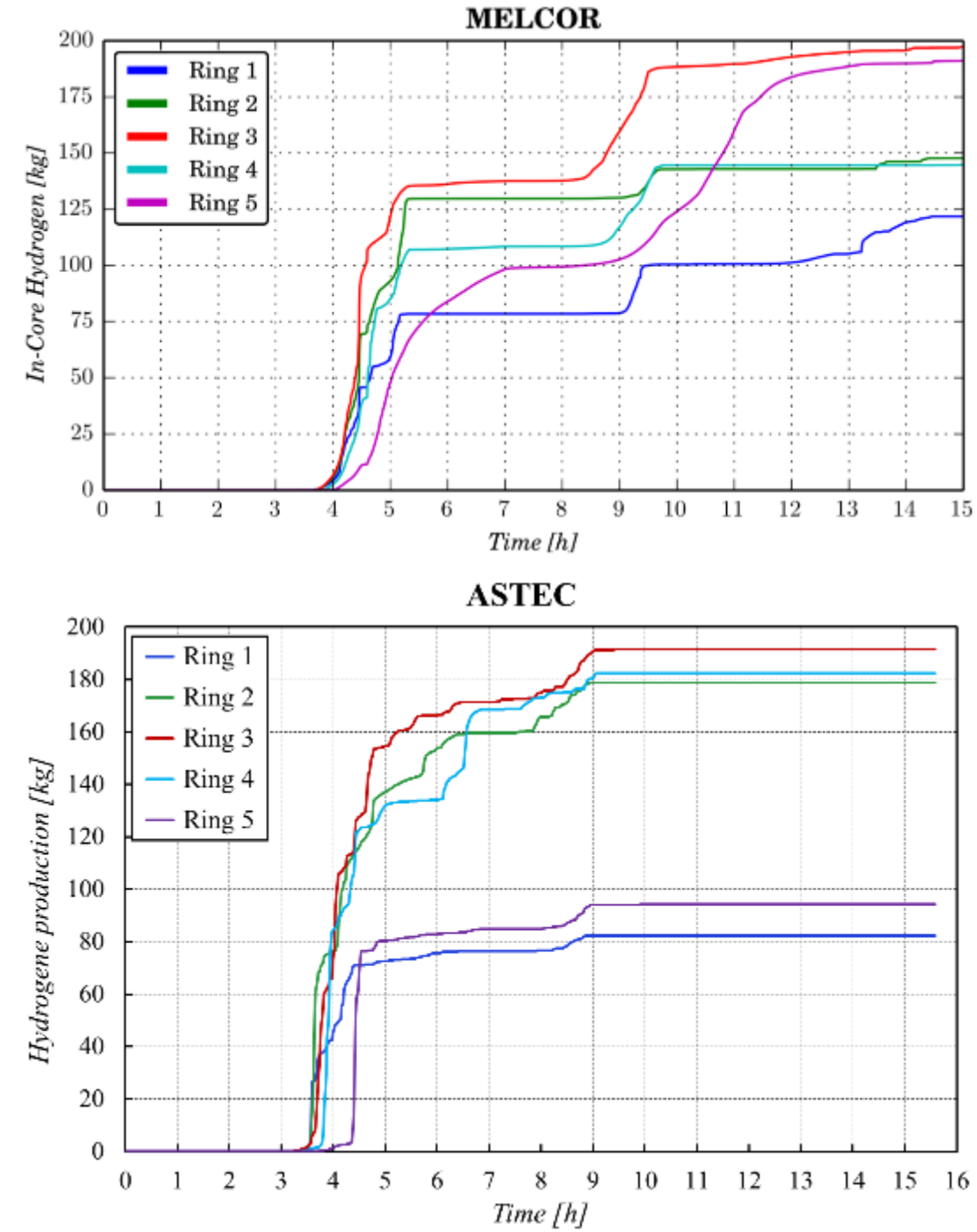

Figure 5-2 In Core Hydrogen Generation by Ring for Both the ASTEC and MELCOR Simulations

5.6 SRV Behavior

This section presents and compares the behavior of the safety relief valves in both ASTEC and MELCOR. Total SRV discharge and hydrogen SRV discharge for both MELCOR and ASTEC are shown in Figure 5-4.

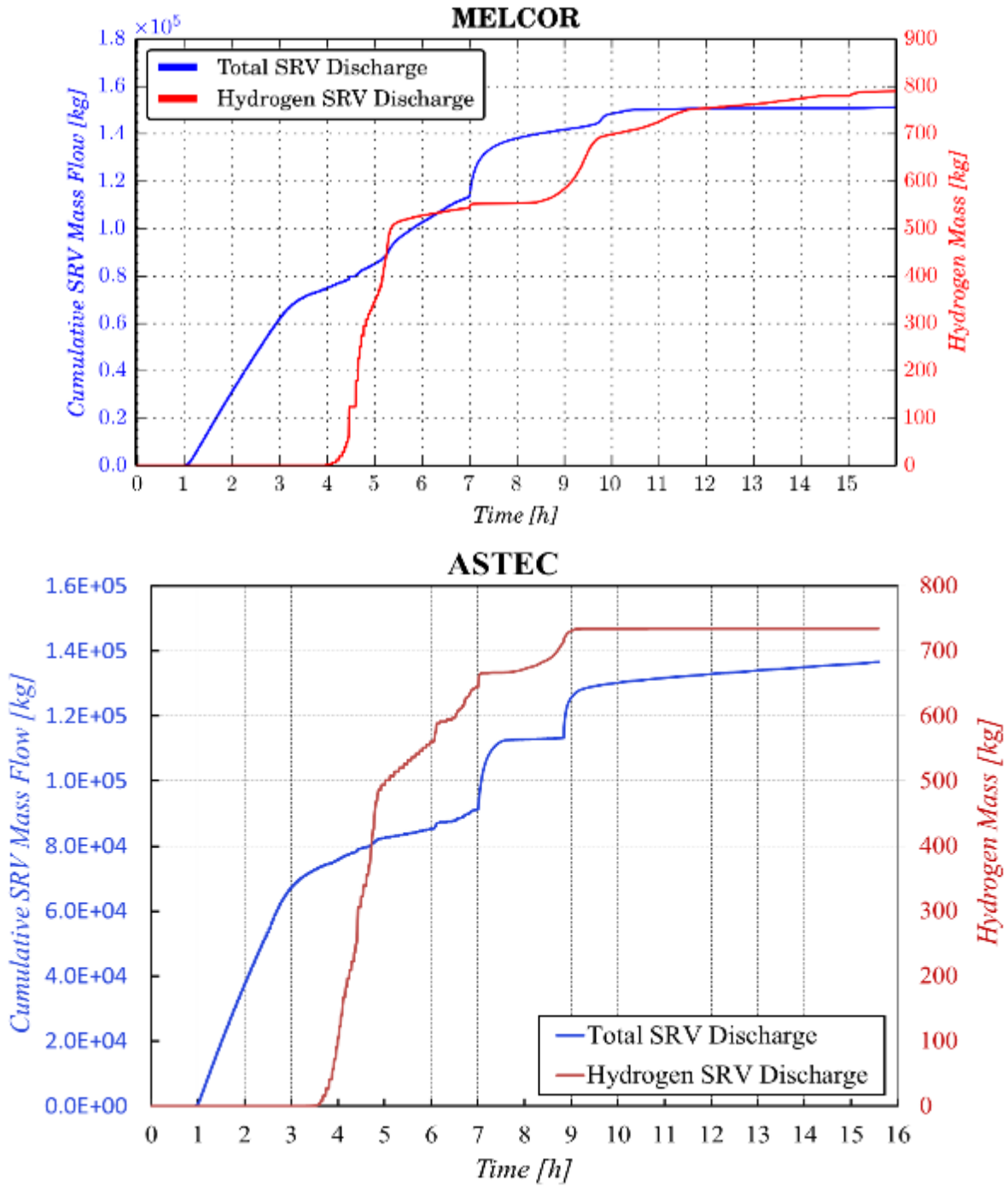

Figure 5-3 Total SRV Discharge and Hydrogen SRV Discharge for Both the ASTEC and MELCOR Simulations

SRV discharge begins at 1.0 hours, which is the time when the SRV begins to cycle. The total discharge predicted by both codes is in close agreement until 5.0 hours. At this time, MELCOR begins to predict more total discharge than ASTEC; this behavior continues through the remainder of the simulation and is discussed later in this section. SRV seizure causes a spike in the total discharge as rapid depressurization forces steam out of the stuck valve. Quenching during the core slumping event also generates a spike in total discharge.

In MELCOR, debris from candling and fuel assembly collapse can relocate to the lower plenum where it is subsequently quenched. The ASTEC core slumping event does not occur until 8.8 hours into the simulation, and there is not fuel relocation to the lower plenum before this point. This means that the MELCOR simulations see significant quenching in the lower plenum much earlier than ASTEC. This leads the total SRV discharge for the MELCOR calculation to be higher after 5.0 hours.

After SRV seizure, the total discharge in MELCOR continues linearly, likely from continued quenching in the lower plenum. The total ASTEC discharge ceases after a SRV, indicating a lack of steam production. Discharge in ASTEC then continues again after the core slump. This implies that there is minimal steam generation (and pool heating) in the lower plenum in ASTEC until the core slumps. The response magnitude after core slumping also varies across each code. The response is governed by the RPV water inventory. The MELCOR RPV experiences total dryout after the core slump as quenching boils the remaining water away. The continuous discharge after the core slumps in ASTEC is due to steam generation of water remaining in the downcomer.

As expected, the hydrogen discharge is proportional to the amount of hydrogen generated in each simulation. The same trends discussed in the oxidation section are likely responsible for the hydrogen discharge behavior. It is worth noting that all hydrogen in the ASTEC simulation escapes the RPV. MELCOR predicts that a few kilograms of hydrogen remain in the RPV at the end of the accident sequence. But hydrogen production still continues in the MELCOR simulation. It is possible that hydrogen is being produced at a slightly faster rate than it can exit through the SRV at the end of the simulation time.

Figure 5-4 shows the mass flow rate through the SRV during the accident sequence, serving as a supplement to the previous discussion.

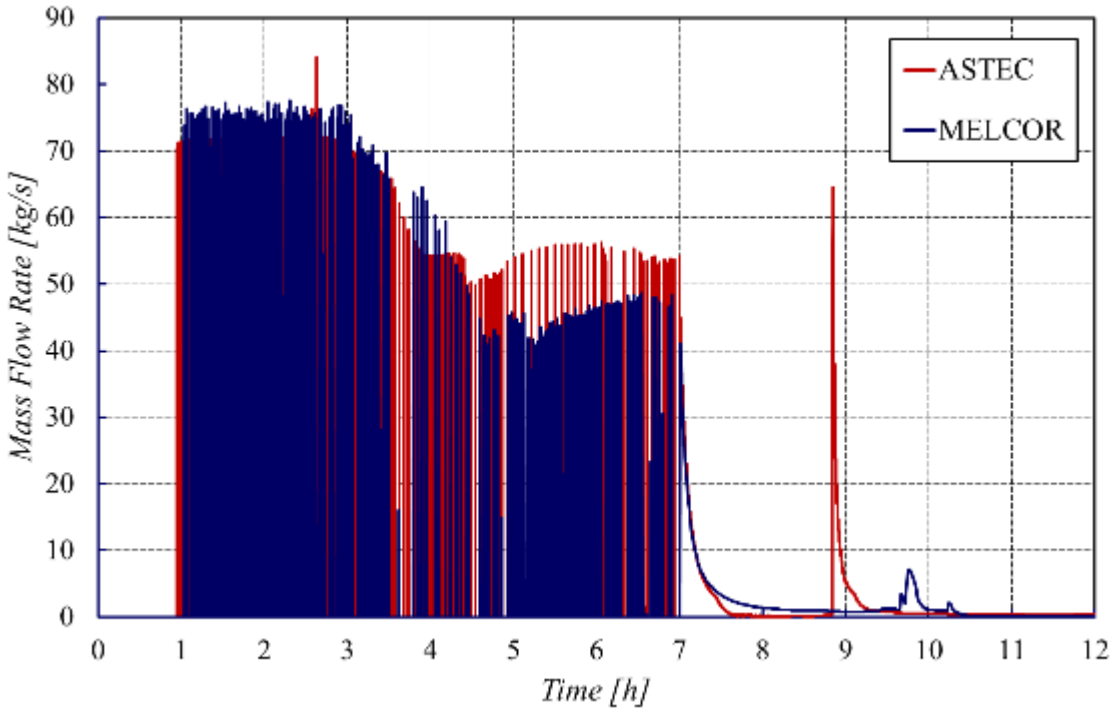

Figure 5-4 SRV Mass Flow Rate for Both the ASTEC and MELCOR Simulations

The mass flow rate reflects the rate of steam generation in each core. As more steam is generated, the pressure increases in the RPV, triggering the activation of the SRV. MELCOR exhibits a constant cycling rate. This implies steady steam generation in the MELCOR simulation.

The core slumping response is proportional to the amount of material that slumps. In ASTEC, the entire core mass effectively slumps leading to a large amount of steam generation and mass discharge. Due to candling and assembly collapse, less mass slumps in MELCOR. Also, the RPV water inventory in MELCOR is lower than ASTEC prior to core slumping, and the MELCOR RPV completely dries out post-slump. For these reasons, less steam is generated in the MELCOR core slump; hence the lower mass discharge rate.

5.7 Lower Plenum Treatment

Within the lower plenum, both MELCOR and ASTEC treat particulate debris. Within ASTEC, corium slumping to the lower plenum can lead to the formation of a debris bed, which is caused by fragmentation of the molten material as it is quenched. When in the lower plenum, a debris bed will form both at the bottom of the plenum and on the top of the corium present. In addition to the particulate debris, ASTEC will form an oxide pool layer with a crust. Above this oxide layer is a metallic layer. It is important to note that the thermal conductivity of the metal layer is much higher than that of the oxide crust. (Humphries, 2014) (Chatelard, 2014)

This leads heat to be removed more quickly from the metallic layer than the oxide pool. Subsequently, more heat is transferred to the sides of the lower head as opposed to its bottom. This leads the lower head to fail along the side and not at the bottom. Figure 5-5 shows a representation of the lower plenum within ASTEC; all relevant layers within the lower plenum

are shown. Figure 5-6 shows a snapshot of the ASTEC transient at 15.6 hours, just before lower head failure. The different layers in the lower plenum can be seen, which are at different temperatures. The temperature of the lower vessel head can also be seen. The higher temperatures are along the side of the vessel and not the bottom. These higher temperatures accelerate failure. (Chatelard, 2014)

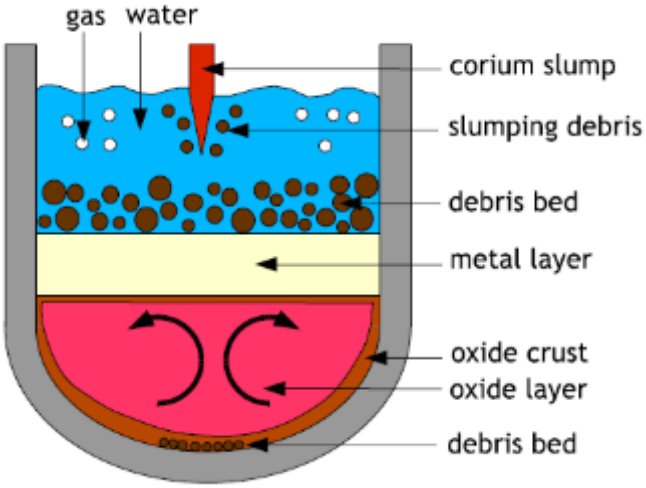

Figure 5-5 Representation of Lower Plenum Characterization in ASTEC

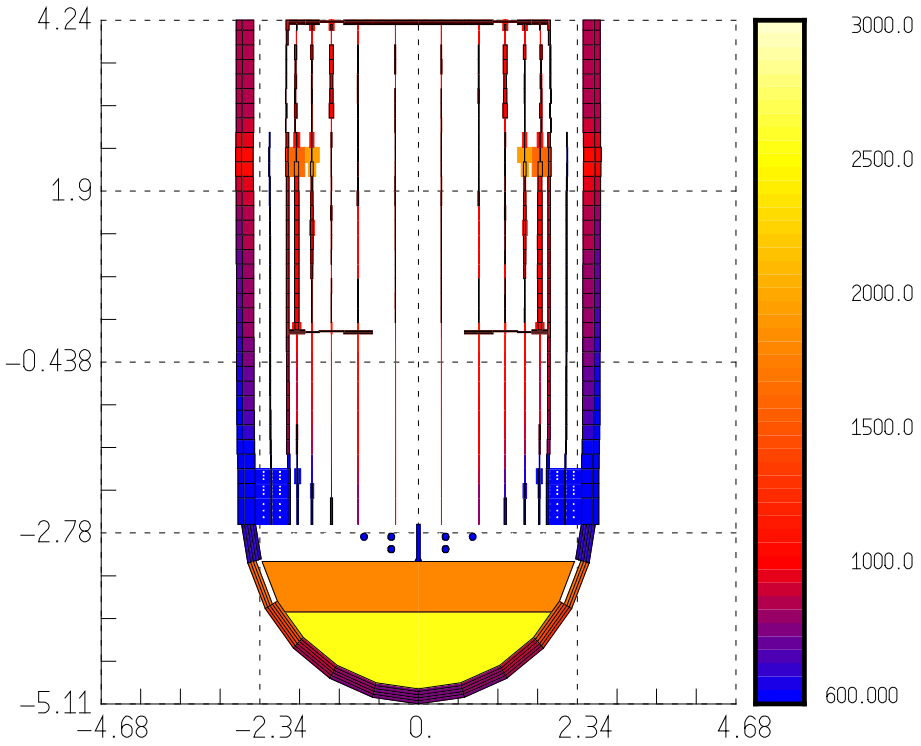

Figure 5-6 Snapshot of Core Degradation Transient, Showing the Temperature Field in the RPV in K at 15.6 hours into the ASTEC Simulation immediately before Lower Head Failure

Similarly, a representation of the lower head model for MELCOR can be seen in Figure 5-7. Within MELCOR, particulate debris and molten pool layers are modeled similarly to how they are modeled within the core region. Within the formed molten pools, there is natural circulation. Heat is also transferred from formed molten pools to particulate debris and the lower head. However, MELCOR generally does not predict molten material formation in the lower plenum for BWR calculations. (Humphries, 2014)

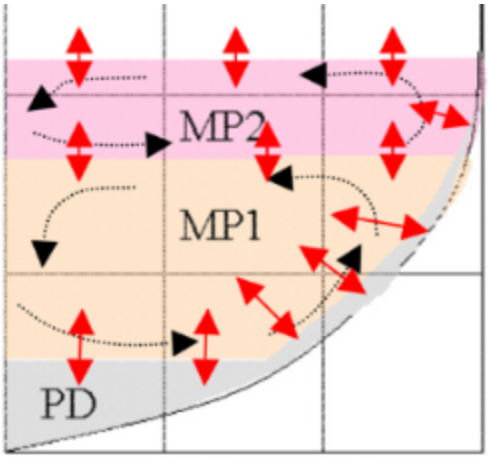

Figure 5-7 Representation of Lower Plenum Characterization in MELCOR (Humphries, 2014)

A snapshot of the core degradation transient at 14 hours in the lower plenum can be seen in Figure 5-8 for the lower plenum region. It this snapshot, it can be seen that there is a large amount of particulate debris (green), minimal molten material (red), and minimal remaining support structures (yellow).

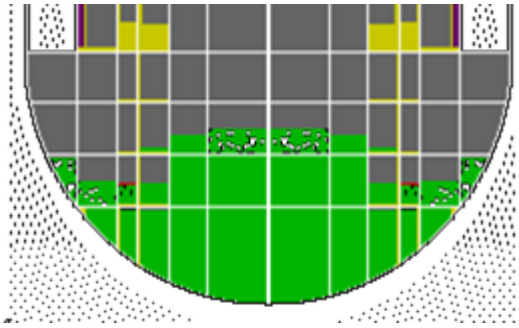

Figure 5-8 Snapshot of Core Degradation Transient in the Lower Plenum Region Showing Particulate Debris Buildup in the Lower Plenum at 14.0 hours into the MELCOR Simulation

5.8 Lower Head Modeling and Failure

Both ASTEC and MELCOR represent the lower plenum similarly. Radial node locations are specified by the user. Then in each radial location a 1D mesh is applied from the internal face RPV-facing side to the external PCV-facing side. This nodal/mesh treatment allows the codes to accurately model the thermal and mechanical stresses on them. Both codes model the stress applied by RPV internal pressure and the stress resultant from structures and mass supported by the lower head. Additionally, both codes take into account thermal stresses. MELCOR, in particular, uses a Larson-Miller expression to model vessel fatigue and failure. A

characterization of the model used for the lower head for both MELCOR and ASTEC can be seen in Figure 5-9. (Humphries, 2014) (Chatelard, 2014)

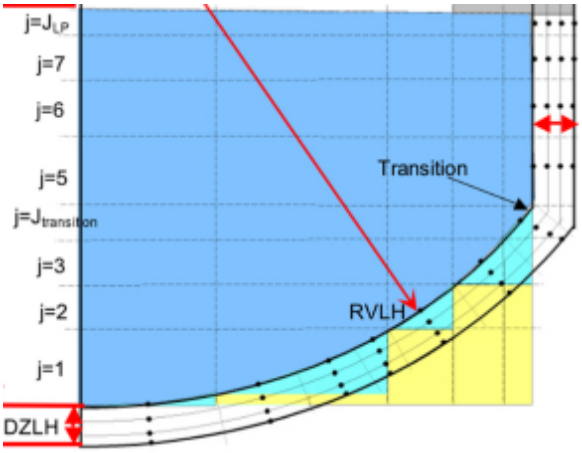

Figure 5-9 Characterization of Bottom Vessel Head Modeling in MELCOR Showing Different Radial Nodes and Discretization within the Shell (Humphries, 2014)

The failure of the lower head in both MELCOR and ASTEC was a result of both thermal and mechanical stress. At the time of lower head failure, in both codes, a significant portion of corium was within the lower plenum placing stress on the lower head. However, the vessel had depressurized by the time of lower head failure. Therefore, it can be concluded that the primary contributor to lower head failure was elevated temperatures. The temperatures in both MELCOR and ASTEC of the hottest node approached the melting temperature of the lower head steel. This can be seen in Figure 5-10 for the MELCOR simulation and Figure 5-11 for the ASTEC simulation.

It should be noted that the failure location of the lower head was different in both MELCOR and ASTEC. MELCOR failed the lower head at the bottom of the RPV, while ASTEC failed the lower head on the side. This can be attributed to ASTEC's lower plenum model, which creates a metallic layer with a higher thermal conductivity on top of the oxide pool layer. That effect is clearly linked to the amount of molten steel in corium and the rapid increase of temperature that can be seen on the Figure 11.

The melt of bottom internals leads to an increase in the fraction of metal in the corium layer and thus the heat flux to bottom head. This leads to more heat transfer to the lower head wall and failure. MELCOR predicts particulate debris within the lower plenum. This particulate debris is better cooled than the ASTEC corium, and takes significantly longer to fail the lower head after the first fuel relocation to the lower plenum. The first relocation to the lower was at 4.5 hours in the MELCOR simulation. At 14.4 hours, the lower head fails in MELCOR. The delay is a result of both increased debris coolability and reduced heat transfer from the particulate debris to the wall of the RPV. As a conclusion, it can be seen that the rupture is globally predicted at the same time for both simulations, but both thermal and mechanical loads are clearly different.

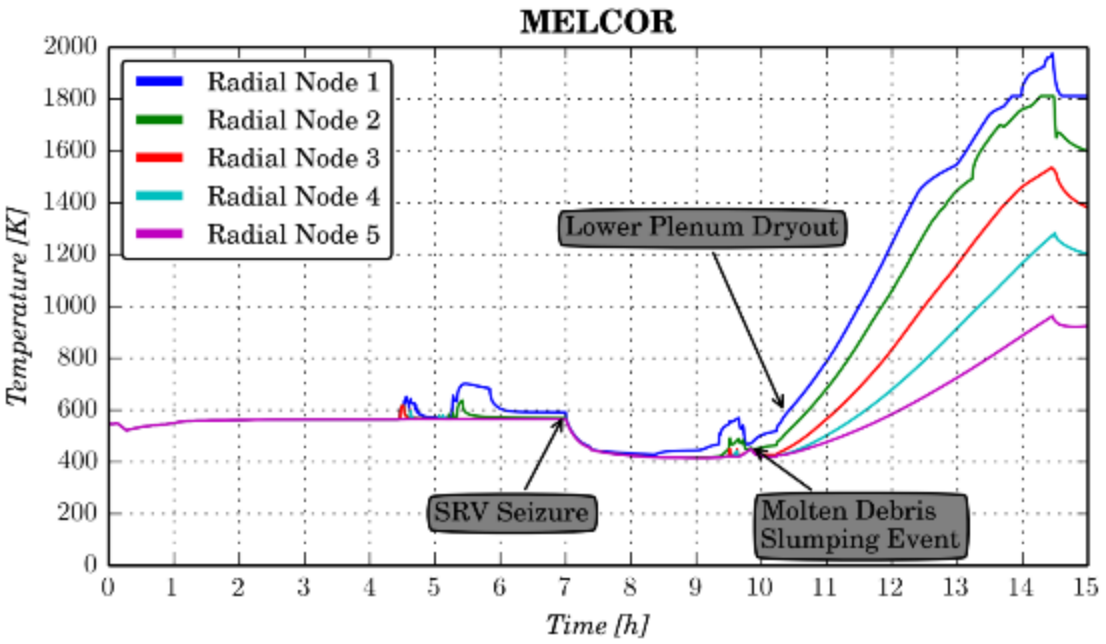

Figure 5-10 Temperature of Inner Mesh of Lower Head Radial Nodes within the MELCOR Simulation (Level 1 corresponds to the bottom of the lower head, while level 6 corresponds to the top of the lower head)

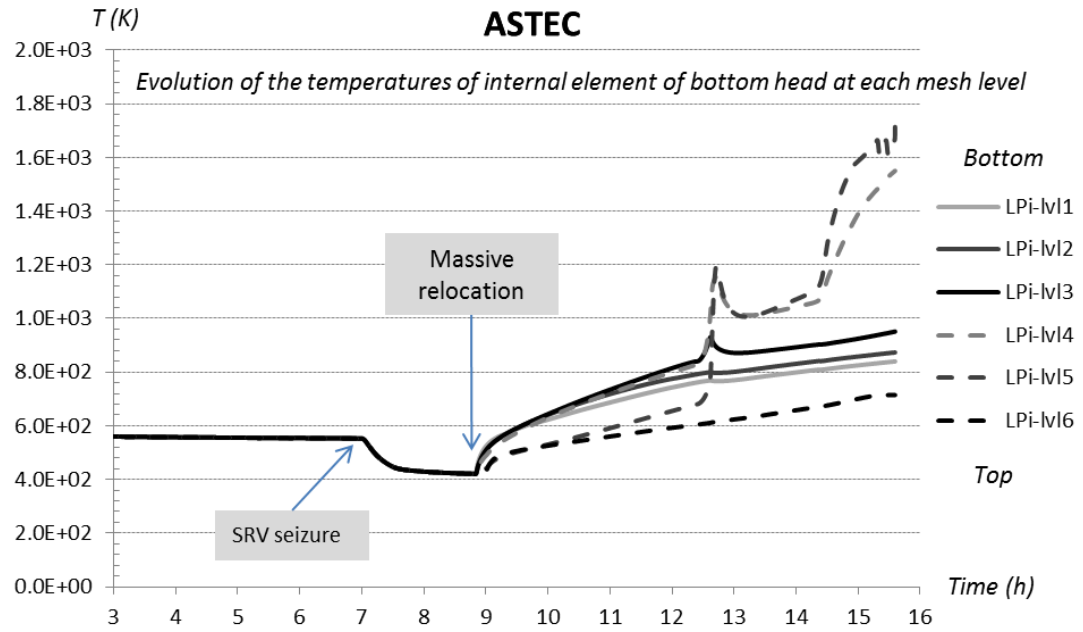

Figure 5-11 Temperature of Inner Mesh of Lower Head Radial Nodes within the ASTEC Simulation (Level 1 corresponds to the bottom of the lower head, while level 6 corresponds to the top of the lower head)

6 SUMMARY AND CONCLUSIONS

6.1 Plant and System Behavior

It can be seen as the accident progresses that the amount of heat removal from convective heat transfer is higher in MELCOR than in ASTEC after the point of initial cladding oxidation. Prior to this point nearly all decay heat was removed via convective heat transfer, which includes steam cooling. ASTEC has more radiative heat loss compared to MELCOR for the first ten hours of the transient; however, after ten hours this trend reverses. Total oxidation energy in both codes is similar, with MELCOR showing slightly more oxidation than ASTEC.

After 7 hours into each simulation, the SRV seizes, resulting in a rapid depressurization of the RPV. Prior to this point both codes show close agreement in RPV pressure. While both codes calculate a post-seizure pressure of 0.34 MPa, MELCOR calculates a relatively gradual decrease in pressure, where the final pressure is reached one hour after the SRV seizure. ASTEC calculates a sharp drop in pressure over 0.25 hours. The difference in depressurization rates may be tied to a steam flow rate out of the SRV immediately after failure, with ASTEC predicting more steam discharge than MELCOR. After SRV seizure, both codes experience pressure transients as debris slumps in the lower plenum. It is likely that the slumping transients are governed by how each code simulates core support plate failure.

Both codes predict a containment pressure increase from 0.1 MPa to near 0.35 MPa at the point of vessel failure. During IC operation and periods of SRV discharge, both codes simulate a gradual increase in containment pressure as steam from the RPV condenses in the suppression pool. Both codes see a marked increase in pressure when runaway oxidation begins to occur in the core at nearly 4 hours into the simulations. This hydrogen then is discharged through the SRV, pressurizing the wetwell. ASTEC predicts a slightly higher containment pressure until just after the corium slump to the lower plenum.

Both codes show close agreement in wetwell water temperature until the energy removal rate from convective heat transfer begins to decrease in the ASTEC simulation near 5 hours into the scenario. Upon SRV seizure, ASTEC calculates a temperature increase of about 10 K, whereas MELCOR calculates a slightly higher temperature increase of approximately 13 K. Greater convective heat transfer from the degraded core in MELCOR could be responsible for the slightly higher wetwell temperature.

6.2 Core Degradation Behavior

In the first minutes of heatup, both codes predict that heatup progresses from top to bottom. The initial hottest spot is located in the center of core (1st ring) and in the top half part of the core (seen at 3.56 hours for ASTEC and at 4.25 hours for MELCOR). Degradation then starts at the top of the active zone in the ASTEC simulation, whereas MELCOR predicts it in the middle of the core region. A possible explanation for the difference in location of the initial hottest spot is that the ASTEC domain over the core upper plate is adiabatic, with the exception of steam exhaust from the area. There is no radiative heat transfer over the upper core plate in ASTEC.

Because of the difference in treatment of degraded core morphology, the accident progresses differently in MELCOR and ASTEC. MELCOR treats debris as a combination of both particulate debris and molten debris. Were the MELCOR eutectic model fully implemented and active, the conglomerate debris that fills the pores could be molten. ASTEC treats degraded fuel as a

unified field called “magma.” This “magma” field more closely resembles molten debris as opposed to the particulate debris predicted by MELCOR.

In the uncovered part of the core, the increase in temperature is strongly driven by oxidation of Zircaloy. Accounting for the melt-down or the collapse of fuel rods has a significant impact on the calculation of temperatures. Therefore, ASTEC and MELCOR temperature fields are very different during core degradation. As a consequence, for the ASTEC simulation, fuel melting also occurs in the 5th ring.

As the core degradation process proceeds, the “magma” formed in the ASTEC simulation leads to significant blockage of flow channels. As these channels become blocked, a minimum fraction is imposed to allow for chemical interactions such as oxidation to proceed. In contrast, the particulate debris predicted by MELCOR is much more porous. Additionally, as fuel assemblies collapse in MELCOR (something which is not modeled in ASTEC) large areas of the core region become open to flow that were previously blocked by debris.

6.3 Hydrogen, Safety Relief Valve and Lower Plenum Behavior

Because MELCOR and ASTEC solve for oxidation in the same fundamental manner, it is not surprising that the total hydrogen generated in both simulations is within 25 kg, with less than a 10 kg difference in hydrogen from zirconium oxidation.

Both codes respond differently to core degradation with respect to oxidation. Although the MELCOR core is degrading throughout the accident, fuel assemblies do not actually fail until 5.2 hours. So, the majority of oxidation in MELCOR occurs while the core is still in its original geometry. In contrast, the bulk of oxidation in ASTEC occurs during core melt and “magma” formation.

As evidenced in Figure 5-1, zirconium, in ASTEC, oxidizes at a faster, steadier rate with no major periods of slowed oxidation before the slumping event. ASTEC also predicts brief jumps in oxidation. However, MELCOR calculates more gradual oxidation with no sudden impulses and prolonged periods of minimal oxidation. After SRV seizure, ASTEC predicts some oxidation whereas oxidation stalls in MELCOR. Conversely, there is minimal oxidation in ASTEC after the core slump, whereas MELCOR predicts continuous oxidation.

Overall, since transients in each code align with core degradation events, it appears that the variations in core degradation treatment across both codes are primarily responsible for the differing oxidation trends. Core material in ASTEC gradually melts and turns into “magma” throughout the course of the accident. In MELCOR, there is debris formation as core structures fail, but the majority of core degradation occurs when rings of assemblies collapse. This lends to the step-like oxidation behavior observed in MELCOR.

The failure of the lower head in both MELCOR and ASTEC was a result of both thermal and mechanical stress, but the primary contributor to lower head failure was elevated temperatures. The temperatures in both MELCOR and ASTEC of the hottest node approached the melting temperature of the lower head steel.

The failure location of the lower head was different in both MELCOR and ASTEC. MELCOR failed the lower head at the bottom of the RPV, while ASTEC failed the lower head on the side. This can be attributed to ASTEC’s lower plenum model which creates a metallic layer, with a

higher thermal conductivity, on top of the oxide pool layer. That effect is clearly linked to the amount of molten steel in corium and the rapid increase of temperature that can be seen on the Figure 5-11.

6.4 Overall Conclusions

This analysis underlines the fact that severe accident analysis codes assume different effective morphologies (modeling abstractions) to describe and represent degraded core materials. MELCOR calculates the formation of primarily particulate debris with some molten debris. ASTEC calculates the formation of a pool mainly composed of molten materials, with a minimum gas flow area through the pool.

Those morphological representations directly impact the porosity and surface area of the debris, and thus have a significant impact on the coolability and oxidation of these materials. Accordingly, the thermal-hydraulic response can differ greatly at times between the two codes. Despite the fact that these codes can differ in thermal-hydraulic behavior, the overall oxidation predicted by the two codes does not differ significantly. Additionally, the time of lower head failure is also similar, even though the location of lower head failure is different.

ASTEC and MELCOR model fuel assembly loss of integrity in different manners. ASTEC models loss of integrity through the melting of core elements. Upon this melting event the fuel becomes “magma.” MELCOR models fuel assembly failure as a function of time at temperature. The modeling of discrete assembly collapses in MELCOR changes the overall plant system response in relation to ASTEC. When assemblies collapse in MELCOR, they become particulate debris and relocate to the core plate. When assemblies fail in ASTEC, the “magma” remains in the same location and gradually heats adjacent mesh locations, eventually making its way to the core plate. This leads to core heatup and fuel assembly loss of integrity occurring faster within ASTEC compared to MELCOR.

As a next step there is interest in comparing the two severe accident codes during a core reflood event, limiting the core damage. This would provide sufficient information for comparing the thermal hydraulic and quench modeling within the two codes.

Additionaly the new reference version of ASTEC is the V2.1 rev1 for which the backbone of the in-vessel phenomena has been reviewed to strengthen the modelling of T/H and fuel assembly degradation modelling and fo which specific functionalities for the description of canister walls, cruciform control blades and in-core multichannel flows have been developed. (Chatelard, 2016) Models for reflooding of degraded core, cladding oxidation and corium behavior in the lower head have also been improved to account with recent R&D developments. This analyses and comparison with MELCOR will so be made again with ASTEC V2.1 rev1 in the next future probably leading to a review of these conclusions.

7 REFERENCES

[1] Cardoni, J., Radionuclide Inventory and Decay Heat Quantification Methodology for Severe Accident Simulations, Unclassified Unlimited Release, SAND2014-17667, September, 2014.

[2] Chatelard, P. et al, ASTEC V2 Severe Accident Integral Code Main Features, Current V2.0 Modeling Status, Perspectives, *Nuclear Energy and Design*, Vol. 272, pp. 119-135, 2014.

[3] Chatelard, P., Belon, S., Bosland, L., Carénini, C., Coindreau, O., Cousin, F., Marchetto, C., Novack, H., Piar, L., & Chailan, L., Main Modelling Features of ASTEC V2.1 Major Version, *Annals of Nuclear Energy,* Vol 93, pp. 83-93, July 2016.

[4] Humphries, L. L., Cole, R. K., Louie, D. L., Figueroa, V. G., & Young, M. F., MELCOR Computer, Code Manuals Volume 2: Reference Manual, *SAND Report*, SAND2015-6692 R, (2015).

[5] Institut de Radioprotection et de Sûrete Nucléaire (IRSN), The ASTEC Software Package, http://www.irsn.fr/EN/Research/Scientific-tools/Computer-codes/Pages/The-ASTEC-Software-Package-2949.aspx, Accessed May 11, 2017.

[6] Luxat D., Hanophy J. & Kalinich D., Modular Accident Analysis Program (MAAP) - MELCOR Crosswalk Study Phase 1, EPRI Technical Report, Report 3002004449, (2014).

[7] Nourbakhsh H. P., Miao, G., and Cheng, Z., Analysis of Spent Fuel Heatup Following Loss of Water in a Spent Fuel Pool: A User's Manual for the Computer Code SHARP, NUREG/CR-6441, March, 2002.

[8] OECD Nuclear Energy Agency (NEA), Benchmark Study of the Accident at the Fukushima Daiichi Nuclear Power Plant - (BSAF Project) - Phase 1 Summary Report, *NEA Technical Report*, NEA/CSNI/R(2015)18, (2015).

[9] Pontillon, Y., Malgouyres, P. P., Ducros, G., Nicaise, G., Dubourg, R., Kissane, M. and Baichi, M. Lessons Learnt from VERCORS Tests. Study of the Active Role played by UO2-ZrO2-FP Interactions on Irradiated Fuel Collapse Temperature, Journal of Nuclear Materials, Volume 344, pp. 265-273, 2005.

[10] Sandia National Laboratories (SNL), MELCOR A Computer Code for Analyzing Severe Accidents in Nuclear Power Plants and the Design Basis Accidents for Advanced Plant Applications, https://melcor.sandia.gov/about.html, Accessed May 11, 2017.

[11] Nowack H., Chatelard P., Hermsmeyer St., Sanchez V., Herranz L., CESAM –Code for European Severe Accident Management, EURATOM Project on ASTEC Improvement, *Annals of Nuclear Energy,* Vol 116, pp. 128-136, 2018

NRC FORM 335
(12-2010)
NRCMD 3.7

U.S. NUCLEAR REGULATORY COMMISSION

BIBLIOGRAPHIC DATA SHEET

(See instructions on the reverse)

1. REPORT NUMBER
(Assigned by NRC, Add Vol., Supp., Rev., and Addendum Numbers, if any.)

NUREG/IA-0510

2. TITLE AND SUBTITLE

MELCOR-ASTEC Crosswalk of the Accident at Fukushima-Daiichi Unit 1: Phase I Analysis

3. DATE REPORT PUBLISHED

MONTH	YEAR
June	2019

4. FIN OR GRANT NUMBER

5. AUTHOR(S)

N. Andrews[1], C. Faucett[1], S. Belon[2], C. Bouillet[2], H. Bonneville[2], D. Algama

6. TYPE OF REPORT

Technical

7. PERIOD COVERED (Inclusive Dates)

8. PERFORMING ORGANIZATION - NAME AND ADDRESS (If NRC, provide Division, Office or Region, U. S. Nuclear Regulatory Commission, and mailing address; if contractor, provide name and mailing address.)

[1]Sandia National Laboratories
Albuquerque, NM 87185
[2]Institut de Radioprotection et de Surete Nucleaire
Cadarache, France, BP 3- 13115 St-Paul-Lez-Durance Cedex

9. SPONSORING ORGANIZATION - NAME AND ADDRESS (If NRC, type "Same as above", if contractor, provide NRC Division, Office or Region, U. S. Nuclear Regulatory Commission, and mailing address.)

Division of Systems Analysis
Office of Nuclear Regulatory Research
U.S. Nuclear Regulatory Commission
Washington, DC 20555-0001

10. SUPPLEMENTARY NOTES

D. Algama, NRC Project Manager

11. ABSTRACT (200 words or less)

This analysis compares Sandia National Laboratories' (SNL) MELCOR results for the first phase of the Modular Accident Analysis Program (MAAP)-MELCOR Crosswalk to the Accident Source Term Evaluation Code (ASTEC), developed by the Institut de Radioprotection et de Sureté Nucléaire (IRSN), results for the same accident scenario. Similar to the original MAAP-MELCOR Crosswalk, this analysis integrates system response of both containment and reactor pressure vessel (RPV), core degradation behavior, lower plenum behavior and lower head failure, and finally hydrogen behavior and generation.

The accident scenario developed by the Electric Power Research Institute (EPRI) and SNL for this analysis is stylized after accident progression of Fukushima Daiichi Unit 1 to better highlight areas of similarity and differences in the two computer codes studied. Hence, this work is not appropriate for extrapolation to the area of Fukushima forensic study. The behavior of the main steam line isolation valve, control rod drive mechanism, feedwater system, safety relief valve, and isolation condenser were made constant between the two codes. The MELCOR simulation was run to 16 hours, while the ASTEC simulation was run a slightly shorter amount of time before to the point of lower head failure. Ex-vessel behavior was not examined in this analysis.

12. KEY WORDS/DESCRIPTORS (List words or phrases that will assist researchers in locating the report.)

MELCOR, ASTEC, Fukushima, Daiichi, Severe Accident, Benchmark

13. AVAILABILITY STATEMENT

unlimited

14. SECURITY CLASSIFICATION

(This Page)
unclassified

(This Report)
unclassified

15. NUMBER OF PAGES

16. PRICE

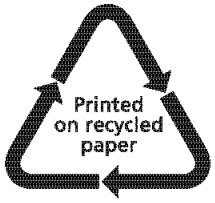

Federal Recycling Program

UNITED STATES
NUCLEAR REGULATORY COMMSSION
WASHINGTON, DC 20555-0001

OFFICIAL BUSINESS